Scuola Internazionale Superiore di Studi Avanzati

Structural Insights Into Alternate Aggregation States Of Mouse Prion Protein

CANDIDATE

Maurizio Polano

SUPERVISOR

Prof. Giuseppe Legname

Summary

Chapter 1: Introduction To Prion Diseases And The Prion Protein

Historical overview

In 1982, the term "prion" was introduced by Stanley B.Prusiner, to christen a particle that, on the basis of clinical and biochemical observations, appeared to be a totally new infectious agent, consisting only of an endogenous cell surface protein [1-3]. This term is a combination of the two adjectives proteinaceous and infectious. The cellular form of the prion protein (PrP^{C}) is hypothesised to be able to induce transmissible spongiform encephalopathies (TSE) in mammals by changing its conformation through, an as yet, ill understood pathway, that results in the formation of a "disease-associated" isoform, called the "scrapie form" of the protein (PrP^{Sc}) [1], [4], [5]. In contrast, to the soluble, monomeric PrP^{C}, PrP^{Sc} has been shown to have a high tendency to associate into insoluble aggregates, such as oligomers or amyloid fibrils, and induce a fatal degeneration of the central nervous system (CNS) in the regions where the aggregates accumulate [6], [7], [8], [9], [10].

TSE or prion diseases are a group of fatal neurodegenerative diseases, which affect the CNS of both humans and animals [3]. Although the pathology of TSE varies from case to case, in general it results in similar neuropathological features, *e.g.* vacuolation, astrocytosis, and neuronal loss [11] showing a “spongy” appearance in the brain.

The first recorded case of a TSE disorder, which was caused by the ‘scrapie’ prion protein, and affected British sheep, was identified and documented more than two hundred and fifty years ago [12] . Since then, scrapie disease of sheep and goats has been known under a multitude of names ("rubbers", "rickets", "goggles", "shakings" "shrewcroft" in England, "scratchie", "cuddie trot" in Scotland, "der Trab", "der Traberkrankheit" lub "die Zitterkrankheit" in Germany, "la maladie convulsive", "la maladie follie", "le tremblante" "la prurigo lombaire" in France and "trzêsawka" in Poland). One of the earliest scientific reports on scrapie was published in the "Agricultural Improvement Society at Bath, as a paragraph in the "General View of the Agriculture of Wiltshire" published by Thomas Davies in 1811 [13]. Interestingly, in 1848, Roche-Lubin claimed that scrapie was caused by the sexual overactivity of rams or, alternatively, by the thunderstorms [13].

The first author who believed that scrapie ("tremblante") was a viral disease, was Besnoit in 1899 whilst the transmissible nature of TSE was proven in the late 1930’s by the seminal experiments of Cuile and Chelle [14]. The contention that scrapie was an infectious disease caused by a filterable agent was accepted with a long-lasting scepticism. In 1938, W.S. Gordon, a deputy director of the famous Moredun Institute in Edinburgh, Scotland, repeated experiments of Cuille and Chelle using 697 animals of which ~200 developed scrapie [15, 16], [17]. The infectious nature of the scrapie agent was confirmed in 1935, when ~ 7% of 18,000 sheep vaccinated against Louping, developed scrapie [15, 16].

This vaccine was produced from formalin-fixed sheep brains and where the scrapie infectivity could survive 0.35% on formalin for more than 3 months. World War II interrupted research, on scrapie, which had been continued by the research of D.R. Wilson [18]. Wilson's research remained largely unpublished due to his reluctance to present data on such an unorthodox pathogen. However, the 'scrapie' community became well aware of the unusual properties of the scrapie agent, in particular, its high resistance to formalin and high temperature[19].

In the next era of the history of prion discoveries, scrapie was transmitted from sheep to mice by Morris and Gajdusek [20] and from goats to Chandler mice [21]. This led to wide-scale laboratory research and the production of many whimsical hypotheses, with an average frequency approaching one every year or two. The infectious agent has been claimed to be a self-replicating membrane [22-24] a subvirus (not well envisaged) linked to a membrane with a "linkage substance" [25], a viroid [26], a spiroplasma [27] or a retrovirus-like element [28, 29].

Fig. 1. A typical image of a sheep with a disease caused by scrapie. In this figure, wool loss through rubbing and gnawing can be seen at the head, basis of the tail, and the sides of both fore and hind limbs. If scratched on the back (along the spine) affected animals start nibbling ("Gnubbern") and licking their nose. Other typical symptoms of scrapie disease are often a change in behavior such as separation from the herd, hypersensibility to touch, nervousness and fear of sudden noises (such as clapping of hands). Changes in sensitivity such as pruritus (itching) and related loss of wool complete the clinical picture. Additional symptoms such as apathy, loss of reflexes, salivation etc. can occur but are less frequent. The disease duration can be from weeks to months, resulting ultimately in the death of the animal from the disease. *(source http://www.thedoctorweighsin.com/journal/2007/11/3/prions-can-kill-you.html)*

Another animal TSE is transmissible mink encephalopathy (TME), which was recognized in ranch-raised mink by Gaylord Hartsough [30].

Another member of the family of TSE, is the chronic wasting disease (CWD). CWD is a transmissible neurological disease of deer and elk that produces small lesions in brains of infected animals. It is characterized by loss of body condition, behavioral abnormalities and death. CWD is classified as TSE due to clinical symptoms similar to scrapie in sheep. Since the 1960s CWD has affected captive mule deer, white-tailed deer, and Rocky Mountain elk in North America; in the 1990s, CWD has also been found in free-ranging deer and elk [31].

Human TSE can be classified into three different forms: sporadic, inherited, or acquired by infection. Approximately 85% of TSE cases occur sporadically, in the absence of any obvious trigger [32]. The inherited forms include Gerstmann–Sträussler–Scheinker syndrome (GSS) fatal familial insomnia (FFI) and ~15% of the cases of Creutzfeldt–Jakob disease (CJD) [33-35].

The first recorded event of a TSE disorder in humans was kuru (Fig. 2), which was discovered by Zigas and Gajdusek (1957) [36, 37]. The elucidation of kuru opened a new field in human medicine and initiated 40 years of research, which has contributed enormously to our understanding of neurodegenerative disorders of the central nervous system, which includes Alzheimer's disease [38, 39]. The name kuru came from the Fore language, which means to shiver or to shake from fever and cold. The Fore used the noun of the kuru-verb to describe the always-fatal disease, which principally affected their children (Fig. 2) and adult women. It has been and still is restricted to natives of the Fore linguistic group at Papua New Guinea's Eastern Highlands and those neighboring linguistic groups, which intermarry with the Fore tribe. Ritualistic endocannibalism (i.e eating of the relatives as a part of a mourning ritual but not as an alimentary habit) was a practice not only in the kuru area, but in many surrounding Eastern Highland groups which never developed kuru. In the late 1930's and 1940's, many gold miners, protestant missionaries, and government officials made contacts with the northern periphery of the kuru region, and they and later anthropologists, became thoroughly familiar with the ritual endocannibalism of Eastern Highland peoples. When the fatal epidemic in the kuru region was announced, most of the local Caucasians made the obvious assumption that it must have been spread by the cannibalistic practices.

It was the publication of this disease by Gajdusek, which led to the first possible suggestions that scrapie in animals and kuru in humans could be linked to the same family of disorders and caused by the same protein [40]. In 1959, Gajdusek, received a letter from the veterinarian William Hadlow [41], which highlighted analogies between kuru and scrapie, and had been successfully transmitted experimentally by the French group in 1936 (for review [42]).

Fig. 2. Example of people affected by kuru disease. A preadolescent child totally incapacitated by kuru in 1957. The child had such severe dysarthria that he could no longer communicated by word, but he was still intelligent and alert. He had spastic strabismus. He could not stand, sit without support, or even roll over; and had been ill for less than six months, and died within a few months of the time of photography [42].

Gajdusek's reply to Hadlow, resulted in him reconsidering the infectious aetiology of kuru. In view of the chronic cerebral infections, such as Iin syphilis, toxoplasmosis, and trypanosomiasis, inoculated laboratory rodents and monkeys were held for longer observation periods than had been carried out previously in 1957, therefore he was

attempting to obtain a better inoculum in the form of autopsied brain tissue (for review [40]).

In light of these discussions, Gajdusek, successfully transmitted kuru to chimpanzees in 1965 [36], followed later, by transmission of Creutzfeldt-Jakob disease [43] and GSS [44]. Fatal familial insomnia was finally transmitted in the late 1990s [45] [46].

A further animal TSE disorder was described in 1987, when Gerald A. H. Wells and his colleagues from the Central Veterinary Laboratory, described a case of a single cow, in the UK, with a novel form of a TSE disorder. This eventually was called bovine spongiform encephalophy (BSE). Incidentally, although the paper came out one year later, the first case of what turned out to be BSE was reported in a nyala (*Tragelaphus angasii*) by Jeffrey *et al.* [47].

An epidemic of this disorder broke out in the UK, which reached a climax in 1992, where more than 35,000 cases were diagnosed. However, due to the implementation of strict farming measures and bans on the sales of gelatin since the peak of the epidemic, the number of BSE cases diagnosed in the UK, has seen a steady decline since; 1,443 cows in 2000, 1,137 in 2001 and 438 in 2002. In relation to this TSE disorder, in1996, Will *et al.* reported a finding of a new variant of CJD (nvCJD or vCJD), which they suggested most probably resulted from transmission of BSE to humans [48]. This epidemiological conjecture was subsequently substantiated by laboratory studies [49, 50], [51], [52, 53], [54]. The number of vCJD cases is still increasing albeit it more slowly since their discovery although discussions about the extent of the outbreak is become disturbing. On the other hand, the BSE epidemic and appearance of vCJD in humans,

has accelerated TSE research and changed it from a rather small obscure field into a major scientific endeavour.

Human-to-human transmission of TSEs was confirmed by iatrogenic CJD cases caused by direct contact of the CNS with contaminated material during the course of medical treatment [55].

In reality, prion diseases are still rare in humans [55], and up until the 1980s, knowledge of these diseases was limited to a small community of neuroscientists. However, since 1986, from the recognition of BSE, (or 'mad cow disease') in combination with its spread in the UK, where more than 180,000 cattle were affected[56]. Attention to prion diseases has increased substantially from both the scientific and public communities [57]. BSE is believed to have been transmitted to humans by consumption of contaminated beef products, and it is believed to have resulted in the outbreak of the novel form of vCJD in England [51]. As a result of this, TSE continue to draw enormous attention from the scientific and public communities, and has even resulted in the awarding of 2 Nobel Prizes, (Gadjusek 1976 and Prusiner 1997) for research in this field, a rarity for most scientific fields.[57].

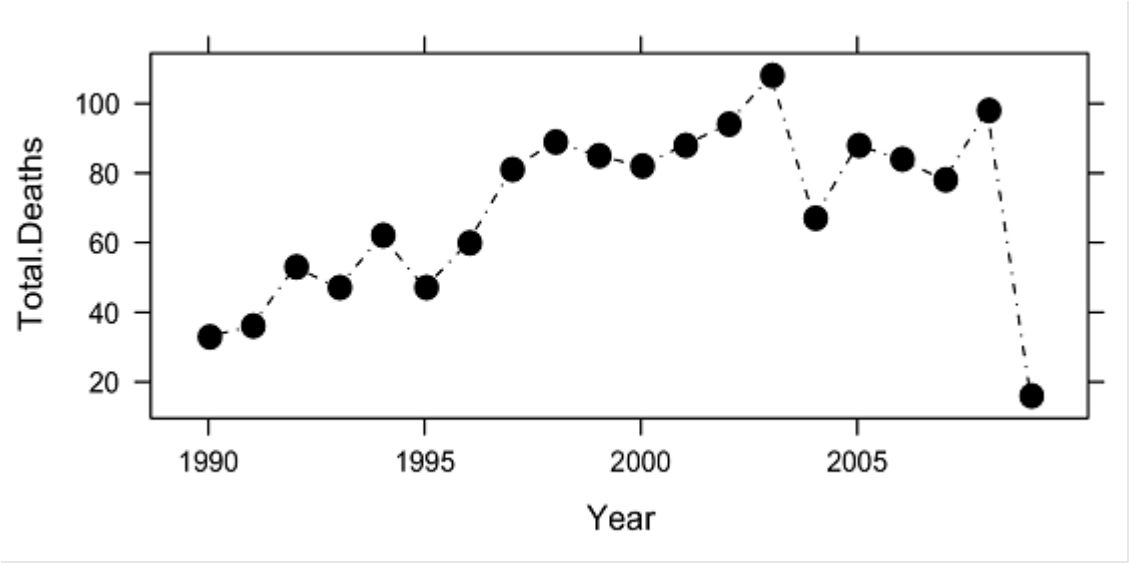

Fig. 3. The number of deaths from TSE in humans since 1990 in the UK. TSE in human have been analyzed from 1990. Case of TSE in human start decrease. (http://www.cjd.ed.ac.uk)

The prion concept – infectious proteins

The protein-only hypothesis was first outlined in general terms by Griffith [4], and formulated in more detail by Stanley B. Prusiner, [2]. It states that the partially protease-resistant and detergent-insoluble PrP^{Sc} is identical with the infectious agent and that the infectious agent is devoid of nucleic acid. Additionally, the propagation of the agent is mediated by PrP^{Sc} and requires a conformational change from PrP^{C} to PrP^{Sc}. Prions are formed by a post-translational conformational remodeling event in which a cellular protein, PrP^{C}, is converted into the disease-associated infectious form, PrP^{Sc} and can be differentiated from PrP^{C} by an increased resistance to digestion with proteases such as proteinase K (PK), poor solubility in non-ionic detergents, an increased β-sheet content, and its propensity for forming higher order structures such as oligomers amyloid fibrils [2]. The protein-only hypothesis is unique in offering explanations for all three etiologies of prion diseases (Fig. 4). In infectious disease, exogenous PrP^{Sc} enters the host, recruits copies of host-encoded PrP^{C} and then templates their conversion, resulting in prion replication and disease pathogenesis. In the literature, protease resistant PrP (formed by the digestion of PrP^{Sc} with PK) is frequentally referred to as PrP^{res} (or PrP27-30) in order to distinguish it from full-length PrP^{Sc} (Fig. 4 and Fig. 5). The use of the term PrP^{Sc} implies that the protein is infectious, whereas PrP^{res} does not necessarily imply infectivity.

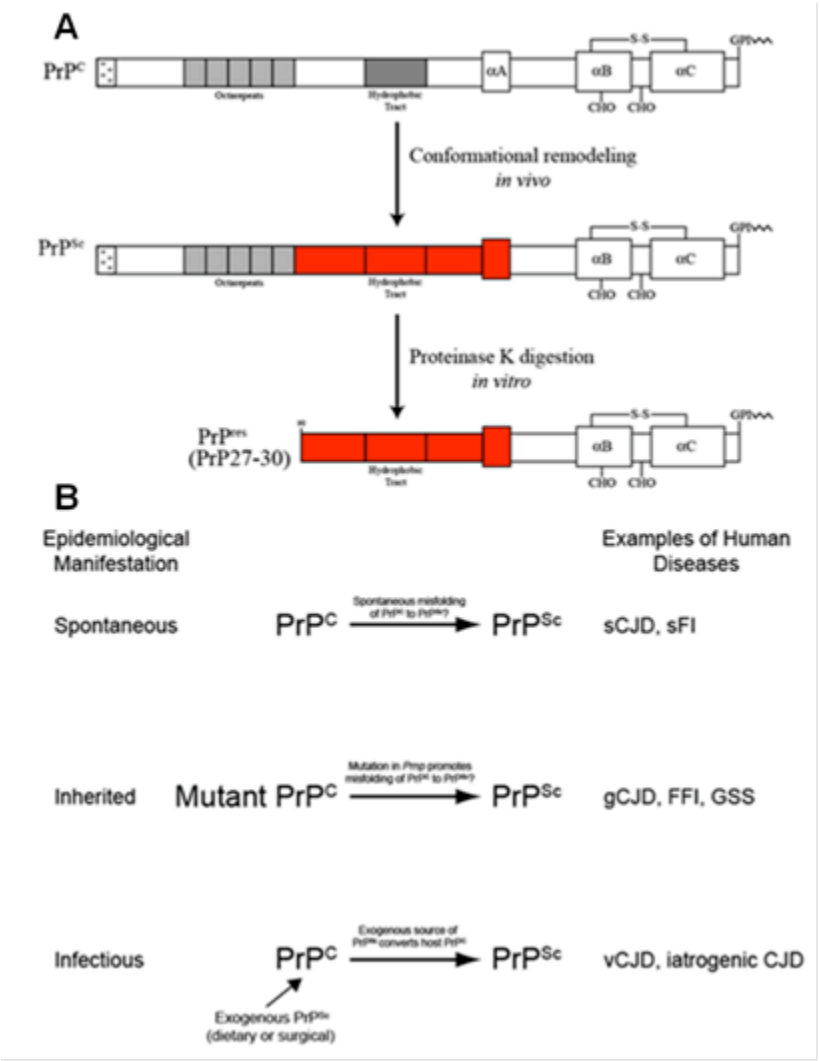

Fig. 4. Prion disease nomenclature and modes of acquisition. A: In prion disease, the host-encoded cellular prion protein (PrP^{C}) undergoes a conformational transition to a disease-associated conformer termed PrP^{Sc} or PrP^{D}. The approximate region of PrP^{C} conformationally altered in PrP^{Sc} is shown in red, although the exact boundaries are unknown. Detection of prion disease is commonly achieved in vitro by treatment with PK, which cleaves PrP^{Sc} near residue 90, to generate the protease-resistant fragment termed PrP^{res} or $PrP^{27\text{-}30}$. **B**: Prion diseases are unique in the fact that they are infectious [58].

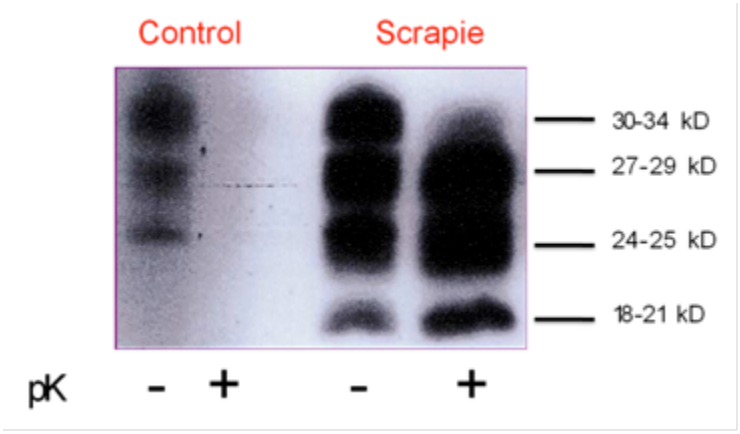

Fig. 5. Differential susceptibility of PrP^{C} and PrP^{Sc} to PK digestion. Demonstration of the different resistance of the protein with PK treatment. On the left the control sample (not abnormal PrP is present in the sample), on the right the abnormal PrP^{Sc} is resistent to PK treatment [58, 59].

Studies show that mammalian prions form fiber-like aggregates rich in β-sheet structures, which often have characteristics of a typical amyloid structure, being rod-like shape in electron micrographs and show apple-green birefringence under polarized light after staining with Congo red [2]. Amyloid fibers are also associated with other neurodegenerative diseases such as Alzheimer's disease and Huntington's disease. However, so far, it has been proven that only prion disorders can be transmitted.

On the other hand, recent data has indicated that at least some amyloid-related disorders, once thought to be noninfectious, may also be transmissible under appropriate circumstances. For example, cerebral injection of brain homogenates from Alzheimer's patients into transgenic mice expressing a mutant β-amyloid precursor protein has been shown to result in neuronal amyloid deposition and neurodegeneration within several months [60]. However, since control (untreated) animals used in these studies developed a similar disease pathology later in life, it was difficult to conclusively

determine whether the diseased brain homogenate used in this study acts as a bona fide infectious agent or simply accelerates a predetermined clinical endpoint. Perhaps even more intriguing, are reports pointing to potential transmissibility of systemic amyloidoses in animals. In the case of mouse senile amyloidosis, marked apolipoprotein A-II amyloid deposition has been observed following either injection or oral ingestion of isolated apolipoprotein A-II fibrils [61]. Amyloid found in fecal matter and milk of these infected animals has also been demonstrated to induce amyloidosis, providing evidence for more natural routes of transmission [62]. For serum amyloid protein A, recent data suggests that amyloidosis may be transmitted from one species to another, where amyloid present in the feces of captive cheetahs was used to accelerate amyloidosis in mice treated with an inflammatory stimulus [63]. Whilst these studies have offered an intriguing glimpse into the relationship between amyloid and infection, it remains unclear whether prion-like transmission is a common property of all amyloid disorders under the appropriate experimental conditions.

Most cases of TSE arise spontaneously, but the infectious nature and spread of the disease has attracted the greatest scientific and public interest. Whilst in the laboratory setting, the TSE agent is typically delivered by intracerebral inoculation into experimental animals, the most common mechanism for the natural spread of the disease is through ingestion. For example, strong evidence suggests that the feeding of BSE-contaminated meat and bone meal to livestock was responsible for the outbreak of BSE in the 1980s, in England, and subsequent consumption of diseased cattle by humans was believed to be responsible for the emergence of vCJD [64, 65].

Neuroinvasion typically begins upon ingestion of the TSE agent. However, the process of infection remains unclear. One possible mechanism is depicted in Fig. 6.

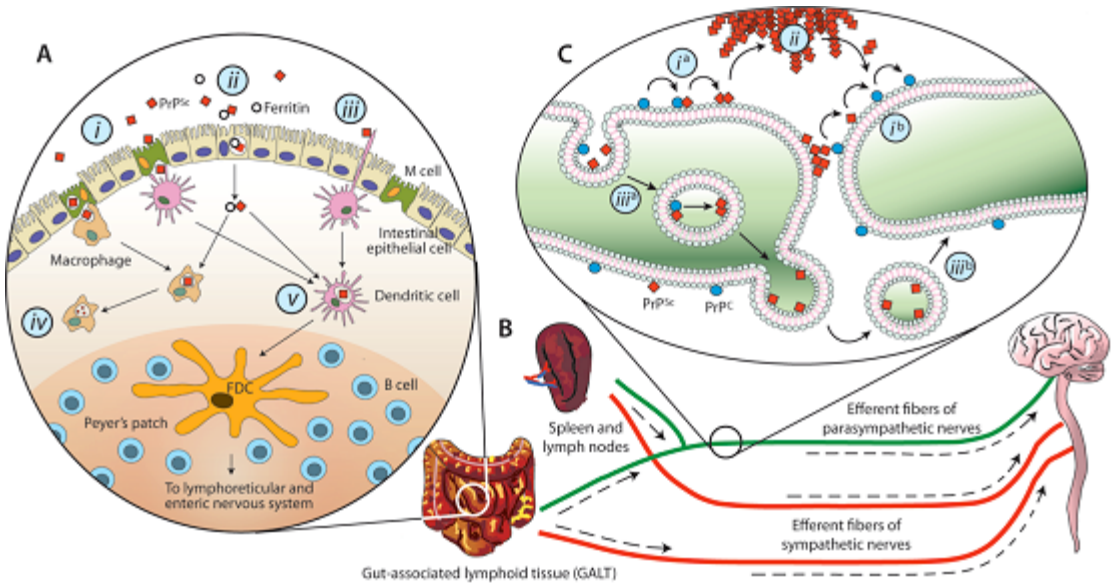

Fig. 6. Schematic representation of the potential mechanism of neuroinvasion in TSE. A: Inital uptake of the TSE agent from the intestinal lumen has been proposed to occur through a number of alternative mechanisms, including M cell transcytosis(i), ferritin-dependent trancytosis through intestinal epithelial cells (ii), or via direct capture by dendritic cells (iii). While phagocytic cells such as macrophages appear to degrade PrP^{Sc} (iv), dendritic cells may deliver the TSE agent to follicular dendritic cells (FDCs) where early accumulation of PrP^{Sc} occurs (v). **B**: After amplification of the TSE agent in lymphoid tissue such as the GALT and spleen, invasion of the nervous system is believed to proceed through peripheral nerves. Retrograde transport of the TSE agent is believed to occur along two distinct pathways, following efferent fibers of the sympathetic and parasympathetic nerves to the CNS. **C:** Retrograde transport and propagation of PrP^{Sc} along neuronal processes may occur by step-wise interactions along the cell surface (ia, ib), via extracellular deposits (ii), or by vesicle-mediated mechanisms (iiia, iiib) [65].

The mechanism seems possible due to the infective particle crossing the intestinal epithelium where probably microfold (M) cells play an important role [66]. Moreover, it is reasonable to postulate that the initial uptake of the TSE agent was made by migratory dendritic cells, which have the ability to capture antigens within the intestinal lumen.

Once past the epithelial wall, PrP^{Sc} is probably sphagocytosed by macrophages and or dendritic cells. Whilst macrophages appear to serve a more protective role [67], some experimental evidence suggests that dendritic cells can deliver the infective molecule to follicular dendritic cells located in the germinal centers of B cell-rich follicles present in Peyer's patches and other gut-associated lymphoid tissue (GALT) underlying the intestinal epithelium (Fig. 6A). After incubation in lymphoid tissue, such as the GALT and spleen, PrP^{Sc} spreads to the CNS via the enteric nervous system. This invasion occurs in the retrograde direction along efferent fibers of both sympathetic (*e.g.*, the splanchnic nerve) and parasympathetic (*e.g.*, the vagus nerve) nerves [67] (Fig. 6B). It is unknown how the retrograde transport between synaptically linked peripheral nerve cells occurs: by step-wise interactions involving direct contact between PrP^{Sc} and surface PrP^{C} along the axolemmal surface, through a vesicle mediated mechanism, or via free-floating extracellular aggregates (Fig. 6C). Once within the CNS proper, further retrograde transport of the TSE pathogen eventually results in infection of the brain, leading to characteristic spongiform degeneration and astroglial activation.

Prion diseases are thus very important to study as they enlighten two important concepts in biology: (1) proteins can have different structures with the same primary structure but with different functions and (2) some structures can be infective because they are capable to self-replicate.

Prion diseases

Mammalian prion diseases belong to a group of invariably fatal neurodegenerative disorders of both animals and humans, and are resultant of the self replication of the protein from its conversion of the host-encoded PrP^{C} into a misfolded form (PrP^{Sc}) that tends to aggregate and may be neurotoxic [11]. There are four principle neuropathological observations for prion diseases (Fig. 7) spongiform change (vacuolar degeneration of brain parenchyma) death of neurons, astrocytic gliosis (in itself a non-specific reactive response to CNS damage but of an unusual intensity in prion disease [68], and the presence of extracellular amyloid plaques in some, but not all, varieties of prion disease. The majority of prion diseases (including scrapie, mouse-adapted scrapie, BSE, and CJD) are characterized by large amounts of spongiform degeneration and the accumulation of PK-resistant PrP, but with little or no PrP amyloid plaque formation.

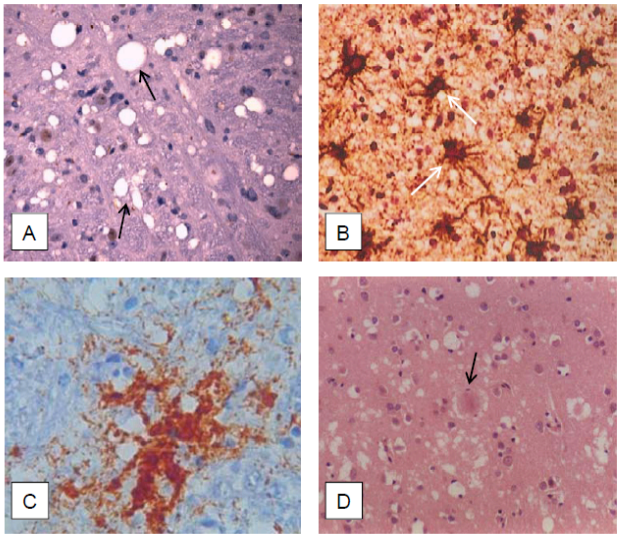

Fig. 7. The neuropathological hallmarks of prion disease. A: Spongiform (vacuolar) degeneration in the grey matter of the brain of a mouse infected with the RML strain of prions. Vacuolation of the brain (black arrows) is observed in most prion diseases and causes the degeneration of neuronal processes and eventually results in the death of neurons. **B**: Activation of astrocytes (reactive astrocytic gliosis: white arrows) in the brain of a patient with CJD as observed by immunostaining for glial fibrillary acidic protein (GFAP). (Image taken from [68]. **C**: Deposits of PrP amyloid as observed by immunohistochemistry in the brain of an elk infected with CWD (Image taken from [58] **D**: 'Florid' plaque (black arrow) consisting of a central PrP amyloid deposit surrounded by a halo of spongiform change in the brain of patient with vCJD. (Image taken from [48])

The mechanism(s) by which PrP^{Sc} causes disease are unclear. One study which used *Prnp*$^{0/0}$ mice that had been grafted with *Prnp*$^{+/+}$ tissue demonstrated that only the tissue which expressed PrP^{C} was damaged, despite the large amounts of PrP^{Sc} in *Prnp*$^{0/0}$ tissue [69]. This suggests that the presence of PrP^{C} is required for prion pathology and that PrP^{Sc} is not inherently neurotoxic. In contrast, in mice expressing PrP^{C} exclusively in astrocytes, pathology in prion-inoculated mice has been observed in tissue surrounding astrocytes (*i.e.* in tissue lacking PrP^{C}) whereas astrocytes remain undamaged [70]. Recent studies using transgenic mice expressing PrP lacking its GPI anchor (*i.e.* secreted PrP) have shown that these mice produce large amounts of PrP^{Sc} ,

but fail to develop clinical prion disease following prion challenge [71]. This suggests that membrane anchorage of PrP is essential for prion pathology, perhaps implying the existence of a transmembrane protein which mediates PrP^{Sc} toxicity [72]. There is also considerable debate as to whether the accumulation of cytoplasmic PrP may play a role in prion toxicity. Transgenic mice expressing cytoplasmic PrP exhibit a neurodegenerative phenotype (albeit one that differs from classical prion disease) and accumulation of PrP in the cytoplasm results in the generation of a PrP^{Sc}-like molecule [73] [74]. However, other investigators have failed to find any toxic effect associated with cytoplasmic PrP [75].

The spectrum of prion diseases appears to be increasing and several new prion diseases of animals have recently been described [58]. Abnormal presentation of prion disease in two cattle in Italy was sufficiently distinct from BSE as to suggest a distinct neurological syndrome denoted bovine amyloidotic spongiform encephalopathy (BASE) [76] [77]} BASE is transmissible to mice confirming that it is a veritable TSE and strikingly, its properties in mice were indistinguishable from BSE suggesting that BASE may represent the original source of BSE [78]. Another disease, Nor98, sometimes referred to as atypical scrapie, was first detected in Norwegian sheep [79], [80]. There is no evidence of lateral or horizontal transmission, with cases (one per flock) observed in geographically dispersed locations. Furthermore, Nor98 possesses distinct genetic, biochemical, and histopathological signatures from scrapie. Nor98 is transmissible to mice, confirming its classification as a prion disease [81]. The origins of BASE and Nor98 are unclear, although it is conceivable that both represent distinct sporadic prion diseases of animals.

Prion strains are prion isolates, biologically cloned, which display unique biological properties and result in characteristic phenotypes when propagated in a given species. Strains can be identified and differentiated on the basis of clinical manifestation (such as the “scratching” and “drowsy” strains of scrapie when given to goats) [17], differential incubation times [82] pathological lesion profiles (*i.e.* different strains target different neuroanatomic areas of the brain) the ratio of glycoforms (unglycosylated, monoglycosylated and di-glycosylated) within protease-digested preparations of PrP [49], the size of the PK-resistant PrP fragment [83], [84] differential reactivity to luminescent conjugated polymers [85], [86], and other biochemical properties such as conformational stability [87]. The existence of prion strains comprises one of the main challenges to the protein-only hypothesis and opponents argue that such diversity cannot be encoded in the absence of a nucleic acid [88]. Indeed, multiple prion strains can exist for a given PrP amino acid sequence suggesting that strain variety is encoded by a different mechanism. Accumulating evidence suggests that strain-specific properties are encoded by the conformation of PrP. Subtle changes in conformation could lead to the phenotypic differences observed, such as differential sizes of PK-resistant fragments and neuroanatomic target areas [84]. This hypothesis has not been definitively proven for mammalian prions to date, in large part due to the lack of high resolution structural data for PrP^{Sc}. Studies on various prion strains using the conformation-dependent immunoassay suggest that individual strains have differential availability of antibody epitopes implying that each strain has a different PrP conformation [9]. Also, small changes in amino acid sequence of a mutant PrP23-144 molecule led to distinct ultrastructural properties of prion fibrils *in vitro* [89] [90].

Furthermore, prion strains which are more susceptible to chemical denaturation have the shortest incubation times and vice versa suggesting that the conformational stability of a given strain governs it replication rate [91]. However, the strongest evidence for the conformational encoding of prion strains has come from studies on yeast prions. Amyloids of the Sup35 protein, prepared at different temperatures have led to unique conformations, which are stably propagated. When these variants are introduced into yeast, different strains of [PSI+] are obtained, suggesting that conformation of Sup35 amyloid governs strain-specific [92]. Furthermore, the structural differences in Sup35 strain variants have been probed by hydrogen/deuterium exchange revealing that differences in the length of the amyloid β-sheet core dictate strain structure and biological properties [93]. Nonetheless, the issue of prion strains will remain an open question in prion biology until parallel high-resolution structures exist for different strains of mammalian prions.

The cellular form of prion protein - PrP^C

The PrP^C protein is a widespread cell surface tethered protein expressed mainly in the tissues of the CNS. Mature PrP^C is a ~210 amino acid protein which largely localizes to detergent-resistant subdomains known as 'lipid rafts', located on the outer surface of the plasma membrane via a C-terminal glycophosphatidylinositol (GPI) anchor (Fig. 8) [3] [94].

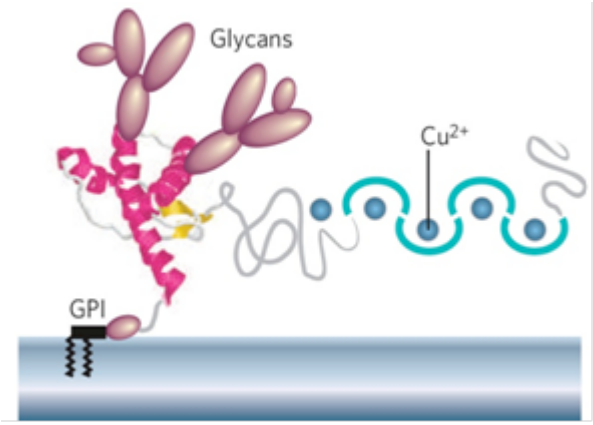

Fig. 8. GPI-anchored plasma-membrane glycoprotein. Picture highlights the three-dimensional structure of PrP^C. Here is depicted the glycosilation site and the putative copper binding site (from [95]).

Moreover, mature PrP^C undergoes endoproteolysis at the cell surface, being subjected to two posttranslational cleavages during the course of its metabolisms. The 'normal' constitutive cleavage of PrP^C, in the brain and in cultured cells, occurs inside this neurotoxic region of the protein (between residues 110 and 111), leading to the formation of a 9 kDa soluble N-terminal fragment (N1; residues 23–110) and a 17 kDa C-terminal fragment (C1 or PrP-II) that is still attached to the membrane through the GPI anchor [96], [97].

Any modification can have an effect on the topology and the function of the PrP. In fact, the PrP protein has been observed in many topological forms and each could be expressed for different roles and interactions for the protein. Due to the fact that the majority of PrP is found outside of the membrane, it is possible that during its passage to the plasma membrane, the mature protein could take on different partial structures and features such as transmembrane variants or cytoplamatica variants. Many authors have speculated about this but as of yet, nothing is conclusive [98, 99].

High-resolution magnetic resonance nucleic (NMR) studies of bacterially expressed recombinant (rec) PrP, a model for PrP^{C} lacking any post-translational modifications, have revealed a folded C-terminal domain and an N-terminal region which is largely unstructured [100]. Depending on the species, the flexible N-terminus contains at least four glycine-rich octapeptide repeats which display a particular affinity for Cu^{2+} [101], with reports of weaker binding to other divalent cations such as Zn^{2+}, Fe^{2+}, Ni^{2+}, and Mn^{+2} [102] (Fig. 8-9).

The PrP globular domain is highly conserved over many different species, consisting of two short β-strands and three α-*helices*, with a disulfide bond bridging *helices* 2 and 3. This domain also contains two potential sites for N-linked glycosylation (Fig. 9) [100].

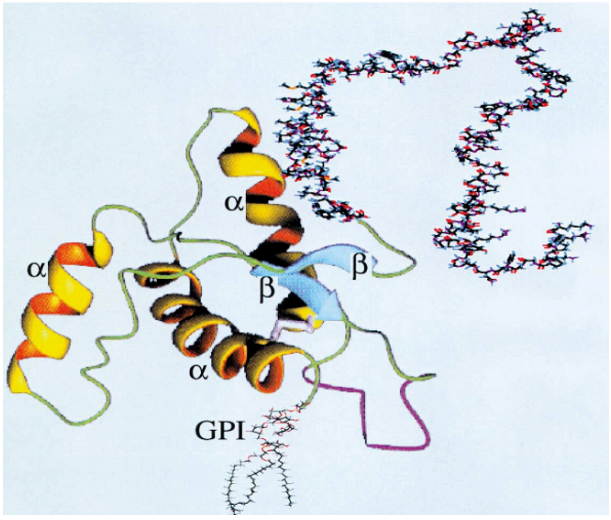

Fig. 9. Model of three-dimensional prion protein. PrP protein is made of a globular domain (amino acid 121-231) which includes three α-helices and two small antiparallel β-sheet structures, and a long flexible tail whose conformation depend on the environment condition (from [59])

The physiological function(s) of PrP^C

The physiological function of PrP^C remains elusive. Much hope was pinned on the use of PrP^C knock-out mice to unveil the function of the protein, but no obvious phenotype was observed [103]. Even postnatally induced *Prnp* ablation does not elicit any phenotype [104]. Aging mice show demyelination in the peripheral nervous system, albeit without clinical symptoms [105]. A number of subtle abnormalities, *e.g.* abnormalities in synaptic physiology [106] and in circadian rhythms and sleep [107] have been described in PrP-deficient mice, but their molecular basis is undefined. The only definite phenotype of $Prnp^{0/0}$ mice is their resistance to prion inoculation [103].

An astonishing number of independent lines of mice lacking PrP^C have been generated by homologous recombination in embryonic stem cells in many laboratories. Mice with disruptive modifications restricted to the open reading frame are known as $Prnp^{0/0}$

[Zurich I] [103] or *Prnp*$^{-/-}$ [Edinburgh] [108]. They developed normally, and no severe pathologies were observed later in life. As predicted by the protein-only hypothesis, these mice were entirely resistant to prion infections [103].

Several physiological roles for PrP^C have been proposed; cell adhesion, signaling, neuroprotection and metabolic functions related to its copper-binding properties. Cell culture experiments reveal a constitutive internalization process of PrP^C from the plasma membrane into endocytic organelles, yet most of the protein recycles back to the membrane without degradation [109]. The existence of a recycling pathway suggests that one physiological role of PrP^C may be to serve as a receptor for uptake of an extracellular ligand. One attractive candidate for such a ligand is the copper ion. It has been shown that copper ions, at physiologically relevant concentrations, rapidly and reversibly stimulate endocytosis of PrP^C from the cell surface [110].

Moreover, it has been reported that PrP^C can bind copper ions and possesses superoxide dismutase activity [111]. Additionally, amino-proximal truncated PrP^C appears to depress endogenous dismutase activity [112], suggesting a role for copper binding of the N-terminal octapeptide-repeat segment. However, PrP^C does not make any measurable contribution to dismutase activity *in vivo* [113]. Given the localization of PrP as a GPI-anchored protein in rafts or caveolate, it has been proposed that PrP, as with other GPI-anchored proteins, could be involved in signal transduction [95]. Crosslinking of PrP^C with F(ab)'2 antibody fragments has been reported to activate Fyn tyrosine kinase [114]. Since Fyn is associated with cellular proliferation and cellular survival, cell surface PrP might modulate neuronal survival. However, it has been

reported that PrP-mediated Fyn activation in cerebellar granule neurons might be responsible for neurite outgrowth rather than neuronal survival [96]. Other studies indicate that PrP^C may interact with components of signal transduction pathways, such as Grb2 [115]. Grb2 is an adaptor protein that mediates growth factor receptor signals and also plays an important role in neuronal survival. Engagement of PrP^C with certain antibodies, a PrP^C binding peptide [116] or with a molecule called stress-inducible protein I (STI 1), leads to activation of both the cAMP/ protein kinase A and the Erk signaling pathways [117] [118]. PrP^C-mediated activation of the cAMP/ protein kinase A (PKA) pathways has a cytoprotective effect in nervous tissue [118]. Taken together, these studies clearly support a neuroprotective role for PrP through signal transduction events.

PrP has been shown to interact with the 37 kDa/67 kDa laminin receptor precursor [119], [120], and heparan sulfate [120], suggesting a possible role in cell adhesion and/or signaling. Perhaps PrP^C does not possess any intrinsic biological activity, yet it modifies the function of other proteins. Multiple PrP^C interacting partners have been identified in recent years: the antiapoptotic protein Bcl-2 [121], caveolin [122], N-CAM, [123] and neurotrophin p75 receptor [124]. None of these interactors, however, have yet revealed functional pathways in which PrP^C could be involved *in vivo*.

PrP^C associations with raft membranes, adhesion molecules and signalling pathways are consistent with its involvement in the assembly of new cellular structures such as neurites and synapses in neurons, and projections in leukocytes (pseudopodia) and follicular dendritic cells (dendritic processes). At the same time, there is evidence that

PrP^C negatively modulates the phagocytic activities of macrophages and other phagocytic cells in a manner that might control inflammatory responses to damaged or apoptotic cells [65]. Notably, PrP^C is expressed at relatively high levels in the brain, where overly aggressive inflammatory responses might be particularly damaging and irreversible. One curious characteristic of PrP^C that is not obviously connected to the assembly of cellular structures, but might be related to clearance or scavenging mechanisms, is its propensity to bind metals, nucleic acids, porphyrins and their analogues. The presence of free forms of these PrP^C ligands in the extracellular spaces would ordinarily be unexpected, unless they were released from pathogens, dying or damaged cells, or perhaps debris from decommissioned cellular structures such as under-used axons, dendritic spines and synapses. The detection and control of potentially harmful factors is an important part of the responses of the innate immune system and glia to infections, tissue damage, stresses, developmental changes (such as apoptosis) and restructuring. It is tempting to speculate that PrP^C might modulate such responses in various cell types by scavenging nucleic acids, metals, porphyrins and similar factors for delivery to appropriate receptors or subcellular sites for degradation and/or signalling. In this context, the binding of PrP^C by cell-surface GAGs might keep PrP^C molecules occupied until preferred ligands appear, because GAGs can compete for the same sites on PrP^C [125]. Most of the known PrP^C ligands - for example, NCAMs, laminins, laminin receptors and HSPGs - are involved in cellular adhesion, and these molecules, and their binding partners, are notorious for being polymorphic. Thus, one likely possibility is that PrP^C functions as a part of complexes comprising multiple proteins and membrane subdomains that are modulated by cell

type, developmental stage, differentiation state, and both extracellular and intracellular cues (Fig. 10).

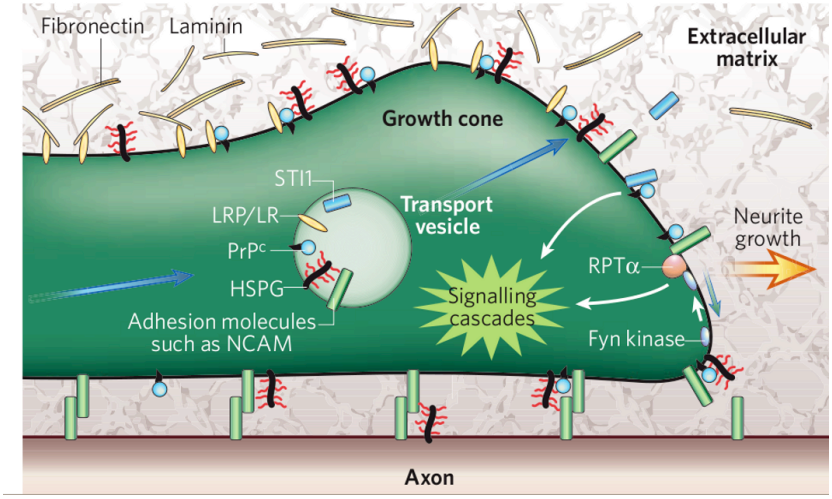

Fig. 10. Model of potential PrP^C interactions associated with axonal growth. PrP^C seems to be important for neurite (nascent axon and dendrite) growth and synapse formation in neurons (from [95]).

Chapter 2: Mechanism Of Prion Protein Conversion: Lessons From In Vitro Studies

Protein aggregation: oligomers vs amyloid fibrils; their toxic role they play in neurodegenerative diseases

Proteins are essential parts of living organisms and participate in virtually every process within living cells. In the last several decades, a great deal has been learned about the various structural forms that the protein molecules adopt in their native states and their functional roles in cellular systems. Moreover, we are also beginning to have a basic understanding of the complex protein folding mechanism at a molecular level and how biological systems have evolved to optimize the protein structure and to ensure the correct folding of proteins. In more recent years, this knowledge has led to the development of numerous computational methods that predict the structures and functions of proteins from their genomic information, which has become largely available from the various genome projects.

Due to the importance of proteins and their roles in cellular systems, failure to synthesize, or misfolding of proteins, may cause the malfunctioning of cellular mechanisms and serious harm to the host organism. Thus, biological systems have evolved elaborate protection procedures to prevent this failure to synthesize or misfolding of proteins by detection and degradation of proteins when misfolding occurs.

However, despite these inherent cellular level controls to prevent protein's misfolding events, a number of human diseases are still associated with protein misfolding and the

subsequent aggregation of proteins [126, 127]. This includes a wide range of diseases from cystic fibrosis and familial emphysema to non-neuropathic systemic and localized diseases such as Type II diabetes, and neurodegenerative diseases such as Alzheimer's disease, Parkinson's disease, Huntington's disease, and prion diseases [128], [129]. These diseases are often inherited and sporadic, but they can also be infectious like in the case of prion diseases. Each disease is associated with a particular protein or aggregates of these proteins, which are thought to be the direct or indirect cause of the pathological conditions associated with the disease [127].

Lately, most research has focused on a group of diseases that involve protein misfolding or the destabilization of the normal soluble structure of proteins followed by subsequent conversions to insoluble fibrillar aggregations, which accumulate in a variety of organs including the liver, spleen and brain [130]. These fibrillar forms of ordered aggregates are known as amyloid. Although proteins that are involved in these amyloid diseases are structurally and evolutionarily unrelated in their native states, the misfolded fibrillar form of proteins bear similar features.

Abnormal protein aggregation is a key feature of a number of other neurodegenerative diseases such as Alzheimer's disease, Parkinson's disease, Huntington's diseases and amyelotrophic lateral sclerosis [131] [132]. These protein aggregates share several physicochemical features: a fibrillar morphology, a predominantly β-sheet secondary structure, birefringence upon staining with the dye Congo red, insolubility in common solvents and detergents, and protease-resistance. None of the polypeptides implicated in these diseases exhibit any primary sequence homology, nor do they derive from

similar sources. However, non-conservative gene mutations have been identified for each of these disorders, contributing to protein misfolding, aggregation and eventual deposition in neuronal inclusions and plaques. These diseases lead to extensive degeneration of neurons.

In Huntington's disease, neuronal loss is believed to be directly mediated through the aggregated state of the huntingtin protein [133]. In other cases (for example the β-amyloid and α-synuclein proteins in Alzheimer's and Parkinson's disease, respectively), presumptive neurotoxic oligomeric protein-intermediates, referred to as protofibrils, have been suggested to mediate cell death [134].

In prion diseases, the precise role of misfolded, aggregated PrP^{Sc} in the neurodegenerative process remains controversial. The protein-only prion hypothesis of protein replication [4] [2], states that the prion (of which PrP^{Sc} constitutes the major, if not sole component) is the infectious and neurotoxic agent. However, work by Brandner *et al.* [69] and recently by Mallucci and coworkers [135] provide evidence *in vivo* that accumulation of PrP^{Sc} in the brain per se, may not cause neurodegeneration. Rather, this neurotoxicity may be mediated by the conversion of PrP^{C} to disease-associated isoforms, PrP^{Sc}, specifically within or on neurons expressing PrP. Or, because PrP^{Sc} binds PrP^{C} [136] it may cause a loss or alteration of the physiological function of PrP^{C}. However, postnatally induced *Prnp* ablation does not elicit any phenotype [104] hence prion pathology is unlikely to come about by a loss of PrP^{C} function.

A general mechanism for neurotoxicity in all neurodegenerative diseases based on protein aggregation has recently been suggested [137] [138] [139]. Bucciantini and

colleagues demonstrated that the aggregation of non-disease associated proteins exhibit inherent cytotoxicity. Moreover, it has recently been demonstrated that different types of soluble amyloid oligomers potentially share a common structure that is recognized by a single antibody, irrespective of the primary amino acid sequence [138]. The binding of this antibody neutralizes the cytotoxic effects of these oligomers, again suggesting a common mechanism of toxicity for all these oligomers. However, despite this recent progress, understanding of the precise pathophysiological mechanisms that eventually lead to the death of neurons is currently lacking.

For more than forty years amyloid deposits were believed to be the causative agents in the degenerative process [140]. Although many studies supported this notion, newer studies with improved techniques are challenging this view [141]. In fact, the current thinking is that it is a group of still poorly defined pre-amyloid species, rather than the amyloid deposits themselves, that are the true toxic conformations [138] [142].

A structural view on amyloid fibrils

The term amyloid was introduced in 1854 by the German physician scientist Rudolph Virchow [143]. Utilizing the best scientific methodology and medical knowledge available at the time, Virchow used iodine to stain cerebral corpora amylacea that had an abnormal macroscopic appearance. The macroscopic appearance of the brain tissue was similar to previous descriptions of other tissues, perhaps as early as 1639, as lardaceous liver, waxy liver, and spongy and “white stone” containing spleens. During the 19th and early 20th centuries, investigations on the nature of amyloid evolved from the macroscopic observations of Virchow and contemporaries to classifications of clinical symptoms.

The term amyloid is often used in different ways. In the context of diseases it was defined by the Nomenclature Committee of the International Society of Amyloidosis as *”extracellular depositions of protein fibrils with characteristic appearance in electron microscope, typical X-ray diffraction pattern, and affinity for Congo Red with concomitant green birefringence”* [144].

Amyloid fibrils may form with distinct kinetics. Amyloid fibril formation typically shows a kinetic curve typical of a nucleation mechanism with a characteristic lag phase. Seeding of the amiloid formation solution with preformed fibrils can shorten this lag phase [128] (see Fig. 11, below for more details). Before formation of mature fibrils, prefibrillar aggregates, sometimes termed amorphous aggregates, occur which can have a spherical shape. Interestingly, specific antibodies can be designed which bind to the prefibrillar aggregates of different proteins but not to the mature fibril [138].

Furthermore, it has been demonstrated that the prefibrillar aggregates are generally more toxic to cells than the mature amyloid fibrils [145]. This led to the speculation that amyloid cytotoxicity is based on the structural properties of the prefibrillar aggregates [145]. However, little direct data exists on how the structure of the prefibrillar aggregates compares with the arrangement of the polypeptide chain in mature amyloid fibrils to truly validate this belief.

Amyloid fibrils also exhibit certain distinctive features. They may be long fibril entities (μm range) with lateral dimensions in the range of 6–13 nm with a distinctive X-ray diffraction fingerprint that results from the cross-β structure (Fig. 11).

They share a common molecular skeleton, the protofilament core structure, which is a continuous β-sheet assembly [146].

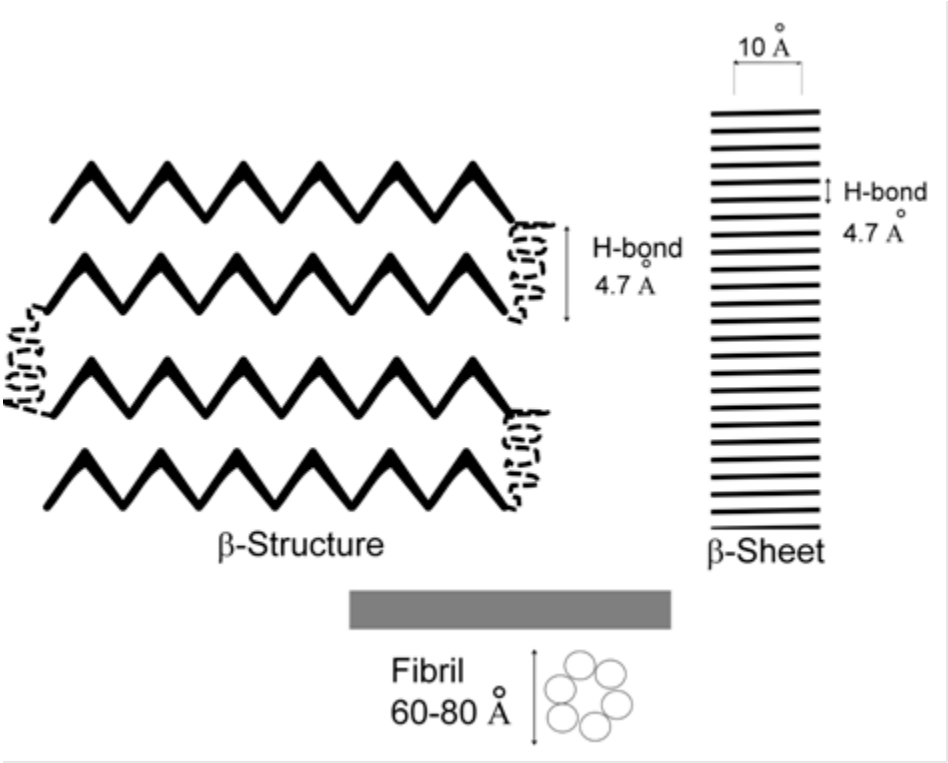

Fig. 11. Amyloid structure. Hierarchy of structure from protein folded into a β-plated structure to amyloid fibril. The 4.7 Å correspond to the hydrogen bonding distance between two β-strand, the 11 Å correspond to the distance between β-sheet and the 60-80 Å distance corresponds to an average fibril diameter (adapted from [147]).

The X-ray diffraction reflections at approximately 4.7 Å on the meridian and 10 Å on the equator are characteristics of fiber diffraction pattern for all amyloids. The structural repeat of 4.7 Å along the fibre axis corresponds to the spacing of β strands and the 10–12 Å spacing corresponds to the face to face separation of the β sheets [148].

Whilst little structural data, exists on whether prefibrillar aggregates and mature fibrils are similar, one study on Aβ(1-40), has shown that the fold of the toxic prefibrillar aggregates and the mature amyloid fibrils are similar [149].

Mature fibrils are the end point of the aggregation process and thus are easily accessible for structural studies. Due to the non-crystalline insoluble nature of amyloid fibrils a variety of methods has been applied to elucidate their structure. The most widely applied technique is electron microscopy, which typically shows straight, unbranched amyloid fibrils, which are 0.1-1.6 μm in length and have a diameter of 60-120 Å. They are built from protofibrils with a diameter of 25-35 Å [147]. Similar proteins may form amyloid fibrils with different morphologies exhibiting a twist of the fibril or lateral association forming an untwisted fibril. Oriented amyloid fibrils show a typical so-called cross-β X-ray diffraction pattern with a meridional 4.6-4.8 Å spacing, which results from the main chain distance within β-sheets running parallel to the fibril axis [148]. The variable equatorial 8-12 Å spacing corresponds to the distance between two β-sheets [145]. Interestingly, amyloid fibrils show a different amide I' band in FTIR spectra in comparison with native β-sheet-rich globular proteins [150]. However, it is the underlaying common structural properties of amyloid fibrils lead to specific reactions with staining dyes (Congo Red [151], Thioflavin T [152] and antibodies [153]).

In vitro conversion studies

The available experimental evidence *in vitro* indicates that the kinetics of fibril formation are complex and can be often separated into a nucleation (or lag) phase and an elongation phase (Fig. 12), followed by the equilibrium between isolated polypeptides and the fibrils [154], [153]. Moreover, multistep kinetics, with the presence of intermediates have also been reported [155].

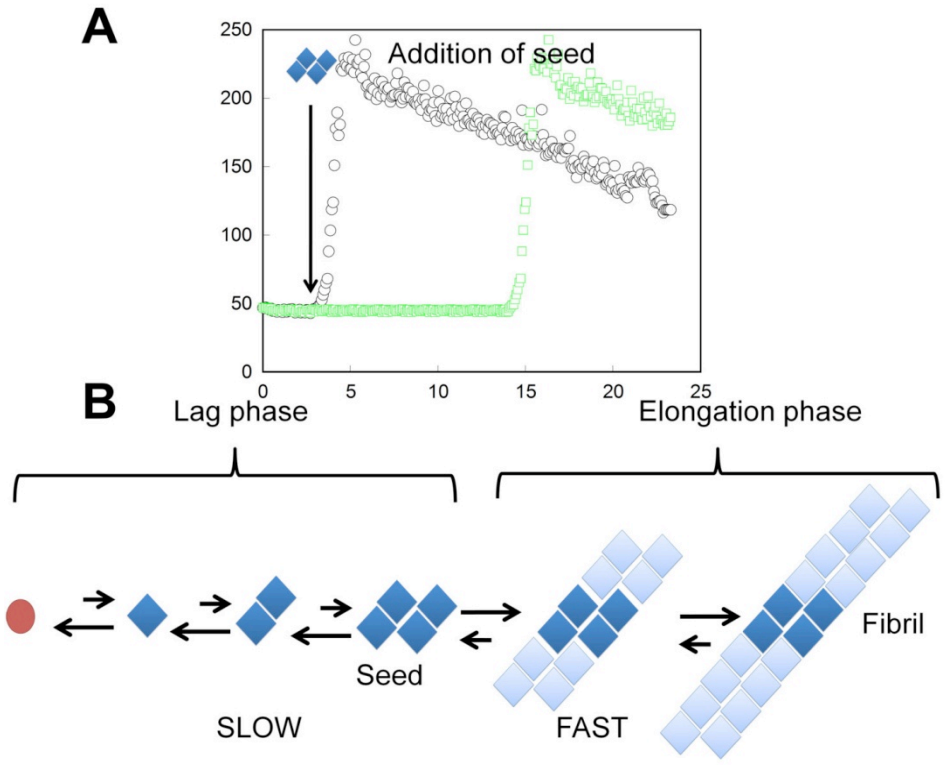

Fig. 12. Mechanism of prion replication and the seeding–nucleation model of amyloid formation. Compelling evidence suggests that PrP^{C} to PrP^{Sc} conversion as shown in (**A)** follow a crystallization-like process known as 'seeding–nucleation'. In this model, formation of a stable oligomeric structure that is capable of further sustaining and catalyzing polymerization of the protein is the key and kinetically limiting step. **A**: The kinetics of amyloid formation usually exhibits an initial lag phase, in which no detectable amyloid is formed, whereas monomers nucleate to form fibers when mixed together with a fresh pool of soluble protein. Moreover, fragmented amyloid fibrils can shorten the lag phase and initiate rapid amyloid formation; a phenomenon known as seeding; **B**: Amyloid formation consists of two kinetic phases. In the 'lag phase', oligomeric nuclei are formed in a slow process that involves misfolding of the protein and unfavorable intermolecular interactions. Once these 'seeds' are formed, a much more rapid 'elongation phase' results in fibril formation. The limiting step in the process is the formation of seeds to direct further aggregation [154]. Amyloid formation can be substantially accelerated by the addition of preformed seeds (circle line) representing the structure that is inherently infectious.

Pathways of fibril formation, fibril morphologies and stability of protofibrillar intermediates are influenced strongly by experimental conditions (*e.g.* protein concentration, pH and ionic strength [156]) and elongation rates can depend on the stability of aggregation of the protein and the folding intermediates [157]. *In vitro* generation of infectious prions from recombinant PrP is considered as the final proof of the "protein-only" hypothesis. In addition, compared to slow and costly conversion experiments in animals and cell culture [3], cell free conversion systems simplify the experimental environment, and opens an opportunity to understand the mechanism of the conversion. Many scientists endeavored to study *in vitro* PrP conversion (despite inherent caveats to the procedure) using short, synthetic PrP peptides [158-162]. Although these short peptides were found to form amyloid fibrils under certain conditions, their relevance has always been questioned since these fibrils have never been found to be infectious *in vivo*.

Difficulties in purification of large quantities of PrP^{C} from natural brain source and the insolubility of PrP^{Sc} are limiting factors in studying biophysical aspects of the $PrP^{C} \rightarrow PrP^{Sc}$ conversion reaction. However, new opportunities for obtaining purer and larger volumes of protein are available from the development of expression systems for the production of recPrP [163]. The methods for production of PrP with either the presence or absence of tag are utilized for purification [164-166]. The use of a tag in the production of the protein gives the best possible results compared to systems without the use of the tag.

Studies with human recPrP fragment corresponding to the Y145stop variant have demonstrated the possibility to transform the monomeric state in fibrillar state *in vitro* [167] and then use it for studies on the species barrier and strain diversity [89].

Studies performed with other peptides such as PrP106–126, a region located near the N-terminal of the protease-resistant PrP^{Sc} has attracted interest, and has demonstrated toxicity in both in vitro and in vivo toxicity of aged 106–126 peptide in a rat retinal model [168]. Whilst these studies provide us some clues with regards to the enigmatic infectivity of prion diseases, they do not explain the process in its entirety.

Moreover, it is known that a broad variety of proteins that rapidly fold into monomeric or oligomeric cellular forms under native-like conditions can also be refolded into β-rich, amyloid forms under conditions that destabilize the native state [126].

In recent years, different protocols for producing fibrils from recPrP or PrP^{C} *in vitro* have been developed by several groups. In contrast to yeast prions in which the amyloidogenic regions are natively unfolded, the PrP domain associated with mammalian prion infectivity is structured and thermodynamically stable [169].

Initial studies using recPrP suggested that the conversion of PrP^{C} to PrP^{Sc} requires the reduction of the disulfide bridge that connects residues Cys179 and Cys214 and that the conversion occurs via a soluble β−sheet monomer. However this conversion does not necessarily bring to an infective form although it can form a β-rich isoform and consequently fibrils [170]. Moreover, it has been recently shown that, the recMoPrP can be folded either to its native, monomeric α-helical isoform or to a β-sheet rich,

oligomeric form with the folding regulated by kinetic control [162, 171]. In addition, it has been shown that an equilibrium between the α-helical and the β-sheet-rich isoforms, where partially denaturing conditions (acidic pH and urea) and with increased concentrations of PrP, favors the conversion to the β-oligomer. Interestingly, whilst both abnormal isoforms, the β-oligomer and the amyloid form, coexist at pH 4–6 [172], the formation of the β-oligomer is favored at pH below 5.5, whereas optimal pH for the conversion into amyloid fibrils is between 5 and 7 [172].

Further still, the conversion to β-sheet of recPrP is strongly dependent on pH, denaturant concentration, and the presence of salts [166, 173].

Because chemical denaturants and elevated temperatures are the most common ways to manipulate the dynamic balance between different unfolding intermediate states, it is not surprising that the first experimental protocols for producing amyloid fibrils from the structured C-terminal domain of α-recPrP (recPrP(90–231)) utilized partially denaturing conditions, such as chemical denaturants [170] [174, 175] or combinations of elevated temperature and high pressure [176]. Moreover, detailed studies of the effect of the denatured agent used have shown how the concentration and the type of agent denaturant can affect the rate and the state of the PrP protein. In 0.4 M urea and at 37°C, the protein maintains its native state [166].

As no unique protocol for making fibrils exist, modifications have been made, which are dependent on the aim of the scientist making the fibrils. Most studies have used the truncated form of recPrP [166]. Although recently a protocol to produce fibrils from full-length PrP has recently been developed. [174]. These protocols evolved around using

the same conditions for amyloid formation that was used when the first synthetic prions were produced (MoSP1) [174, 177].

An alternative to the system above, Riesner and co-workers have established an alternative conversion procedure, where amyloid fibrils are produced by incubating recPrP(90– 231) or PrP^{C} in the presence of low concentrations of sodium dodecyl sulfate (SDS) or in the presence of lipids [178, 179].

Cell free conversion studies have demonstrated similar findings to studies *in vivo* upon the role of PrP to the transmission and the pathogenesis of TSE. The work of Kaneko *et al.* with labeled PrP^{C} demonstrated a high specificity in the PrP^{C} to PrP^{Sc} conversion [180]. Using a similar approach, Bossers *et al.* have shown that the nature of PrP^{Sc} has an impact on the yield of the conversion reaction [181]. In contrast, evidence exists that suggest that the complete disaggregation and denaturation of PrP^{Sc} in the presence of high concentrations of denaturant abolishes the conversion, whereas unfolding of PrP^{C} has no influence on the converting activity [180].

In order to explain the mechanism by which a misfolded form of PrP could induce the refolding of native, normal PrP molecules into the abnormal conformation, two distinct models have been postulated: (A) the template assistance or 'refolding' model, and (B) the nucleation-polymerization or 'seeding' model (Fig. 13).

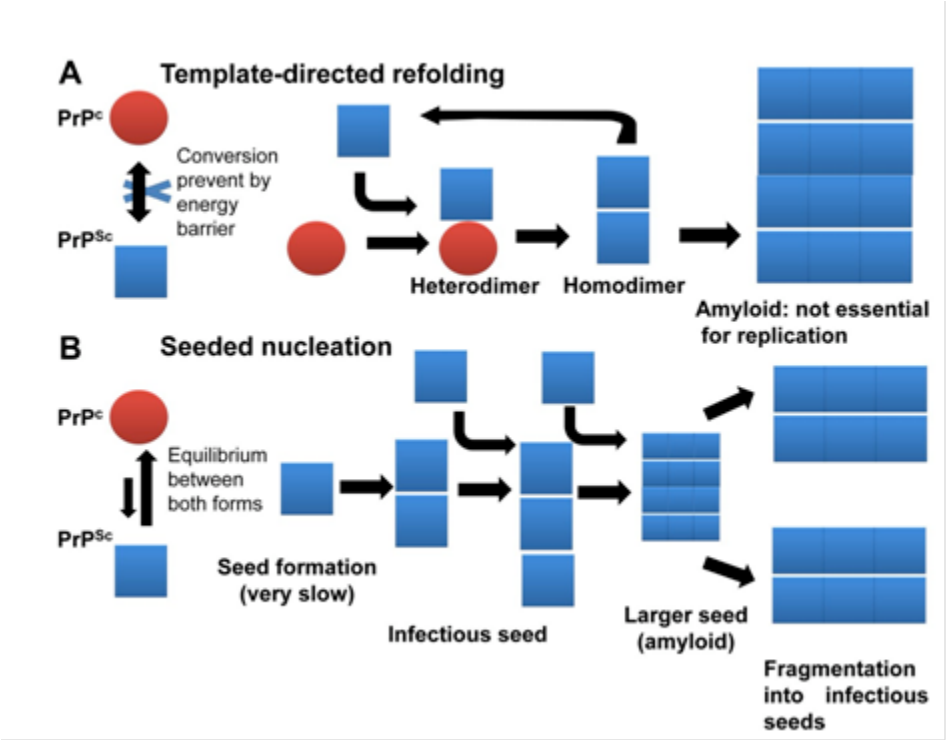

Fig. 13. Proposed models of prion replication. A: In the template-directed refolding model, PrP^{Sc} is not normally present in the brain and its spontaneous formation is impeded by a large energy barrier between PrP^{C} and PrP^{Sc}. Exogenous PrP^{Sc} recruits host PrP^{C} and templates its conversion to an additional copy of PrP^{Sc}. Amyloid formation is a byproduct of prion replication and does not figure explicitly in the mechanism. **B**: In the seeded nucleation model, an equilibrium exists in the brain between PrP^{C} and PrP^{Sc} (although the balance is shifted greatly towards PrP^{C}). The formation of a PrP^{Sc} seed occurs slowly and is favoured by the introduction of exogenous PrP^{Sc}. Once the seed has formed, recruitment of additional PrP^{Sc} occurs rapidly allowing the formation of larger amyloids. Fragmentation of amyloid into smaller pieces generates new seeds and allows prion replication to progress (Figure modify from [182]).

The first model postulates an interaction between exogenously introduced PrP^{Sc} and endogenous PrP^{C}, which is induced to transform itself into further PrP^{Sc}. A high-energy barrier may prevent spontaneous conversion of PrP^{C} and PrP^{Sc} at detectable rates [183]. This reaction may involve extensive unfolding and refolding of the protein to explain the postulated high-energy barrier and could be dependent on an enzyme or chaperone, provisionally designated as protein X [84]. In the second model, *i.e.* the nucleation model, PrP^{C} and PrP^{Sc} are in an equilibrium strongly favoring PrP^{C} [184],

[185]. Only if several monomeric PrP^{Sc} molecules are mounted into a highly ordered seed, can further monomeric PrP^{Sc} be recruited which will eventually aggregate to form amyloid assemblys. Within such a crystal-like seed, PrP^{Sc} becomes stabilized. Furthermore, fragmentation of PrP^{Sc} aggregates increase the number of nuclei, which can recruit further PrP^{Sc} molecules and thus result in apparent replication of the agent. Consistent with the latter model, cell-free conversion studies indicate that PrP^{Sc} aggregates are able to convert PrP^{C} into a protease-resistant PrP isoform [180, 186]. Moreover, this model postulates that small amounts of PrP^{Sc} are present in a healthy brain. Supporting this idea, PrP^{res} has been shown to be amplified from control healthy brain samples using the protein misfolding cyclic amplification (PMCA) procedure [187].

Synthetic mammalian prions

The most stringent criteria for judging whether prion infectivity is generated *in vitro de novo* are the bioassay in animals. Recently, it was shown that the transmissible form of prion disease could be induced in transgenic (Tg) mice that expressed PrP(89–231) at high levels (Tg9949) by inoculation with amyloid fibrils generated in vitro from MoPrP(89–230) [87]. However, these fibrils did not cause disease up-to 600 days after the inoculation into wild type mice. Most interestingly, after the first passage in Tg9949, the synthetic prions were transmitted to both Tg9949 and to wild type animals in the second passage [87].

Similar to the fibrils formed from recPrP(89–230), a chemically synthesized 55-residue peptide (residues 90 to 145) harboring a P101L mutation and refolded *in vitro* into a β-conformation was shown to induce disease in transgenic mice that express PrP(P101L) [180]. In contrast to the Tg9949 mice, the TgPrP(P101L) mice were found to develop disease spontaneously, even in the absence of the synthetic peptide [188]. On the other hand, Tg9949 mice did not develop any clinical signs of spontaneous disease, nor did they produce transmissible scrapie upon aging.

With regards to biochemical and neuropathological features, the two studies showed different findings. In the Tg9949 mice which had been inoculated with fibrils a novel strain of TSE were discovered [189]. Whereas the disease associated PrP conformer identified in TgPrP(P101L) mice and inoculated with the synthetic 55-residue peptide, the conformation of the protein was indistinguishable from that seen in the same Tg mice that developed disease spontaneously [190]. Taken together these data argue,

that the 55-residue peptide accelerated a slowly progressing, spontaneous form of the disease, whereas the fibrils of recPrP(89–230) caused prion disease *de novo*.

Perplexing though was that the incubation times observed upon inoculation of fibrillar MoPrP(89–230) were much longer than those exhibited by most known PrP^{Sc} strains. Because the length of incubation time is typically used as a measure of prion infectivity titer, this assay brought to the hasty conclusion that synthetic prions would exhibit a very low infectivity titer. However, this conclusion cannot be accepted because the infectivity of natural TSE strains has been tested only on a particular host and not all strains. Based on the knowledge of the molecular mechanism of prion conversion, Soto *et al.* developed the PMCA technology (Fig. 14), designed to mimic PrP^{Sc} autocatalytic replication *in vitro* [191]. In a cyclic manner, minute quantities of PrP^{Sc} (as little as one single particle) induce misfolding of large amounts of PrP^{C} in a process catalyzed by ultrasound waves to multiply the number of converting units. Moreover, they recently demonstrated that it is possible to produce a synthetic PrP from the PMCA and observe directly an effect in wild type mice. Whilst this finding has high importance there are technical issues to consider, such as whether another molecule besides PrP^{Sc} could have been enriched in the process of PMCA that caused the effect [192].

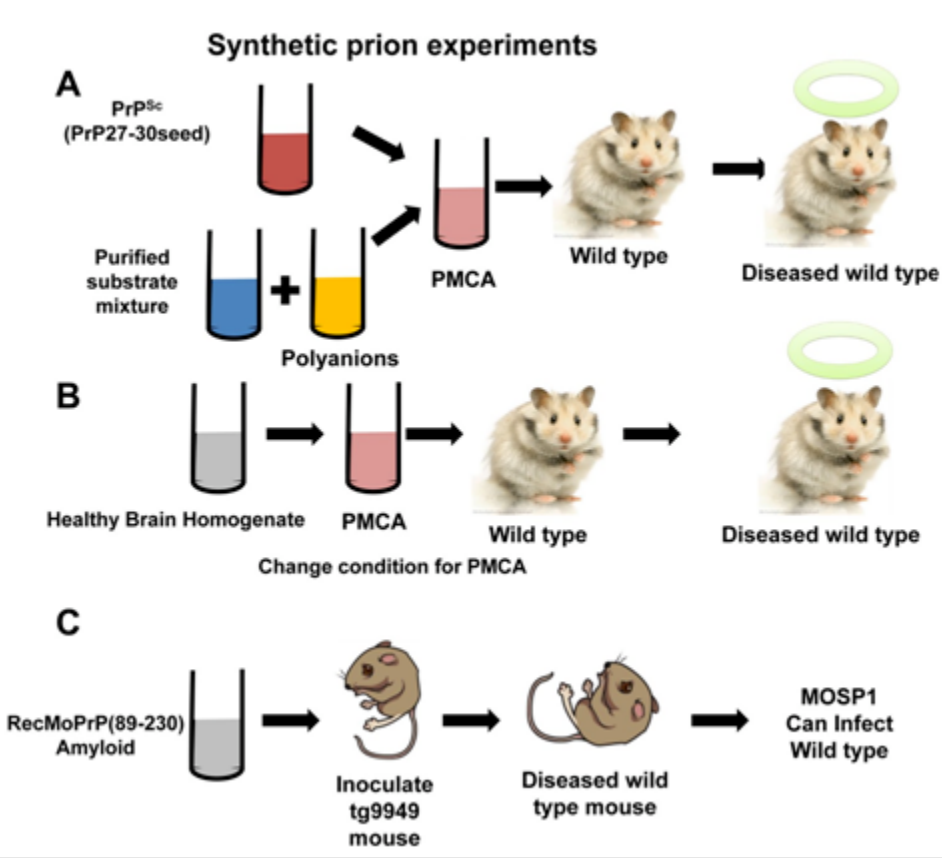

Fig. 14. Schematic representation of methodologies used to produce synthetic prions using purified substrates. A: Schematic diagram of the production of new synthetic prions using the PMCA method by serial dilution and propagation of PrP^{Sc} starting by purified PrP^{C} [193]. **B**: Schematic representation of the procedure for the production of synthetic prion without use a seeding of PrP^{Sc} with changes in the condition of PMCA for mimic sporadic condition. **C**: Schematic representation of the procedure for production of the first synthetic prion using recPrP [87].

In vitro assay for the infectivity

Conversion of PrP^{C} to PrP^{Sc} has been successfully reproduced in cell-based and animal systems in which PrP^{Sc} is propagated and prion infectivity is maintained. As mentioned in the previous section, several *in vitro* conversion assays have been introduced over the past 15 years to investigate how PrP^{C} is conformationally altered by PrP^{Sc}.

However, molecular conversion, in various cell-free systems have failed to completely reproduce the proposed prion conversion process. Although close, none of the *in vitro* systems simulate perfectly prion propagation. Conversion of PrP^{C} to PrP^{Sc} seems to be difficult in most cell-free reactions unless other molecules besides PrP isoforms are also present. The continuous evolution of *in vitro* assays mimicking the conditions of prion conversion and propagation is still under progress.

Table 1 gives a summary all currently used *in vitro* conversion assay systems.

The most recently developed system is the so-called amyloid seeding assay (ASA) developed by Colby *et al*. [194] (Table 1). The assay can detect the infectivity in biological sample. Furthermore, the assay shows that many prion strains are capable of seeding the polymerization of recPrP into amyloid, and that property of each strain can be used as a means for the detection of prions in biological samples [194].

In terms of data, the quickening of the kinetic profile indicates the presence of infective molecule. Taking into account the capabilities of this assay, it is one of the fastest and most reproducible protocols to use.

Conversion Method	Conversion Buffer	Incubation	Sonication/Agitation	PrP^{C} source	PrP^{Sc} source	Reference
Mixing	PBS with protease inhibitors	37 °C≤24 hr		Lysate of N2a cells expressin MHM2 PrP^{C}	PrP^{27-30} purified from prion-infected mouse brains	Raeber et al. 1992
Metabolic Radiolabeling	PBS with protease inhibitors	37°C≤ 24 hr	none	Lysate of ScN2a cells expressing [35S]-PrPC	Endogenous PrP^{Sc} of ScN2a cells	Raeber et al. 1992
Microsomal Membranes	20 mM Tris buffer pH 7.5	25 °C1 hr	none	[35S]-PrP^{C} synthesized by cell-free translation systems	Microsomal membranes from scrapie-infected hamster brain cells	Raeber et al. 1992
Cell-Free Conversion	0.75 M GdnHCl 130 mM NaCl 10 mM Tris-HCl pH 7.0	20°C22 hr	none	[35S]-PrPtextsuperscriptC expressed in mouse fibroblast cells	Brain-derived PrPtextsuperscriptSc treated with 2 -3 M GdnHCl for 5 h at 37°C	Kocisko et al. 1994
Cell-Lysate Conversion	50 mM Tris, pH 7.4, 150 mM NaCl, 0.5% Triton X-100, 0.5%SDS	37°C48 hr	none	Lysate of CHO cells expressing MHM2 PrP^{C}C	Brain-derived mouse PrP^{Sc}	Saborio et al.2001
PMCA	PBS with 0.05% Triton X-100, 0.05% SDS protease inhibitors	37°C10-72 hr	40 sec sonication	Normal, uninfected crude brain homogenate	Prion-infected crude brain homogenate 20 -100 fold increase of PrP^{Sc}	Castilla ey al. 2006
PMCA under non-denaturing conditions	PBS with 1% Triton-X 100, 0.5 mM EDTA	37°C16-48 hr	Continuous agitation, 800 rpm	Purified brain -derived PrP ^{C}C	PrP27-30	Lucassen et al.2003
rPrP-PMCA	PBS with 0.05-0.1% SDS, 0.05-0.1% Triton X-100	v37°C24 hr	40 sec sonication	recPrPC expressed in E.coli	vPurified PrP^{Sc} or crude homogenate of prion-infected brains	Atarashi et al 2007
QUIC	PBS with 0.05% SDS, 0.05% Triton X-100	45°C46 hr	10 sec agitation, every 2 min	recPrP^{C} expressed in E.coli	Prion-infected crude brain homogenate	Atarashi et al. 2008
AutocatalyConversionAssay	β-oligomer sequentialdilution with 5 M urea, 2mM NaOAc,0.2 M NaCpH 3.7, and with 1 M ure20 mM NaOAc, 0.2 M NaCl, pH 5.5	20°C16 hr	recPrP^{C} expressed in E.coli	none	none	Baskakov et al. 2002
AutocatalyConversionAssay	see above	37°C10-72 hr	Continuous agitation, 600-900rpm	recPrP^{C} expressed in E.coli	none	Baskakov et al. 2004
ASA (Amyloid Seeding Assay)	PBS 0.4 M GdnHCl	37°C24-48 hr	continuos agitation 600 rpm	recPrP^{C} expressed in E.coli	none	Colby et al. 2008

Table1. Summary of in vitro conversion assay develop in prion field.

Current structural models for PrP^{Sc}

As the structure of PrP^{Sc} is still elusive because of its insoluble nature and because is inaccessible to conventional methods of protein structural biology, such as NMR spectroscopy or X-ray crystallography, alternative combination of methodologies have been utilized to produce structural data. In 2002, Wille *et al.* used electron microscopy in combination with computational imaging and modeling methods, to study the structure of two-dimensional crystals of PrP27-30, and produce from the reconstructed images, a model showing that the repetitive unit of the crystals had hexagonal symmetry [195]. Assuming PrP^{Sc} has a similar structure to currently known proteins, the authors suggested that the hexagonal symmetry came from a trimeric structure, and proposed a "left handed β–helical model," as shown in Fig. 15 [196].

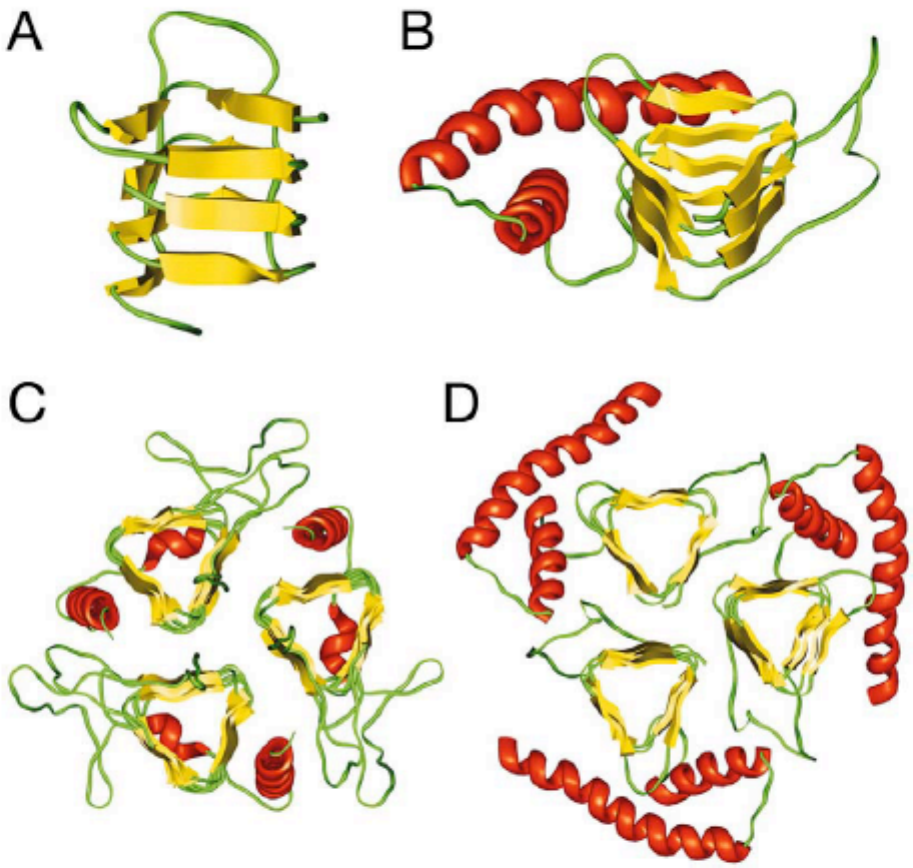

Fig. 15. Model of PrP^{Sc}. Left handed β–helical model [196] **A**: The -helical model of the N-terminal part of PrP 27–30 **B**: Model of the monomer of PrP 27–30. The -helical region (residues 177–227) as determined by NMR spectroscopy (PDB ID code 1QM0 [PDB]) was linked to the -helical model shown in A. **C**: The crystal structure of the trimeric carbonic anhydrase from Methanosarcina thermophila (PDB ID code 1THJ [PDB]). **D**: Trimeric model of PrP 27–30 built by superimposing three monomeric models onto the coordinates of the C 's of the 1THJ [PDB] structure.

In their model, the N-terminus of each monomeric subunit (residues 89-175) forms left-handed β-helices in the core part of the trimer, whereas the C-terminus (residues 176-227) largely preserves the disulfide-linked α helices at the outer part with the glycosyl groups pointing away from the center. The structures proposed are highly regular and repetitive, and symmetrical fold formed by the coiling of elongated β–sheets into helical 'rungs'. Left-handed β-helices are stacks of triangular rungs that typically incorporate 18 residues per rung. This model is derived directly from the experimental electron crystallography data, which clearly show the circular-elliptical form. DeMarco and Daggett utilized molecular dynamics to simulate PrP conversion, which resulted in another theoretical model being proposed, the "spiral model", as shown in Fig. 16 [197].

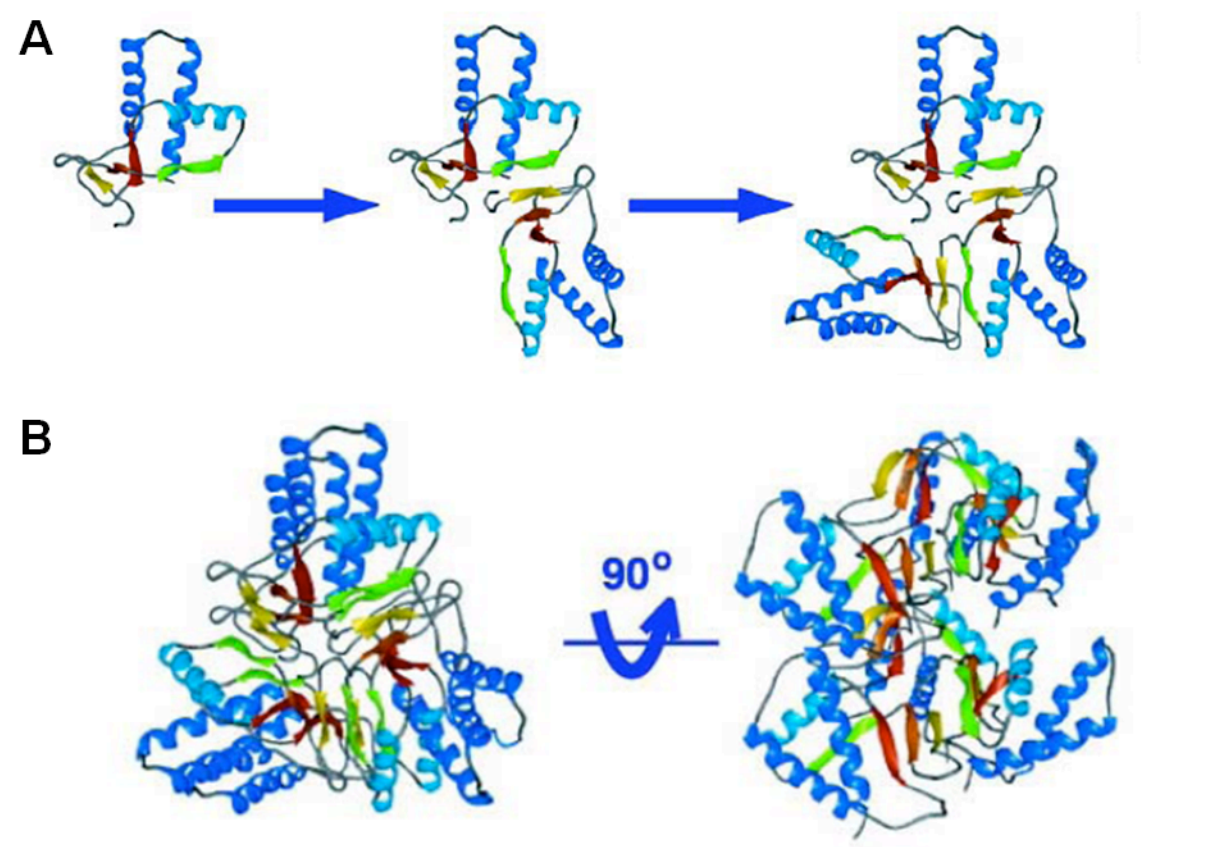

Fig. 16. The spiral model A: Building of a protofibril with 3_1 axis (viewed down the fiber axis). The oligomerization site occurs between the isolated strand and a three-stranded sheet of the adjacent monomer. **B**: Views of hexameric representation of protofibril showing maintenance of symmetry on oligomerization and propagation of the extended strands between monomers to form extended sheets (from [197]).

In this model, each monomeric subunit in PrP^{Sc} preserves all three α-helices, but has increased β-sheet content in the 116-164 region, consisting of a three-stranded sheet and one isolated strand. During polymerization, each isolated strand is connected with the adjacent monomer's three-stranded sheet to form a continuous four-stranded sheet, which leads to a spiraling protofibril. This model was developed targeting the dimension

of a small aggregate studied by EM. The minimum and maximum diameters, excluding glycans of the spiral model are 58 Â [195].

In 1994, Reed Wickner proposed that two non-Mendelian genetic elements of yeast *Saccharomyces cerevisiae*, [PSI+] and [URE3], were also caused by a self-propagating conformational conversion of protein [198], which extended the prion concept from the infectious agent of TSEs to heritable elements in yeast. To date, six prions in yeast and other fungi have been identified [199]. Although fungal prions do not share amino acid sequence identity with mammalian PrP, these fungal proteins display prion-like mechanisms of propagation. The aggregation of soluble fungal prion proteins into amyloid fibrils changes the phenotype of cells, and these characteristics can be cytoplasmically transferred from mother to daughter cell, showing that the altered phenotype is heritable. Studies on these fungal prions have been proven extremely valuable [200]. For example, one of the best-studied fungal prion, the translation termination factor Sup35p, can aggregate into distinct forms of amyloid fibrils *in vitro* under different experimental conditions [201]. Infection of normal yeast cells with these distinct amyloid fibrils was found to generate different [PSI+] strains, providing an opportunity to understand the molecular basis of this phenomenon [202].

HET-s is the prion of the yeast *Podospora anserina* and is involved in heterokaryon incompatibility, a mechanism that controls vegetative cell fusion [203]. Up until recently, the only known high-resolution amyloid fibril structure has been obtained by magic-angle spinning (MAS) NMR spectroscopy on fibrils formed by the prion domain of HET-s consisting of the C-terminal residues 218-289 [204, 205].

An earlier study, proposed that the β-strand regions were derived from proton-deuterium exchange experiments and solid state MAS NMR chemical shifts [206]. In contrast to other MAS NMR studies of amyloid fibrils, the observed lines are very narrow. Interestingly, in CP-MAS spectra only 43 of the 78 residues were detected [207, 208]. Most of the missing residues were, however, observed using proton detection and solution NMR techniques, indicating a high mobility in some parts of the protein [207]. In addition, the observed chemical shifts suggest a random coil conformation of these residues which comprise the N and C-terminus of the protein and residues in the loop regions.

Now, high resolution structures for HET-s(218-289) have been presented [205]. The monomeric unit forms eight short β-strands. Six of them are arranged in a manner similar to a left-handed β-helix or β-solenoid with two coils per monomeric unit, Fig. 17. Thereby, the β-strands incorporated in the same β-sheet are pseudo repeats of each other. Between strands three and four a long loop region, not incorporated in the fibril core, is observed.

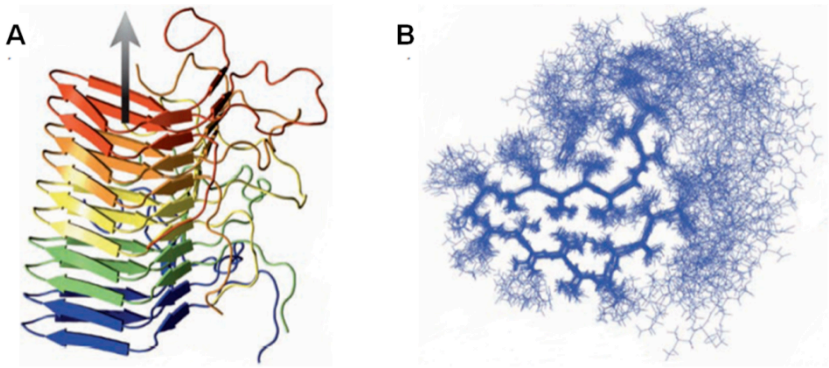

Fig. 17. Representations of the high resolution MAS NMR structure of HET-s(218-289). A: backbone fold of five monomeric units, the single monomeric units are shown in different colours, **B**: structural ensemble of a monomeric unit. From [205].

Aim of this work

Despite considerable research efforts, the mechanism by which the PrP converts into the pathological abnormal form remains enigmatic. Whilst people have begun to show that is it possible to produce the infectious molecule in the test tube no clear evidence exists for the structure of this molecule. Solubility problems and the reproducibility of the preparation of the fibers are still outstanting problems.

The major aim of this study has involved a systematic analysis of the different conditions under which fibrils can be formed, with the ultimate aim to produce a reproducible protocol to use for biochemical and biophysical studies.

As a starting point, my project commenced, using other proteins; α-synuclein, β protein, insulin, in order to learn the commonalities of the methodologies to produce fibers and further improve the approach and understanding of aggregation studies, in particular to that of PrP.

For the production of fibrils from the PrP, I have analyzed in great details the effects of changes in the environmental conditions on the morphology of the fibrils, with particular attention to the conditions, which appear to aid in demonstrating the presence of an infective molecule.

Chapter 3: Materials and Methods

Preparation of recPrP

The recMoPrP(89-230) was a kind gift of the Prusiner laboratory, University of California at San Francisco, San Francisco, USA [163].

Monitoring of the kinetics of *in vitro* amyloid formation

To monitor the formation of amyloid fibrils in our samples, lyophilized recMoPrP(89-230) was initially dissolved in 6 M GndHCl, to a protein concentration of 1-5 mg/mL. The aliquots were kept frozen at -80°C until used. Upon use, the stock protein solution was made to a final protein concentration of 50 µg/mL. This was then incubated in 1X PBS buffer pH 7, 10 µM thioflavin T (ThT) with different concentrations of guanidinium hydrochloride (GdnHCl) (0.4 M to 4 M) in a reaction volume of 200 µL in 96-well plates (BD Falcon 353945, BD Bioscience).

For the seeding experiments, which were performed to provide information as regards to the autocatalytic nature of the reaction, small amounts of preformed aggregates were added to the reaction mixture at t=0. To each well, 4 µL of the seeding sample was added to the 200 µL reaction. To the seeding experiments, a glass bead was also added to each well, to increase the production of the kinetic profile. The 96-well plate was covered with sealing tape (Perkin Elmer) and incubated at 37°C with continuous shaking on a plate reader (Spectramax M5 and Gemini EM, Molecular device). The kinetic of fibril formation was monitored by top reading of the fluorescence intensity

every 5 min, using 444 nm excitation and 485 nm emission filters. Each sample was measured in six independent replicates and the differences were evaluated using statistic programs R software. Data were assessed using different methodologies: one was based on [209], the other was based on a qualitative evaluation. The analysis was performed using a R program to verify any statistical differences (See Appendix for mathematical approach).

Dynamic Light Scattering

Dynamic light scattering (DLS) was used to analyse the homogeneity of the fibril formation. To this aim a dynamic light scattering with DLS Zeta sizer Nano zs Malvern (Dispersion Technology Software) was used. After the fibrillization reaction, samples were analysed after dialysis with phosphate buffer. The analysis was performed at the same concentration of the protein, and verified by calculations using the extinction coefficient.

Phosphotungstic acid (PTA) precipitation of PrP^{Sc} from ScGT1 cell lysates

GT1 and ScGT1 cells were grown in DMEM containing 10% fetal bovine serum and 1% penicillin/streptomycin at *37°C* and 5% CO2. Cells were split 1:10, incubated for 7 days and then disrupted using lysis buffer (10 mM Tris HCl pH 8, 150 mM NaCl, 0.5 % NP-40, 0.5 % DOC). Typically, total protein concentration of 1 mg/mL was used for the PTA protocol as described by Colby *et al.* 2008. PTA from a 10% (wt/vol) stock solution (pH

7.4) was added to the sample to a final concentration of 0.5%. Then, it was incubated the sample with constant shaking (350 rpm) for 1 h at 37°C. After incubation, samples were centrifuged at 14,000 g for 30 min at room temperature (RT). The pellet were washed with 500 µL of PBS/2% sarkosyl, containing protease inhibitors, and centrifuged at 14,000 × g for 30 min at RT. The pellet was resuspended in 150 µL of water and then stored it at −80°C until use.

Amyloid Seeding Assay (ASA)

Briefly, total cells extracted in sarkosyl were precipitated with PTA to purify prions. Four µL of PTA purified brain cell extracted were diluted into 400 µL water, then used as seeds in amyloid formation reactions. A 96-well plate was prepared with 180 µL/well of MoPrP(89-230) solution (50 µg/mL recMoPrP(89–230), 0.4 M GdnHCl, 1X̣PBS, 10 µM ThT). Twenty µL of diluted PTA-precipitated brain homogenate were added to each well, with each sample tested with six replicates. ThT fluorescence measurements were taken at 444/485 nm excitation/emission spectra on a Spectramax M5 fluorescence plate reader with continuous shaking at 37°C.

Atomic Force Microscopy (AFM)

MoPrP(89-230) solutions prepared with different GdnHCl molarities were deposited evenly onto a freshly cleaved piece of mica at a concentration of 50 µg/mL, and left to adhere for 1-10 mins. Samples were then washed with distilled water and dried with N_2. Specimen were imaged with a NanoWizard-II BioAFM (JPK Instruments AG, Berlin,

Germany, www.jpk.com) operating in dynamic mode and using non-contact cantilevers (NSG11, NT-MDT – Moscow, Russia, www.ntmdt.com or ARROW-NCR, NanoWorld-Neuchâtel, Switzerland, www.nanoworld.com) with tip radii of <7-10 nm, spring constants of 20-42 N/m, and resonance frequencies of 285-325 kHz.

The images were acquired at line scan rates of 0.5-1 Hz at RT.

The images were analyzed using Gwyddion software (http://gwyddion.net/), which extracts data from the scanned images and evaluates the statistical value of the image. All data was analysed with the R program (http://www.r-project.org/).

Circular dichroism of MoPrP(89-230) at different concentrations of GdnHCl

Circular dichroism (CD) spectra were obtained with a JASCO J-810 spectrometer at 20°C in 20 mM Na-Phosphate pH 7. Far-UV CD spectra (208-250 nm) were recorded at protein concentrations of 0.2 mg/mL in a 0.1 cm cell, with an average of 6 accumulated scans, and at varying GdnHCl concentrations.

Chapter 4: Results

The kinetics and the products from *in vitro* fibril formation assay are affected by the concentration of the denaturant used

In order to gain insight into the physical properties that separate infectious from noninfectious MoPrP(89-230) fibrils, the kinetics of fibril formation was analyzed in greater detail. It is known that the addition of GdnHCl improves the yield and shortens the lag phase of fibril formation, but is also influential in physical properties of the fibrils [210]. Toward this aim, different concentrations of GdnHCl were employed in the fibrilization assay

Previous studies have shown that in an attempt to generate the infectious PrP forms, different strategies have been pursued. There is the PrP^{Sc}-dependent conversion or amplification [211] [180], [191] and the conversion of PrP^{C} or recPrP in the absence of a PrP^{Sc} template [212] [172] [170] [173] approach. Moreover, these topics have been analyzed in several review papers [213] [212].

An alternative approach has more parallels with the sporadic formation of prions, rather than with prion diseases acquired through transmission. In opposition to the amplification approach, where the physical properties of the newly generated PrP^{Sc} are expected to mimic that of PrP^{Sc} seeds, the conversion reaction in the absence of PrP^{Sc} seeds poses question as regards to the uncertainty with regarding the conformation of the final products of the reaction.

By analogy to the studies where the amyloid form has been shown to be equivalent to a prion state for several yeast prions [202, 214] and [202, 214-217], converting recPrP into amyloid fibrils seems to be one of the possible ways for *de novo* generation of mammalian prion infectivity *in vitro*. For the last few years several protocols for producing fibrils from recPrP or PrP^C have been developed by different groups. In contrast to yeast prions in which the amyloidogenic regions are natively unfolded, the domain associated with mammalian prion infectivity is partially structured and thermodynamically stable [169]. Due to the fact that chemical denaturants and elevated temperatures are the most common way of manipulating the dynamic balance between different unfolding intermediate states, it is not surprising that the first experimental protocols for producing amyloid fibrils from the structured Mo(PrP90–231) utilized partially denaturing conditions such as chemical denaturants [170], [218], [166], [25], [219] and [220] or combinations of elevated temperature and high pressure [176].

Amyloid formation can be monitored in solution using the dye ThT [152]. This dye undergoes a fluorescence shift upon binding to amyloid fibers, from 342 to 442 nm and from 430 to 482 nm for excitation and emission maxima, respectively. As ThT does not fluoresce significantly at excitation/emission maxima of 442/482 nm in the absence of amyloid fibers, the background signal tends to be quite low, and hence the dye is used as highly sensitive reporter. When used in conjunction with multi-well plates and automated plate readers that record fluorescence over time, ThT offers ideal solution, of detecting conformational changes of proteins in solution.

In order to get acquainted with the process of formation of fibrils I started to investigate the protocol to form fibrils. There are at least two main different ways to produce fibrils using either (a) discontinuous assay or (b) continuous assay (Fig. 18).

The first procedure is base on the fact the fibrils are made in a pure condition, with the kinetic profile of ThT obtained in a discontinuous time. The kinetic profile is obtained by numerous readings of the sample at different time points. However, this type of analysis gives problems in the reproducibility of kinetic profile, and also depends upon the number of time points read and the operator ability. Moreover, the total protein levels change during the procedure, thus possibly altering the true kinetic reading.

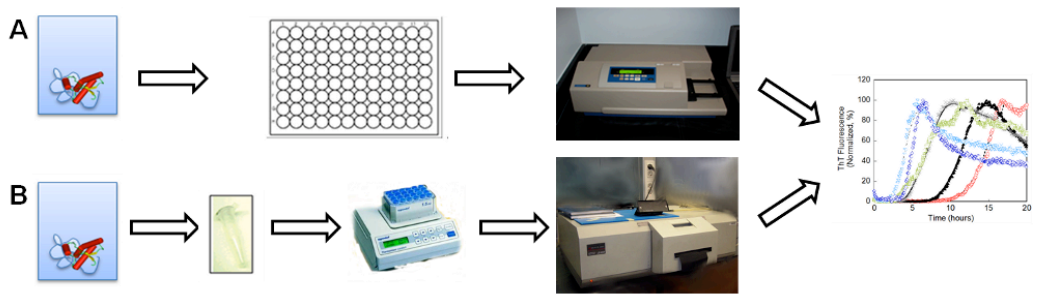

Fig. 18. Schematic production of fibrils. A: Method for preparing fibrils in a continuous assay. Protein is : incubated with the presence of ThT at 37 °C with agitation of 600 rpm. **B:** Method for preparing fibrils in a discontinous assay. Protein dissolved in particular protein concentration and buffer condition and incubatde at 37°C without the presence of the ThT molecule. Aliquots of the solution are taken and read on a fluorimeter in the presence of ThT.

The continuous assay first appeared in the literature authored by the laboratory of Ilia Baskakov, where they demonstrated the possibility of obtaining a kinetic profile, using a plate of 96-well in a plate reader, using a continuous reading without alternating sample readings [174].

The results obtained using this procedure gave reliable results. The protein chosen for that primary purpose was insulin. I performed fibril formation using a simple protocol giving intriguing results. Then we use the discontinuous assay using MoPrP(89-230) in 1X PBS/2 M GdnHCl pH 7. This protocol is a standard protocol for preparing fibrils for many researchs [174, 221]. The kinetic results obtained are summarizes in the Fig. 19.

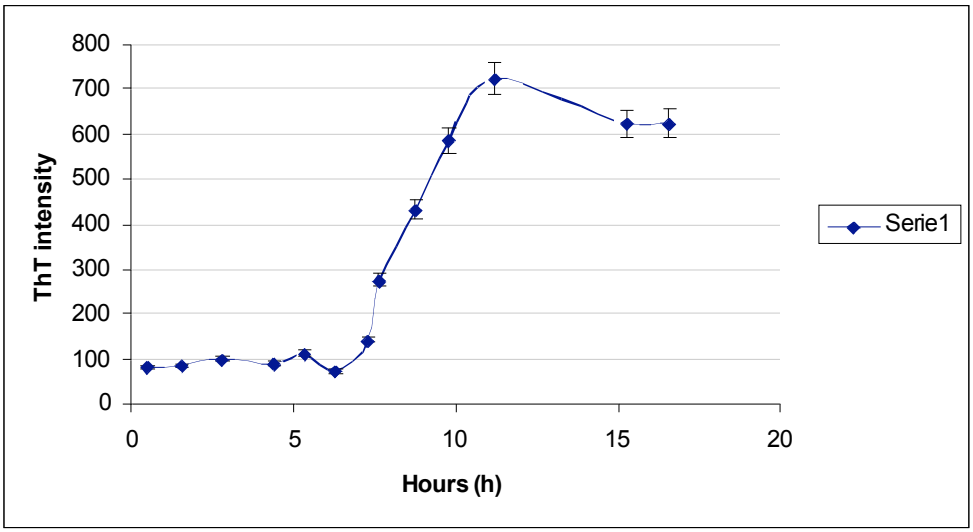

Fig 19. Kinetic profile of MoPrP(89-230) incubated at 37°C with 600 rpm. Here I report time course of MoPrP(90-230) conversion in the presence of 2 M GdnHCl. The reaction was monitored by ThT fluorescence readings.

It was observed difference in the rate of fibrilization using both procedure. The lag-phase starts either at 9-10 hours or at 40 hours or more. For a practically point of view for more experiments we use a continuous assay because allow to follow all process without interruption. Another important factor of the use of continuous assay is that the concentration of the protein in the test tube remains constant throughout the reaction.

However, the procedure employed in a discontinuous assay has been generally used in many paper. Due to the fact the continuous protocol gives better resolution for the

reproducibility of fibril formation. The presence of glass beads inside the well plate helps to obtain a quite reproducible kinetic profile.

The reaction is characterized by a well-defined lag phase followed by a growth phase, consistent with a nucleation dependent polymerization mechanism. Moreover, the conversion seems to be possible even in the presence of high denaturant concentrations, conditions under which the protein is fully unfolded. I have performed a series of kinetic experiments in which an array of different growth condition were employed. The conversion was studied under different experimental conditions and special attention was focused on the influence of denaturants on the conversion mechanism and the morphology of the conversion products. The experiments were performed under vigorous shaking conditions at pH 7, and 37°C. The typical fibril formation process starts with a lag phase in which the amount of amyloid proteins turned into of fibrils is not significant enough to be detected. Afterwards, a drastic elongation phase follows and fibril concentration increase rapidly (see figure below).

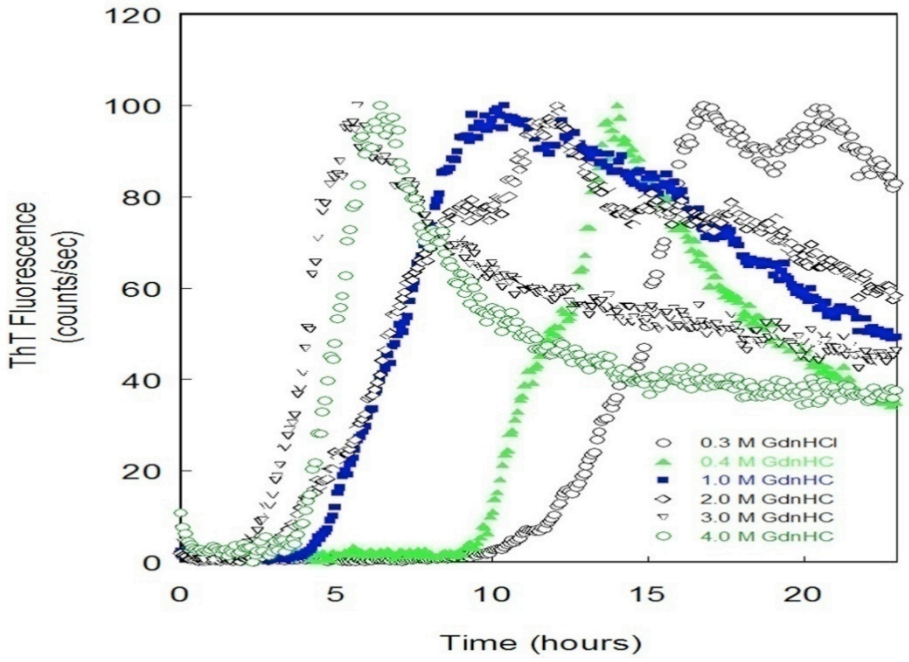

Fig. 20. Kinetic profiles of fibril formation in 96-well by continuous assay. Example of the kinetic profile made by change the concentration of guanidine inside the growth condition. From the right to the left it was possible to observed the decrease of the lag phase.

Low concentration of GdnHCl in solution gives a relative long lag-phase in contrast to high concentration of that denaturant. Above 1M of GdnHCl It was obtained quite the same lag-phase (Fig. 20). These results is in agreement what was found by other authors but contradicts what some author believe that high concentration of GdnHCl increase the lag-phase time [166].

The kinetic data profiles were analyzed using a mathematical approach for calculate the lag-phase value (see Appendix I: Mathematical approach).

Due to the fact recently demonstrated that it is possible to amplify many different prion strains by using a particular concentration of GdnHCl I wanted to analyze in detail the effect of different concentration to the fibril formation. The results support the fact of the reliability of the continuous assay and the *in vitro* approach.

The studies were focused only on two concentrations of denaturant: 2 M GdnHCl and 0.4 M GdnHCl. The first concentration of GdnHCl was already used in many publications by other authors, which gave good results in terms of fibril formation. The second concentration was chosen because this particular concentration gave a read out of the infectivity. Thus, these concentrations were used in discontinuous growth condition [222], [65], [174].

The kinetic profiles extracted by these two concentrations follow the same sigmoidal kinetic curve typical of an aggregation of the protein, which was clearly different between the two preparations (Fig. 21). This kinetic difference was observed in all experimental assay runs.

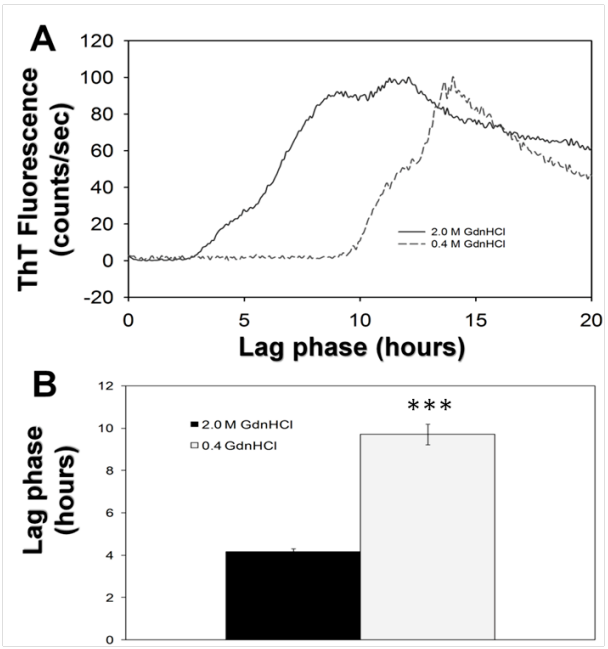

Fig. 21. A: Time course of MoPrP(89-230) conversion in the presence of 2 M GdnHCl (solid line) and 0.4 M GdnHCl (dotted line). The curves results are shown as mean of different kinetic curves. **B**: Mean value of the lag-phase for the two different solvent conditions (2 M and 0.4 M GdnHCl) as calculated using the equation of quadratic and exponential functions Bishop-Ferrone [209]. Bars denote the standard error (n=6; *, p <0.01; **, p<0.05; ***, p< 0.001).

It was observed that the mean lag phase of 2 M GdnHCl condition gave a fast kinetic profile than 0.4 M GdnHCl. ANOVAs analysis shows statistically significant difference each growth condition ($p < 0.001$).

Using different estimation protocol we obtain the same ratio of difference between growth conditions as reported in Table 2 below.

Concentration of GdnHCl	Bishop and Ferrone [209]	Cohlberg et al. [223]	Qualitatively
2 M GdnHCl (n=106)	4.155±0.166	5.22±0.160	4.67±0.160
0.4 M GdnHCl (n=68)	9.72±0.487	10.8±0.495	12.11±0.523

Table 2. Lag-phase values estimated using a script in R program as describe AppendixI:Mathematical approach.

In addition the maximum ThT fluorescence intensities also showed differences between the two preparations. The preparation using 2 M GdnHCl appeared to show a trimodal probability density distribution. In contrast, the preparation with 0.4 M GdnHCl revealed a different probability density distribution (data not shown). With this preparation the probability of the maximum intensity of ThT signal was higher in the lower signal intensities compared to what was found with the 2 M GdnHCl preparation (Fig. 22).

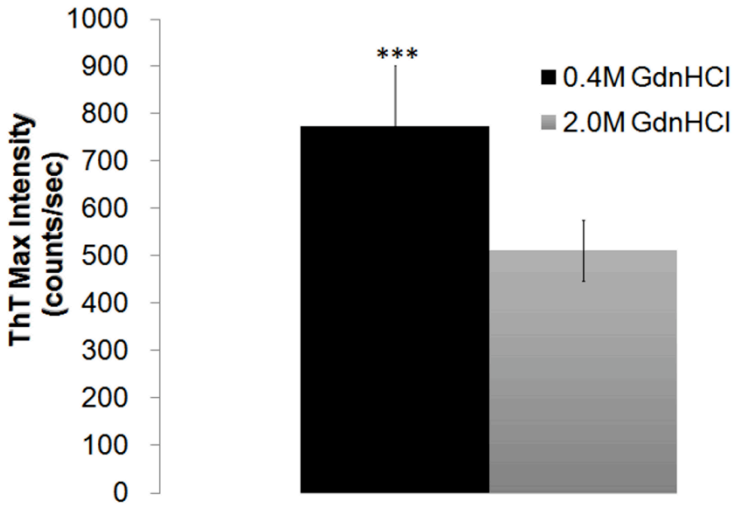

Fig. 22. Mean value of ThT max Intensity in two different solvent conditions(2 M and 0.4 M GdnHCl) as calculated from data before normalization by script run R programs (http://www.r-project.org/).

Furthermore, in the 2 M GdnHCl preparation, a non zero probability density at the higher signal levels was present, which was different from that of 0.4 M GdnHCl. These results suggest that the mechanism, which we used to detect the aggregation process, reveals a different mechanism of fluorescence in terms of intensity between the growth conditions (data not shown).

Changing the concentration of GdnHCl from 2 to 0.4 M revealed an extension of the lag phase (Fig. 21B). This difference in the kinetic trace and the maximum intensity frequency (Fig. 22) was also showed by the differences in the morphology of the aggregates as revealed by AFM (Fig. 26 A-B).

Kinetics of fibril formation is accelerated by seeding

MoPrP(89–230) formed amyloid in the presence of low concentrations of GdnHCl, as measured by ThT fluorescence (Fig. 22). When preformed fibers of MoPrP(89–230) were added to the reaction, amyloid formed much more rapidly. This phenomenon is defined seeding effect. The presence of seeds in an amyloid formation reaction was quantitatively detected either by observing a decrease in the mean lag phase of the reaction compared to control samples, or by observing an increase in the mean ThT signal during the period before negative control samples began to polymerize.

During our analysis of both conditions, we additionally tried to analyze the effects of seeding using different solvent condition. I tested the effect of cross seeding in both solvent conditions and observed a general universal effect of seeding as in agreement with many studies [224], [184], [90], but our data cast light on some differences related to the reaction rate. Homo-seeding was more efficient than the cross seeding in both protocols, which is in agreement with previous studies using full length prion protein for the preparation [210]. In the 0.4 M GdnHCl preparation, fibrils made in 2 M GdnHCl condition had only a small seeding effect although they showed a high effect of seeding in 2 M of GdnHCl (Fig. 23).

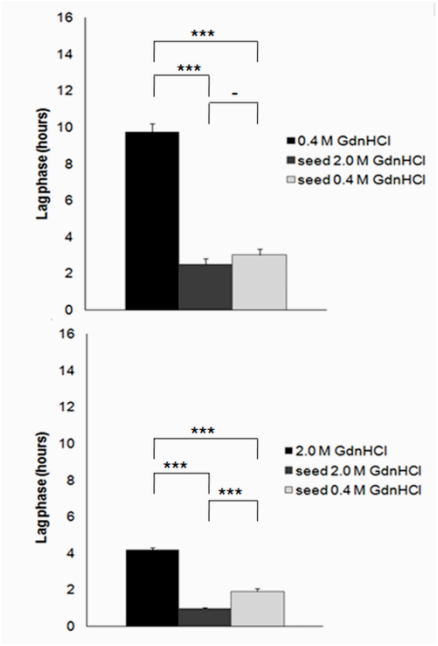

Fig. 23. Effect of seeding of MoPrP(89.230). A: Change in lag phase mean values after seeding 0.4 M GdnHCl. **B**: Change in lag phase mean values after seeding in 2 M.

Seeding effect was seen in all samples. The seeding effect of homogeneous solution in both cases resulted in a decrease of the lag phase (Fig. 23). This was a more apparent decrease for the 0.4 M GdnHCl preparation and more efficient compared to 2 M GdnHCl suggesting that the length of the lag phase could be a key for detecting different prion strains. Probably for this reason 0.4 M GdnHCl was chose as base on the Colby *et al.* protocol.

Atomic force microscopy analysis of end products

The atomic force microscope (AFM) or scanning force microscope (SFM) are very high-resolution type of scanning probe microscopies, with demonstrated resolution of fractions of a nanometer, more than 1000 times better than the optical diffraction limit. The AFM has several advantages: unlike the electron microscope, which provides a two-dimensional projection or a two-dimensional image of a sample, the AFM provides a true three-dimensional surface profile. Additionally, samples viewed by AFM do not require any special treatments (such as metal/carbon coatings) that would irreversibly change or damage the sample. Disadvantages of AFM are the image size and an incorrect choice of tip can lead to image artifacts.

To gain further insight into the structures of the aggregate products in both preparations, we studied their topology using AFM in ambient conditions. The preparations were viewed at the end-point of growth using recombinant MoPrP(89-230) synthesis *in vitro* for both aggregation conditions and revealed different substructure data. Furthermore, Imaging of the samples confirmed that highly polymorphic fibrils form in a single growth condition as described in the literature [225].

The MoPrP(89-230) incubate at 2 M GdnHCl by discontinuous assay was analyzed by AFM show fibril formation. In the first time it was observed a low yield but after improve the manual ability increase the yield of fibrils aggregates.

The scanning was performed in different substrate like mica, glass and silica surface. What was evident the mica is a system more rapidly for analysis the fibrils in AFM as described by Anderson *et al.* [226].

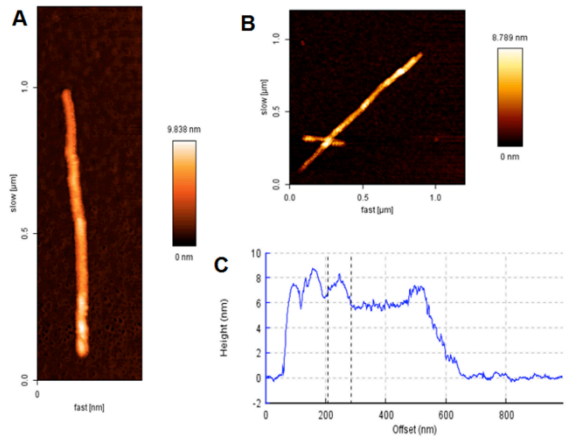

Fig. 24. MoPrP(89-230) fibril preparation in discontinuous assay. A: Topography of the fibrils. B: Topography of one fibrils were was perform the height profile reported in C. C: Distribution of height long x axes of one fibril.

In Fig 24 A and B, AFM scans of mica surfaces prepared in discontinuous protocol gave a typical fibril morphology. Comparison of the data obtained by our readings with the other author they approach these problems, shows the same polymorphic structure [226]. The length of the fibrils made by discontinuous assay was up to 2 μm.

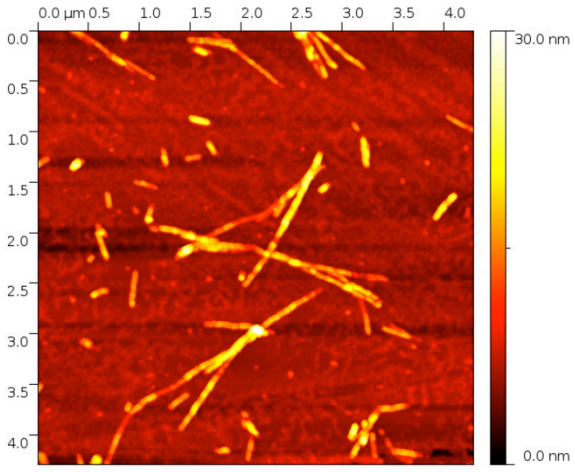

Fig. 25. AFM scan topographical images of PrP deposited mica surfaces made by discontinuous assay. 5x5 µm area was scan acquired by AFM (1024x207 pixel).

Due to the fact we want to characterize the structure of different growth condition we perform many scanning in the sample prepared in the two growth conditions.

The kinetic profile clearly shows difference between two growth conditions. In fact the kinetic profile have a different rate but also the intensity of ThT is different. These differences are due to a different assembly of the aggregates as show by analysis of the AFM scans.

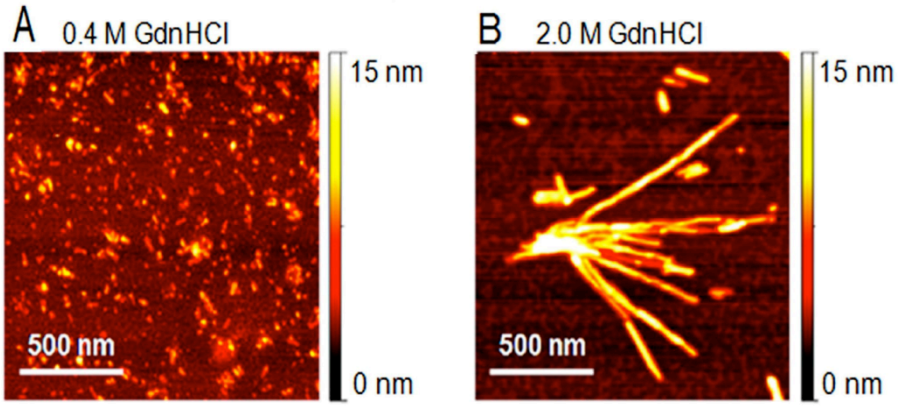

Fig. 26. AFM imaging was performed at the end of the fibrillation reactions. The reaction was formed in two solvent conditions 0.4 M GdnHCl (A) and 2 M GdnHCl (B). Scale bars represent 500 nm as depicted.

In Fig. 26 A and B, AFM scans of mica surfaces prepared with these solutions clearly revealed differences in the two growth conditions of the preparations. The solution with the concentration of0.4 M GdnHCl contained a few nanometer sized, mostly globular, aggregates of the protein in addition to a small number of short fibril fragments with less than 100 nm length. In contrast, the high concentration of denaturant (2 M GdnHCl) solution showed long amyloid fibrils of the protein in addition to a few smaller fibril fragments. Preparation with 2 M GdnHCl resulted in the formation of fully mature fibrils.

The major fibrillar subtypes were either straight or slightly curvy ribbons or rod-shape fibrils, which is in agreement with earlier studies using the same concentration of chaotropic agent, but in a different buffer solutions (Fig. 26F A-B).

The distribution of fibril height in the profiles from both preparations gave differing results (Fig. 27 A-B). The deconvolved line profiles from the blind estimated tip shape

suggested an approximate 5 nm FWHM width of the fibril (data not shown). AFM cannot provide a high precision results about the width of the fibrils because of an effect know as tip convolution. The AFM tip radi are usually about 5-6 times wider than the fibrillar structures.

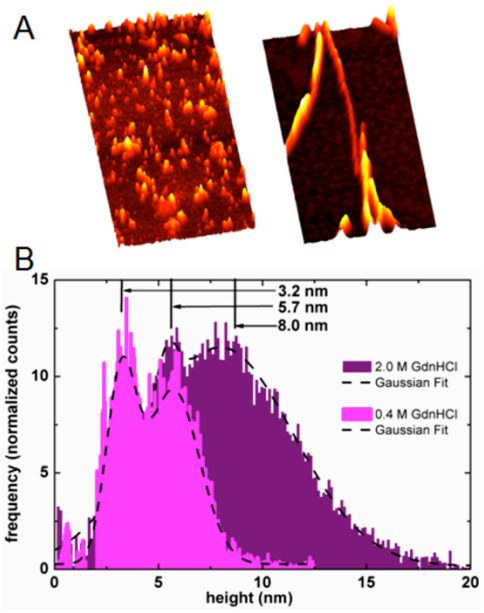

Fig. 27. A 3D representations of the AFM topography images as in Fig. 26. B: Height distribution data obtained from the AFM images in part A. An exponential curve for the low topographical structures was subtracted from the data. The frequency peaks at the levels of 3.2 nm, 5.7 nm and 8 nm are marked by arrows, suggesting an approximate 2.7 nm periodicity in height. The 3-D views revealed structures with different topology (Fig. 27 A-B). Moreover, the frequency peaks height distribution obtained from the Gaussian fits indicated the differences.

The preparation of 2 M GdnHCl gave a peak of the height at 5.7 nm and 8 nm whereas the preparation with 0.4 M GdnHCl revealed peak height levels at 3.2 nm and 5.7 nm. The height distribution associated with 5.7 nm is the common height peak found in the two preparations, and is probably due to the formation of some protofibrillar structures.

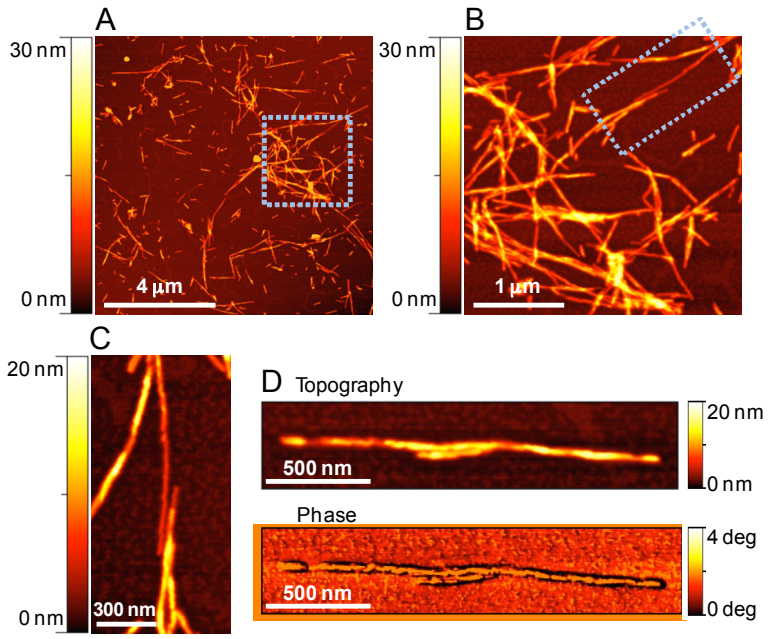

Fig. 28. A: 10 mm × 10 mm AFM topographical image of PrP deposited mica surface prepared with 2 M GdnHCl. **B**: A 3 mm × 3 mm higher resolution scan image belonging to the area marked with a blue dashed square in part A. **C**: A 0.75 mm × 1.5 mm higher resolution scan image belonging to the area marked with a blue dashed square in part B. **D**: Topography and phase images of an amyloid fibril acquired by AFM.

The length of the fibrils obtained with 2 M GdnHCl could be as long as 1800 nm and were composed of straight ribbon-like fibrils, curvy fibrils, and fibrils with occasional branching (Fig. 28 A-C). Moreover, the acquired phase image of an amyloid fibril as seen in Fig. 28D illustrated that protofilaments were formed with different fragment lengths.

Detailed analysis of the fragment size is 0.0859±0.00519 μm length. However the dimension is not always the same there is a variation.

In Fig. 29 show different profile shape for both condition: 2 M show a profile typical in fibrils while the 0.4 M GdnHCl gave typical dimension of spherical shape with a height not more than 5 nm. At the low molarity (0.4 M GdnHCl) preparation, clusters of aggregates ~5-6 nm height were seen. In contrast, the 2 M GdnHCl preparations, as revealed from the profiles “steps”, featured the height profiles ranging between 3 nm to 15 nm (measured from the 2 nm baseline) with approximately 4 nm unit height steps (Fig. 29).The detail in the branching and fragment formation was observed as shown in Fig. 30.

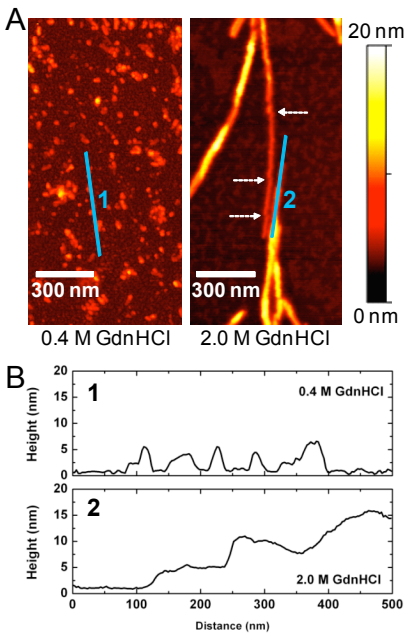

Fig. 29. A: AFM scan topographical images of PrP deposited mica surfaces. The PrP is prepared with 0.4 M GdnHCl (left image) and 2 M GdnHCl concentrations (right image). The white bars show the unidirectional length scale. The color scale of the height is given in far right. On the left image isolated clusters of PrP oligomers, on the right image amyloid fibrils of PrP are clearly observed. The white dashed arrows designate discontinuities along a fibril. **B**: The AFM height profiles along the blue lines in topographical images of part A. The profiles belong to the lines as numbered in the images.

From the analysis of both AFM and kinetics data it can be stated that the solvent conditions are a determinant of the final products of the assay.

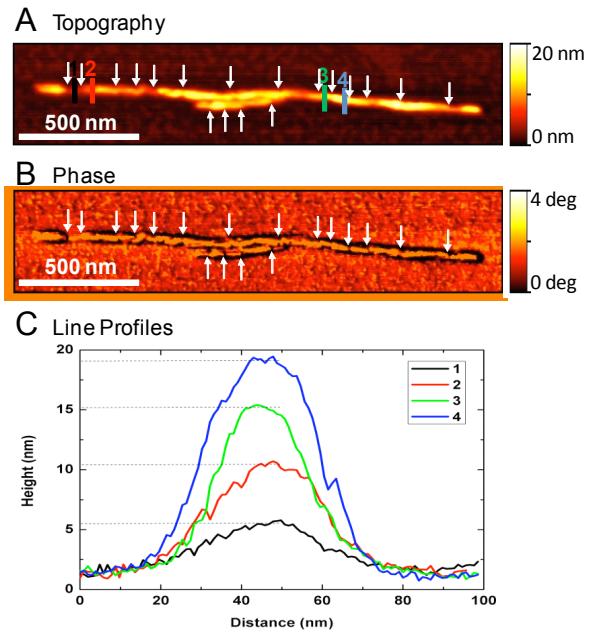

Fig. 30. Dynamic mode AFM scans of an amyloid PrP fibril. A: The height image. **B**: The phase image. The white arrows indicate the points of presumable fragmentation in both of the images. **C**: Height profiles along the lines as color designated and numbered in the height image. The height along the fibril lies between 3 nm to 18 nm (measured from the 2 nm baseline) with approximately 3 nm unit height steps (see also Fig. 29B).

Amyloid Seeding Assay (ASA) from partial purificated PrP^{Sc}

The amyloid seeding assay (ASA) is an alternative protocol for measuring PrP^{Sc} in biological samples. The ASA employs PTA precipitation, similar to the conformational – dependent immunoassay (or commonly known as CDI) [9], but detects prions based on their propensity to hasten the formation of PrP amyloid rather than detection using antibodies. It was found that many prions strains could be detected using the ASA [194].

In our study, the ASA protocol appeared to be related to the formation of a particular assembly of the aggregates not exhibiting long fibrils. Moreover, our analysis revealed how this powerful tool to detect a small quantity of prions, could be associated to the different states of the PrP amyloid. The original ASA protocol condition, 0.4 M GdnHCl gave a better detection in the assay compared to 2 M GdnHCl. The lag phase after the addition of scrapie sample as a seed can be seen in Fig. 31.

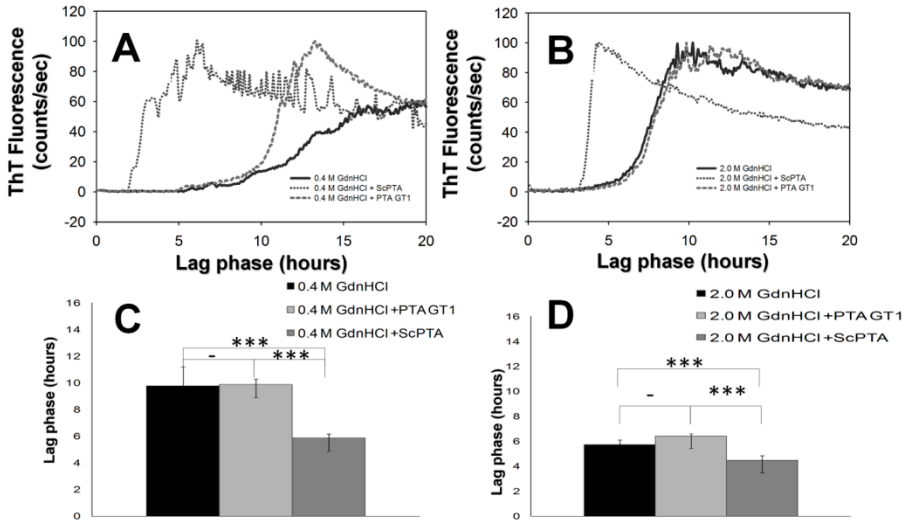

Fig. 31. The ASA assay using PTA from either GT1 or ScGT1 cells. A: Effect of seeding of PTA precipitated of ScGT1 cells using recPrP in the presence of 0.4 M of GdnHCl [194]. **B**: Effect of seeding of PTA precipitated ScGT1 cells using recPrP in the presence of 2 M of GdnHCl . **C** and **D** lag phase measurements from several experiments using **A** and **B** protocols, respectively.

Stability of MoPrP(89-230) was checked also by the effect of the denaturant agent like GdnHCl. In order to understand better the performance of the ASA protocol we attempeted to perform analysis on the effect of hastening the kinetic curve by extracted PTA ScGT1 cells. Increasing the concentration of GdnHCl to the extracted PTA ScGT1 cells does not block the ability of the extracted PTA samples to hasten the kinetic profiles. A titration is presented in Fig. 32.

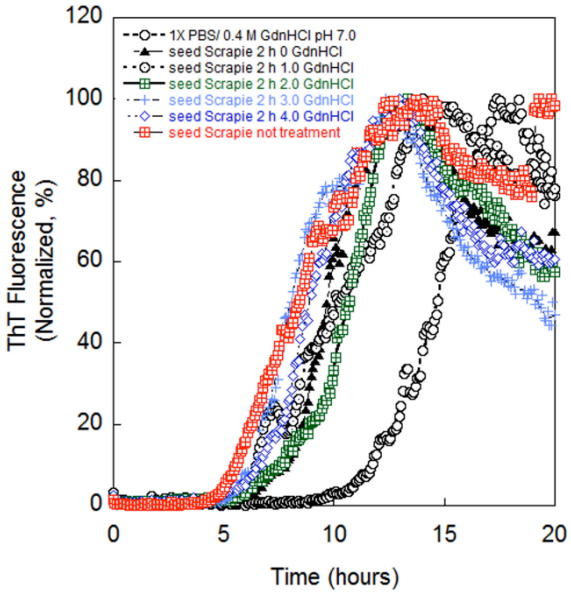

Fig. 32. Effect of increasing GdnHCl concentrations in the ASA protocol.

Comparing two different aggregation conditions by CD and fluorescence

We used CD and fluorescence to elucidate the biochemical features that give rise to the different aggregated states of recPrP using the two ASA protocols. Guanidinium salts are well known for their denaturing action on proteins. In our experiment we use GdnHCl, one of the most effective denaturants. In 6 M GndHCl all proteins with an ordered structure showed partial or total unfolding and most of them become randomly coiled, meaning they do not contain any residual structure. The CD spectral obtained from MoPrP(89-230) in different growth conditions are shown in Fig. 33. The CD spectra of MoPrP(89-230) in 20 mM sodium phosphate buffer revealed prevalently α-helix content in this mixture, without apparent aggregation. Increasing the amounts of denaturant changed the conformation of the recombinant protein, which eventually became unfolded. The results showed the 0.4 M GdnHCl condition is different from 2 M GdnHCl condition of the folded protein. In 2 M GdnHCl we found an increase of random coil with respect to 0.4 M GdnHCl. The α-helical content of MoPrP(89-230) without denaturant was very similar to that of 0.4 M GdnHCl, as indicated by the intensity of the negative maxima at 208 nm and 222 nm (Fig 33). The molecular ellipticity of the recombinant protein at 222 nm decreased at increasing concentrations of the denaturant. This result suggested that MoPrP(89-230) after dilution during the preparation of the working solution in the ASA protocol had the folding of the native protein. This may suggest that different concentrations of GdnHCl can lead to different

structural conformations. Moreover, the changing of the molar ellipticity intensity could be due to the changing of the concentration of GdnHCl.

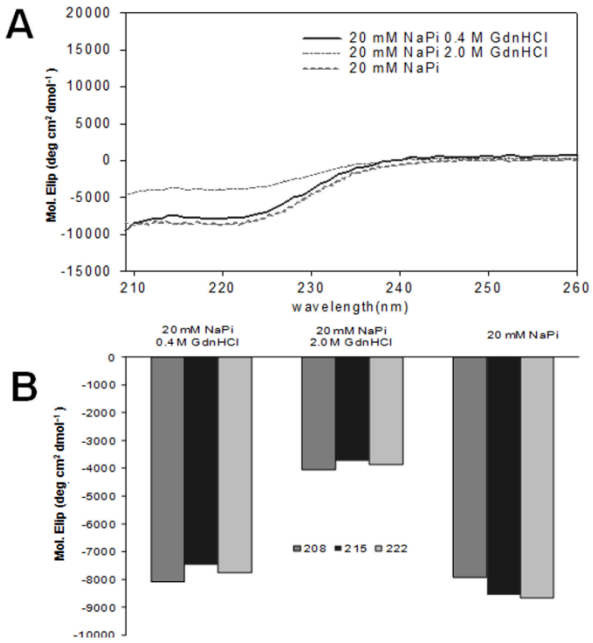

Fig. 33. A: FarUV CD spectra of MoPrP(89-230) at different concentration of GdnHCl. **B**: Variation of intensity mean ellipticity at 208 nm, 215 nm, 221 nm, 222 nm at different concentrations of GdnHCl.

We also analyzed the variation in the fluorescence of particular aromatic amino acids to demonstrate the occurrence of conformational changes. This analysis gives indirect information about how the structure differ in solution and during the formation of aggregates. In fact, the fluorescence of both preparations was different not only at the starting condition, but also at the end of the reaction. The analysis of the intensity ratio of 270 nm and 280 nm fluorescence wavelengths showed qualitative differences in two conditions. In fact, we found the same solution before performing the aggregation

process that the ratio is different between the two growth conditions. These differences were also found at the end of the reaction.

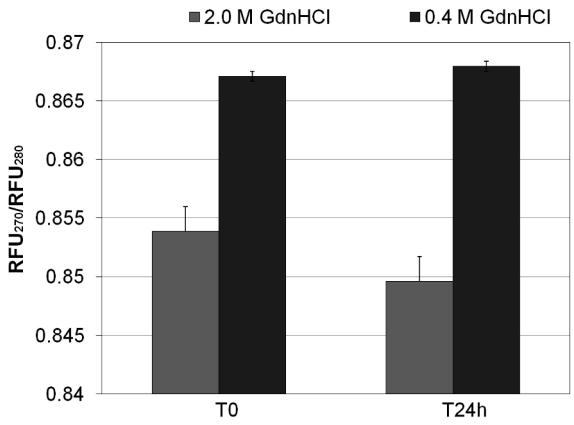

Fig. 34. Variation in the fluorescence intensity from excitations at 270 nm and 280 nm belonging to preparations with 0.4 M and 2 M concentrations of GdnHCl. T = 0 h is the value before starting of the fibrilization process at 37C. T = 24 h shows the same after 24 h.

DLS : effect of mechanical agitation using beads on the kinetic of fibril formation

DLS was used to detect the average size of the assembly (Fig. 35). The preparation with 2 M GdnHCl resulted in a monodisperse solution, whilst a polydisperse solution was observed with the 0.4 M preparation (Fig. 35 A-B). This further supports our observations from AFM and kinetics data analyses, *i.e*. that the two preparations can lead to different protein aggregates.

Using DLS it was also observed how the size changes in the presence of absence of glass beads. These supported the fact the beds help to obtain the select the size made in function of the solvent condition.

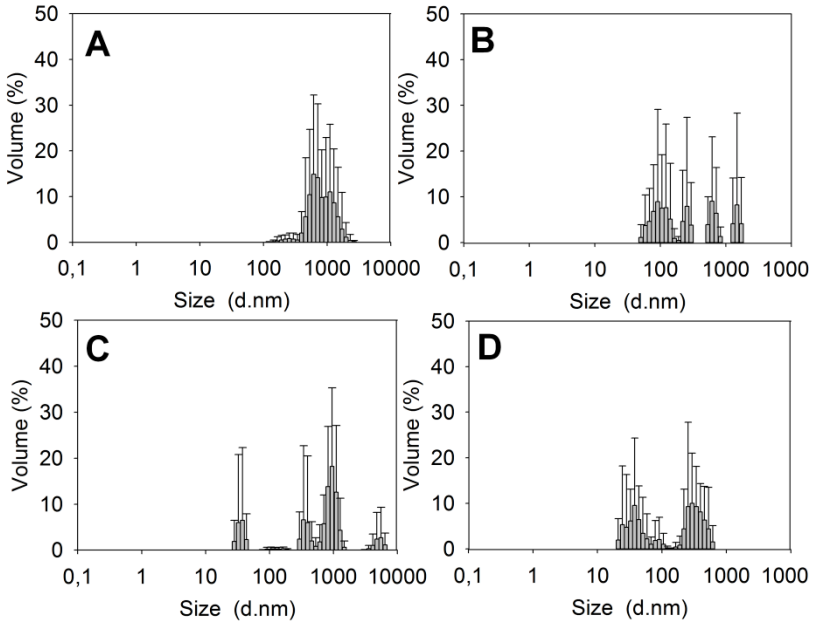

Fig. 35. DLS of fibril formation with or without beads using two different concentrations of GdnHCl. A: Fibrils sizes using 2 M GdnHCl in the presence of beads. **B**: Protein aggregates sizes using 0.4 M GdnHCl in the presence of beads. **C**: Fibrils sizes using 2 M GdnHCl in the absence of glass beads. **D**: Aggregation size of the protein made using 0.4 M GdnHCl in the absence of glass beads.

The absence of the glass beads gave a polydisperse solution in both buffer conditions. However, analysis of 2 M GdnHCl using AFM reveals the presence of much longer fibrils than in presence of the beads. However, 0.4 M GdNHCl does not reveal any fibrils.

Biochemical characterization of fibril assemblies

PrP^{Sc} fibrils produced *in vitro* by a spontaneous conversion of the recPrP have shorter PK-resistant core than those obtained present in brain homogenate with prions. Recently, Bocharova *et al.* reported that the PK-resistant core of Mo and hamster full-length PrP can be extended to ~16 kDa fragment with the N-terminus at residue 97 [174, 224, 227]. MoPrP(89-230) protein after fibril preparation was analyzed by SDS-PAGE and western blotting. No conclusive data were obtained. The result suggests low yields of the aggregation preparations for both protocols.

It was also analyzed the stability of the fibrils at both concentration of GdnHCl. The analysis made did not give conclusive results, indicating that there is probably a loss of proteins during the analysis.

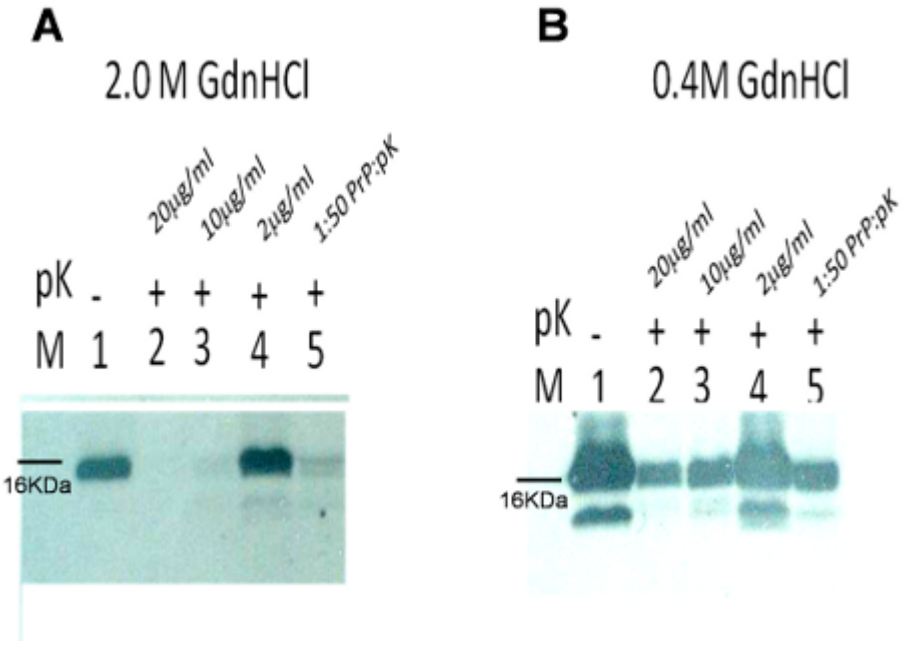

Fig. 36. Wester blots of PK digestion of Mo(PrP89–230) fibrils at two different conditions of GdnHCl. The concentration of PK: or the ratio PK:PrP(wt/wt) is indicated on top of each lane. – or + symbols refer to fibrils made in absence or presence of PK, respectively. Western blots were performed using the antibody D18. On the left 2 M GdnHCl aggregates using PK resistance and on the right 0.4 M GdnHCl.

Chapter 5: Discussion

The discovery of prion disease transmission in mammals, as well as a non-Mendelian type of inheritance in yeast prions, has led to the establishment of a new concept in biology, the prion hypothesis. The prion hypothesis postulates that an abnormal protein conformation propagates itself in an autocatalytic manner via recruitment of the normal isoform of the same protein as a substrate, and thereby acts as a transmissible agent of disease (in mammals). Ironically, while prion researchers have been struggling to provide definite proof that the PrP transmits the disease, other amyloidogenic proteins have been shown to be able to transmit (or cause) certain neurodegenerative or systemic diseases in a prion-like manner [228].

In vitro studies are typically performed using pure protein samples or protein in the presence of other components found in amyloid deposits. Two aspects of amyloid fibril formation can be determined *in vitro*: i) the structure of the fibril; and ii) the process of fibril formation (*i.e.*, the mechanism of kinetics). For both, it is important to first characterise the protein using traditional techniques (*i.e.* SDS-PAGE, DLS, CD, UV-spectra).

However, there are caveats and limitations to the study of amyloid fibril formation and interpretation of data. The single biggest obstacle in the examination of peptides and proteins that can form amyloid fibrils is the preparation of the sample. There have been several reports by different laboratories of batch-to-batch variability and poor reproducibility of experiments [229]. Several factors can contribute to this variability.

One factor to consider is the purity of the peptide or protein sample. Impurities can affect the kinetics of aggregation and, unfortunately, there is no way to predict if a sample impurity has an effect on aggregation. To reduce chemical degradation of pure samples, proper storage conditions are necessary. Typically, peptides are most stable when stored -20 or -80°C as a lyophilized powder, under N_2, in a desiccator, in the freezer. However, even under these conditions, some peptides can undergo chemical modifications [230].

Another factor affecting sample preparation is the ion-pairing agent used in the peptide/protein purification process, since the ion pair can affect the kinetics of aggregation. The purification, particularly of peptides, is performed using buffers that contain either HCl or trifluoroacetic acid (TFA). Since peptides are charged molecules, the negative ion present from the acid (Cl^- or TFA^-) forms an ion pair with the positively charged N-terminus or side chains of the peptide. These two reagents lead to ion pairs that differ in size (Cl^- <TFA^-) and hydrophobicity (Cl^- <TFA^-) and, consequently, can have a significant effect on amyloid fibril formation. The Aβ1–40 peptide, for example, has been shown to be random coil by CD if prepared from TFA but β-sheet if purified using HCl [231]. Equally, dramatic effects of ion pairing agents on the ability of IAPP24–29 to form amyloid fibrils have also been reported [230]. However, in relation to this last point, as yet, no affect seems to have be reported in the PrP.

Another caveat which has to be considered that can influence amyloid formation, is the effect of agitation, which can affect both the morphology and the kinetic output of the fibrils produced. This has been assessed for many proteins [232]. Moreover, recent

studies in the prion field showed the agitation have a big effect on the morphology of the fibril formation [233]. The agitation effect is dependent upon the type of machine used to produce the agitation and the speed of the agitation. Moreover, physical agitation such as shaking could provide an increased kinetic energy for the nucleation units to overcome the repelling force between the surface chemical potentials of two approaching particles and thus increase.

For the experiments carried out in this study, the machine used was a Spectramax M5 (Molecular Devices). No detailed published details exist for this machine and it is assumed from communication by technical staff from Molecular Devices, that the mechanism of agitation produces in the machine is a step moving by chaotic mixing, giving the same centre of agitation and intensity for each well (Fig. 37).

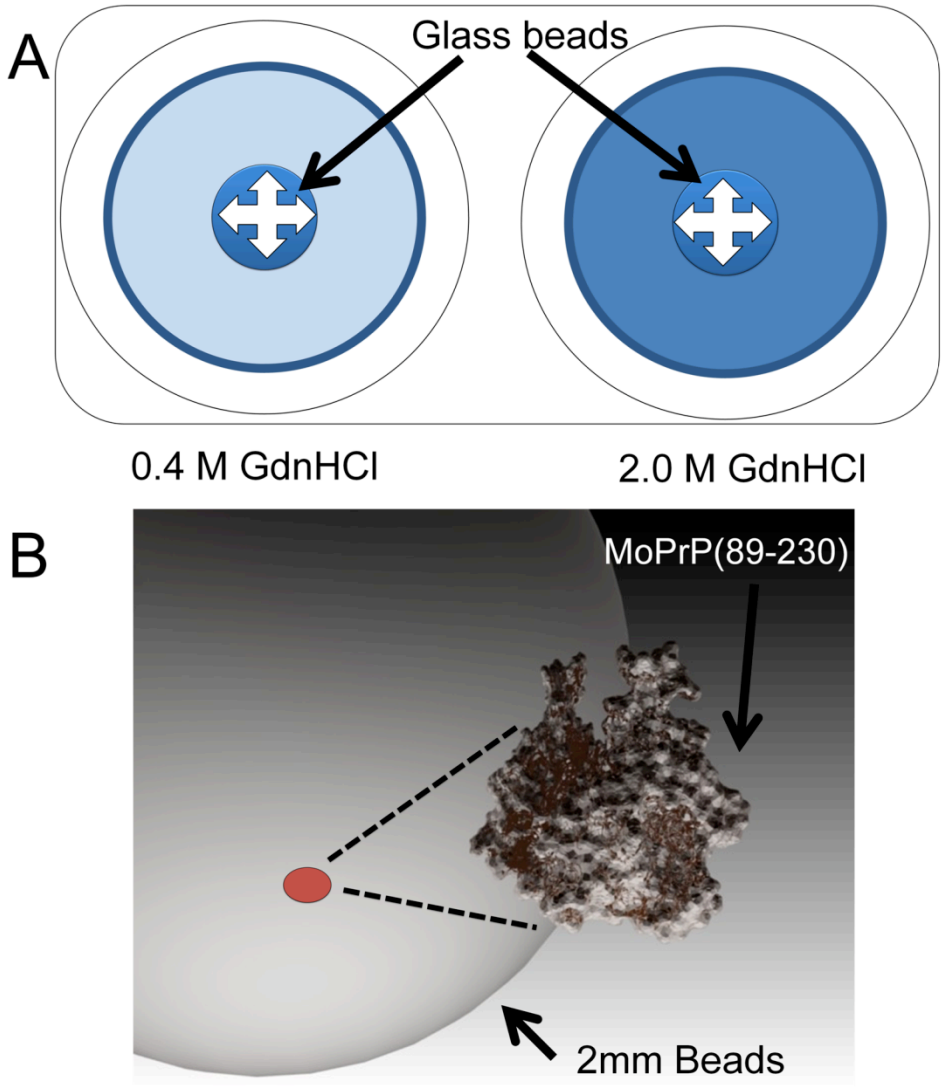

Fig. 37. A: Figure depicting two wells with two different concentrations of GdnHCl as used in this study. The agitation can be longitudinal, transversal or both. **B**: Representation of the ratio between the glass beads and MoPrP(89-230) The surface glass beads can attract protein due to the charge of the protein.

Recently, the development of the ASA has provided a new opportunity to detect prion infectivity in biological samples [194]. However, the discovery that prions can be artificially created by polymerizing recPrP into amyloid has also led to the development of cell-free systems [87]. The ASA assay is based on the availability of prions in biological samples, which can be detected by their ability to hasten the kinetic of aggregation of PrP. This assay measures the infectivity of any given biological sample, in a reasonable time scale, with a high sensitivity to low seed concentration. Moreover, further questions can be posed about the possible structures for detecting prions in biological samples. Additionally the system has been shown for revealing potential anti-TSE drugs [221].

The protocol can make use of 96-well plates with different platforms (Molecular Devices and ThermoLabsystems) and different buffer conditions (Fig. 38).

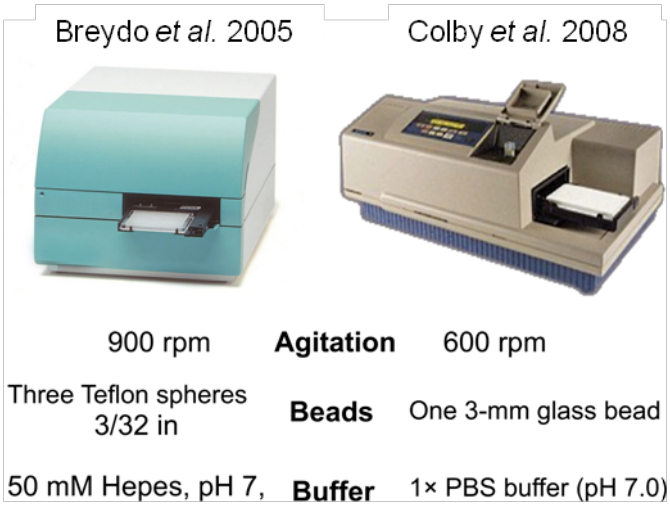

Fig. 38. Parameters of two protocols used to develop PrP aggregation protocol in a 96-well plate format. On the left condition published for revealing anti-TSE drugs properties, on the right for detecting prions in biological sample.

The main focus of my PhD studies was to analyse in detail the process of fibril formation using the ASA assay. Firstly, the initial analysis of the reaction of fibril formation was carried out using a discontinuous assay due to the fact that it is historically the protocol to study amyloid formation. However, I switched to the continuous assay, which uses a 96-well plate, in order to develop this particular assay system.

The parameters of the assay used for making the fibrils, was the same as the one used by Colby *et al.*: Spectramax M5 (Molecular Devices) 600 rpm at 37°C. In order to assess the ASA assay, one parameter was changed for the experimental assay: the concentration of GdnHCl. Intriguingly, the ASA protocol uses only one glass bead (3

mm) inside each well in contrast to that of the protocol by Breydo *et al.* [234] which uses 3 beads (Fig. 37B and Fig. 38).

Two different concentrations GdnHCl were used: 2 M and 0.4 M. These two concentration of denaturant were chosen, because the former concentration is routinely used for fibril production and gives a good production of fibrils, while the latter is used for detecting the infectivity in biological samples [194]. GdnHCl is known to alter protein structure. In the presence of 2 M GdnHCl we observed that recPrP folded completely into a random coil whereas in the presence of 0.4 M GdnHCl, recPrP is mainly α-helical. This latter condition was also postulated and demonstrated with the same concentration of urea [166]. Recently, studies have shown an existence of a strong correlation between the conformational stability of synthetic prions, (determined from PK digestion assays) and the incubation period to prion disease [91]. To explain this relationship between the stability of fibrils and their infectivity, they authors of the study proposed that the conformational stability of amyloid fibrils determines their intrinsic fragility and/or the size of the smallest possible fibrillar fragments. Recently, this model was sustained by analysis of aggregates made in different growth conditions [210].

Interestingly, the kinetic output data was modulated by the concentration of GdnHCl. In difference to that was seen using the discontinuous assay, the increase of concentration of GdnHCl reduces the lag phase. However the maximum rate was obtained at 2 M GdnHCl. An increase in the concentration of GdnHCl above 2 M gives a small decrease in the lag phase in comparison to that one seen in the concentration range between 0.4 to 2 M GdnHCl. The strength of the denaturing environment has an

important impact in the range of possible amyloid structures with those exhibiting high conformational stability.

An aim of these experiments was to find a common structural characteristic of the aggregate formed. Moreover, the main question was to assess if there were different structures formed under the different concentrations. To this aim, a combined AFM and biochemical characterization analysis was performed. The AFM analysis was performed with the help Dr Alpan Bek. We observed, by a systematic analysis of the different growth conditions, that the growth conditions impacted greatly, the assembly of aggregates.

We observed a production of long fibrils using 2 M GdnHCl but only small aggregates using 0.4 M GdnHCl. These differences were also revealed by a different max intensity of ThT.

The ThT dye shows a strong increase in fluorescence upon binding to amyloid fibrils and has hence become the most commonly used amyloid-specific dye. In spite of this widespread use, the mechanism underlying specific binding and fluorescence enhancement upon interaction with amyloid fibrils remains largely unknown. Nevertheless, ThT fluorescence enhancement is strongly dependent on fibril morphology. Our data highlights the fact that the profile of data gives a direct indication of the aggregation process. Furthermore, a difference in the maximum fluorescence intensity from 2 M GdnHCl preparation to 0.4 M GdnHCl was seen. The differences enable an analysis of the seeding effect in detail. The catalytic and the templating effects, the two key features of the amyloid and prion replication, were intimately coupled due to the self-replicating nature of the cross-β structure. The catalytic effect

was observed also in the analysis of the kinetic profile. The templating effect was also demonstrated using ThT intensity. In fact the intensity obtained with cross seeding is not the same as that from the initial analysis. This effect has also been seen in earlier experiments using cross seeding from mouse fibrils and hamster fibrils [234, 235].

Under the growth condition in 0.4 M GdnHCl, seeding had a different impact to that as seen in 2 M GdnHCl. In fact, the homo-seeding condition at 2 M GdnHCl is significantly different to the seeding made by 0.4 M GdnHCl. However, the seeding experiment suggests that low concentration of GdHCl can help to reveal seed effect. Recently, Baskakov *et al.* showed that the effect of seeding can be separated between the catalytic effect and templating effect. The catalytic effect can be visible also with the absence of the templating effect as demonstrated in different recent works [233]. This result is in agreement with our results. In fact, a max intensity of ThT as a marker of templating effect it was found only the catalytic effect (no seed-specific structure eredity) (data not shown). However, we observed the possibility to reveal the infection molecule also in the cells culture. In fact, we observed a seeding effect using PTAScGT1 cells but not in PTAGT1 cells. This is in agreement to the fact the ASA protocol can be useful to that scope. However we observed the catalytic effect also at 2 M GdnHCl.

Inoculation of β-pleated fibrils formed by one protein was sufficient to cause or accelerate the *in vivo* amyloidosis of an unrelated protein in animals [153]. This result suggests the necessity to define in detail the seeding structure definition.

To elucidate more details of structure recPrP in amyloid fibrils, this structure was analysed both at the start and at the end of the preparation under different concentrations. The protein, under the conditions of the ASA assay, shows mainly an α-

helical fold. This suggests therefore that the data obtained in this study highlights the importance of the growth condtions of the fibril for the structure of the aggregate formed. This difference is important in order to explain the heterogeneity of the aggregate preparations. The random coil structure enabled a production of fibrils with a particular assembly in a constant reproducible manner.

Interestingly, the impact of the growth condition revealed from a detailed analysis of the aggregates, a particular distribution of the height of the amyloid assemblies: height of 8 nm and 5.7 nm for the preparation of 2 M GdnHCl. Preparations of 2 M GdnHCl showed fibrils with height profile more than 8 nm (12-20 nm). Preparations also revealed a monodispersity using DLS instruments suggesting a homogeneity in the preparation sizes is aided by the glass beads (Fig. 41). Moreover, this occurrence suggests that the assembly of higher-order fibrils occurred predominantly in the vertical dimension via the stacking of ribbons on top of one another, with the association in the lateral dimension being limited.

Fibrils prepared with 2 M GdnHCl also displayed twists in the fibrils. SAFs (scrapie associated fibrils) extracted from a single source, typically include fibrils consisting of filaments aligned in parallel arrays, fibrils formed by helically twisted filaments, fibrils with a “spaghetti-like” wavy appearance, and fibrils with undefined morphologies. Ultrastructural studies of the full-length PrP, by atomic force microscopy and TEM reveal extremely broad polymorphism in fibrils formed under a single growth condition [226]. Detailed analysis of ultrastructure was attributed to a fibrils with a major subtype height 3.61±0.28 nm, composed of two ribbons, each of which was composed of two filaments. These studies were made, using the same condition used for the production

of the first synthetic prion [87]}. Unexpectedly, the 2 M GdnHCl condition gave fibrils with a particular distribution of height. In 0.4 M GdnHCl growth condition we found aggregates with a similar height profile to that of the aggregates made using a protocol to produce synthetic prions: 3.2 nm and 5.7 nm. A detailed analysis of the volume of the particles suggests the possibility that each aggregate has a variable number of molecules (Fig.39).

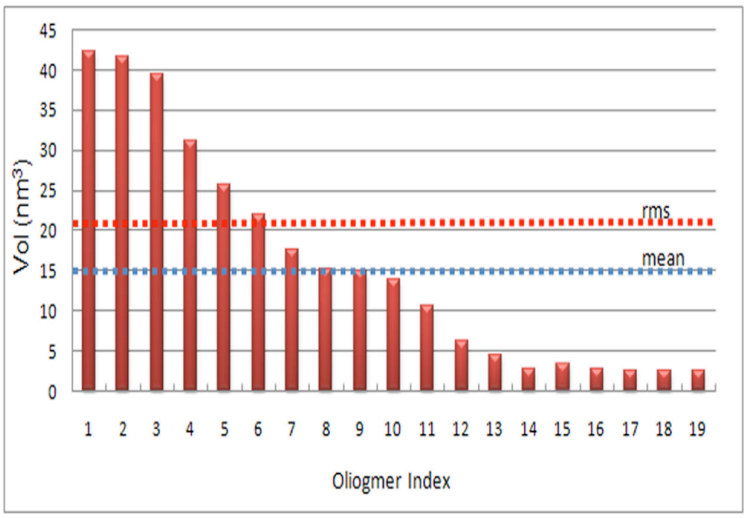

Fig. 39. Number of molecule of MoPrP(89-230) composing aggregates at 0.4 M GdnHCl. This analysis was based on a estimation of the volume of MoPrP(89-230) in 15 nm^3.

However, in the fibril preparation in 2 M GdnHCl, the solutions contain a polydispersed distribution of the aggregates. Moreover, testing the influence of glass beads showed an effect in the kinetics of the aggregates (Fig. 40) also revealed an effect in the size of aggregates by DLS (Fig. 39).

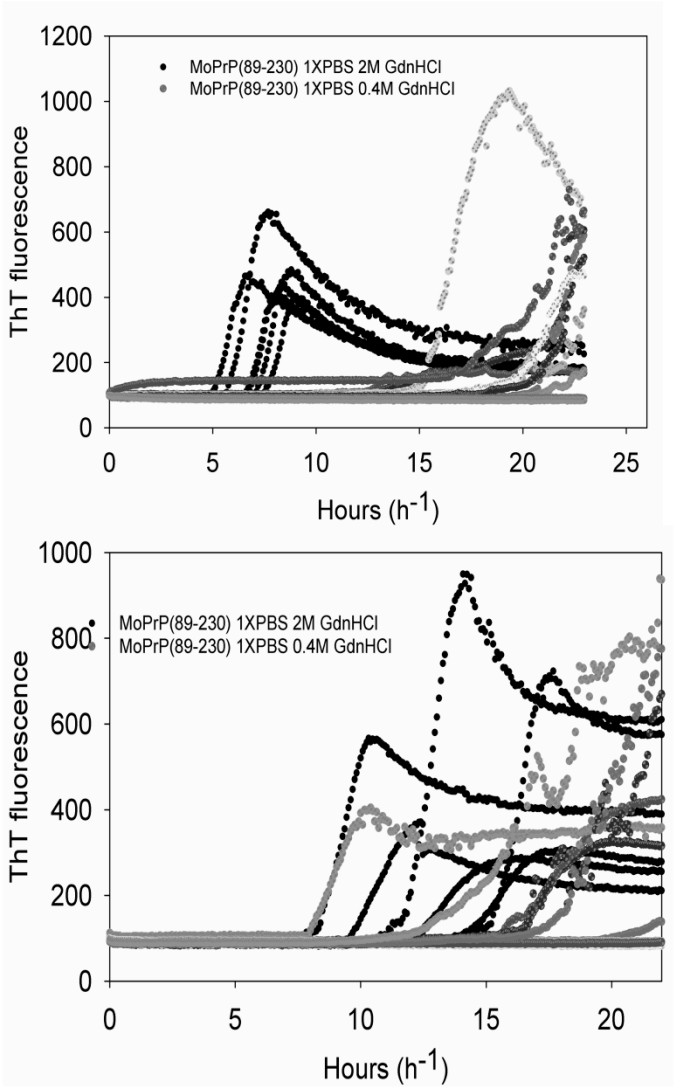

Fig. 40. A: Kinetic curve of MoPrP(89-230) of 2 M and 0.4M GdnHCl in presence of glass beads. **B**: Kinetics curves of MoPrP(89-230) of 2 M and 0.4M GdnHCl in absence of glass beads.

Therefore this data suggests that the associate structure in the ThT intensity profile is not of a particular aggregate form. This could explain why the height of 5.7 nm, as was found in both preparation conditions, probably is in a protofibrillar state and common to both conditions.

The morphological diversity of the fibrils has been previously proposed to appear as a result of a variation in nucleation events. The data here, suggests that the denaturation state can affect both the nucleation event and the aggregate morphology. Many models of structure of prion aggregates have been proposed but the heterogeneity of the preparation makes it difficult to sustain a unique model. The data in this study appears not to support either the model as proposed by Govearts *et al.* [196] but is in agreement what suggested by Caughey group [236] This is supported by the minimum height of the packed fibrils which is in agreement by the spiral model [197]. However the Spiral model does not account for the cross-β fiber X-ray diffraction and that is a great limitation in to validate that model. This study has certain limitations but is in agreement with that as proposed by previous authors [236] showing that the structure proposed by Govaerts *et al.* and by the recent publication by Anderson *et al.*, that aggregates made *in vitro* are not similar to prion fibrils produced *in vivo*. However the *in vitro* aggregates have more similarity with a particular structure encoded in the SAF fibrils. Recently unpublished result show how X-ray diffraction patter of PrP^{Sc} are different with the patter obtain starting by recombinant source. In conclusion, more details on the structural relationships between prion fibrils and SAF fibrils, in contrast with other strains or infective aggregates should be undertaken. Moreover, the data from this study shows that the continuous assay in a 96-well plate has the possibility (using different growth conditions) to differentiate aggregates in terms of their structural morphology and their kinetics traces. One important parameter can be use for that purpose is the concentration of GdnHCl but also the pH and the type of agitation.

Altogether, these results suggest the need to further investigate several other biophtsical conditions. In other words, the approach presented in detail above provides new insights into a new methodology of how to prepare a new generation of synthetic prions and suggest the necessity to improve our knowledge of prion structure and its function.

Acknowledgements

This work would have not been possible without the help of many people. Some of them were directly involved in the work, others taught me a great deal on prion studies and introduced me to the world of structural biology, and supported me during my everyday of PhD-student's life.

I wish to express my gratitude to Prof. Giuseppe Legname for his supervision.

I am grateful to my family for supporting me all these years.

I wish to express my gratitude to Prof. Baskakov , Prof. Negro, Dr. Catharino, Dr. Suzuky, Dr. Culhane, Dr. Susman, Dr. Lazzarino, Prof. Lagazio who helped me throughout these years at different steges and manners. I am grateful to all the technical staff of SISSA, who helped me and supported me these years: in particular to Andrea Tomicich, Tullio Bigiarini, Jessica Franzot, Micaele Grandolfo, Massimo Righi, Alessandra Janousek and Amanda Colombo.

I would like to thank my lab colleagues for the great time outside the laboratories. I would like to thank to Diane Latawiec for the help in the laboratory for her encouraging whenever I needed help.

I would like to thank to Marina Cioffi and Joanna Narkiewicz for great discussion about science in the lab. I would like to thank to Alpan Bek for his help and for his knowledgeble introduction of AFM technology.

A special thank to the family of my girlfriend for their support.

Finally, A special thanks goes to my Chiara who patiently supported and helped me all these years.

APPENDIX I: MATHEMATICAL APPROACH

Method for fitting kinetic profile of MoPrP(89-230)

The kinetics and products of protein aggregation have been measured using at least 18 different analytical techniques, each having its own intrinsic advantages and disadvantages [237]. Typical kinetics of spontaneous *in vitro* fibril formation of MoPrP(89-230) at 37°C showed a substantial lag-phase followed by a rapid increase of amyloid fibrils accumulation as measured by ThT fluorescence. The length of the lag-phase is a important parameter as it can help to detect any effect on the fibril formation. In fact, the difference of the lag phase was used to detect the propensity of prion transmission [166, 174, 224].

The way we can estimated the lag-phase depends on the type of equation used. Therefore, I use three different approaches based on the different starting hypothesis.

The first method was the qualitatively method: this method is base on the fact the operator estimated the lag-phase in function of is experience. This method was used in many papers and don't have any physical meaning. This method was also used by Colby *et al.* [194] as a base for detecting the infectivity in biological samples. In fact, after the determination of the lag phase, the error was estimated using ANOVA procedure.

[162, 166, 212, 224]. The second method is base on the sigmoidal curve develop by Cholberg *et al.* [223]. The authors are careful to note that, “This expression is unrelated to the underlying molecular events, but provides a convenient method for comparison of the kinetics of fibrillation”[223]. These empirical equation has been used to analyze numerous data sets thus allowing for comparisons to be made between related data sets [162, 166, 174, 222, 226]. However, meaningful kinetic and mechanistic information is lacking.

The data were fit to a sigmoidal equation (Eq 1) using

$$F\ ) (F_i + m_i t) + (F_f + m_f t)/\{1 + \exp[-(t - t_m)/\tau]\} \quad \text{(Eq.1)}$$

where F is the fluorescence intensity and t_m is the time to 50% of maximal fluorescence. The initial baseline during the lag time is described by $F_i + m_i t$. The final baseline after

the growth phase has ended is described by $F_f + m_f t$. The apparent rate constant, k_{app}, for the growth of fibrils is given by $1/\tau$, the lag time is calculated as $t_m - 2\tau$, and the amplitude, amp, is given by $F_f - F_i$. Although Eq 1 gave very good fits for the ThT kinetics profiles, the expression is strictly a simple empirical means of providing kinetics parameters for comparing rates of fibrillation from different samples and does not directly reflect the underlying complex kinetics scheme.

Third method was base by quadratic and exponential functions that describe nucleation and elongation stages of fibril formation. These functions are limiting forms of hyperbolic cosine solution (Equation 2) of the first-order approximation of the reaction equation developed by Bishop and Ferrone [209]. for analysis of the nucleation-controlled polymerization.

$$F = A(\cosh Bt - 1),\ F \approx \tfrac{1}{2} B^2 A t^2 \text{ at } Bt \approx 0,\ F$$

$$\approx \tfrac{1}{2} A e^{Bt} \text{ at } Bt \gg 1, \text{ Eq. 2}$$

where F = observable parameter (ThT Fluorescence), t = polymerization time, A and B = fitting coefficients.

These method was used for estimated the length of lag-phase. Toward this aim we use a statistic program for intimately rapidly the lag-phase value. Therefore we use R Program (http://www.r-project.org/) a open source program give a opportunity to write a simple script to analyzed many data sets.

Thanks to the precious help of Prof. Corrado Lagazio it was wrote a script for any type of equation for estimated the lag phase. Each kinetics profile obtain by different growth condition was import by the R program and Normalized. Then the data was fitted using all equation describe above.

Program after many iteration give at the end a simple table with the lag phase estimation. For any analysis give the confidence of the reading and a PDF image to evaluated the properly fitting kinetics (Fig. 1).

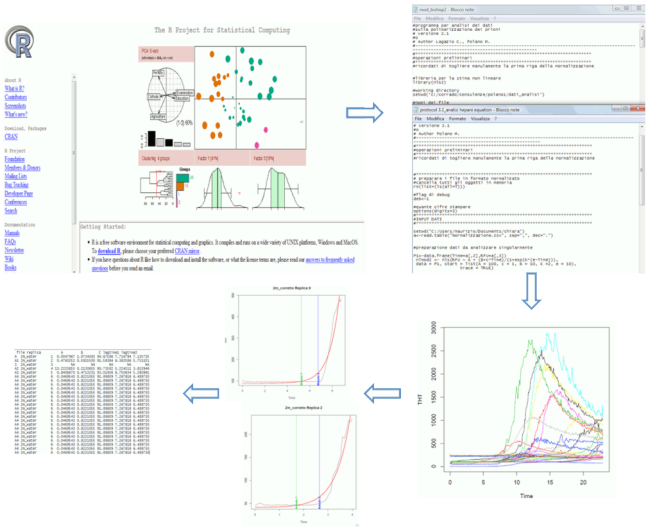

Fig. 1. Example of the normal procedure of analysis using R program.

The estimated lag phase was compare using R program using one way ANOVA.

APPENDIX II: Atomic Force Microscopy (AFM)

The atomic force microscope (AFM) is one of the foremost tools for imaging, measuring and manipulating matter at the nanoscale.This technique uses a probe that consist of a sharp tip at the end of a micromachined cantilever generally made of Silicon or Silicon Nitride. The tip interacts with the sample or better with the surface of the sample, at the atomic level through attractive or repulsive forces, depending on the imaging regime. AFM tip determines with its structure the interactions with the surface. The values of these interactions are recorded while the tip and the cantilever are scanned on the sample surface allowing the reconstruction of the sample topography with sub nanometric high resolution. The tip moves in one direction and returns in the opposite direction generating two images (trace and retrace image) of the same scanline. When all the parameter are set correctly trace and retrace images should be identical. When instead the tip interact and modify the sample trace and retrace could appear dramatically different (see picture below).

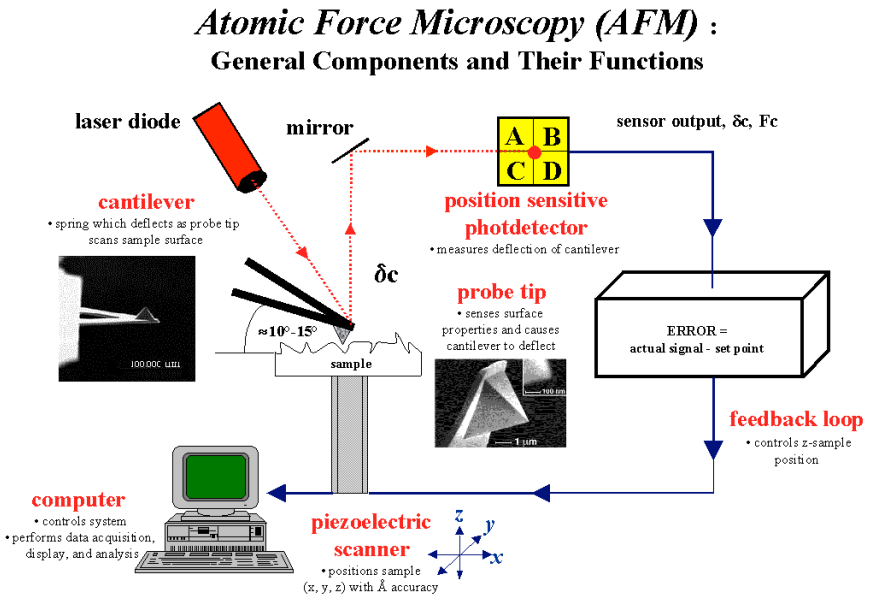

APPENDIX III: Insulin Amyloid Fibril Formation

Introduction

Insulin, a small hormone protein consisting of two polypeptide chains, adopts an α-helical conformation in its native state. The insulin sequence is well conserved among mammalian species, with few variations. Two polypeptide chains are linked by two interchain and one intrachain disulfide bridges [238]. Although insulin does not appear to be directly involved with any known human amyloid diseases, native insulin does readily convert to an inactive fibrillar form under a wide range of conditions [239]. In one clinical study, amyloid fibril–like deposits containing insulin were found at sites of insulin injections in a diabetic patient [240]. An interesting feature of insulin is that its three disulfide bridges are retained in the in vitro and ex vivo fibrillar form [238, 241] [242] [243]. Thus, these disulfide bonds must constrain the possible conformational rearrangements during the α-helix to β-sheet transition [243]. This conformational constraint makes insulin a unique model system for studying protein misfolding and subsequent amyloid fibrillization.

Material and Methods

Preparation of Insulin Protein

Bovine insulin and all other chemicals were of analytical grade or better and were obtained from Sigma–Aldrich and used without further purification. Solutions were made up by weighing out the required amount of insulin and dissolving the dry powder in distilled and deionized water adjusted to pH 2 with HCl. The pH was then checked and, if necessary, adjusted with solutions of HCl or NaOH. It was found by UV absorption at 280 nm that insulin concentrations obtained by this method were precise to within 10%. Solutions were incubated in glass vials at temperatures of 37°C or 65°C for up to 24 h. These protocol was follow in agreement of what publish in 2005 [244]

The fibril preparation has been diluted in buffer solution to a concentration of 10μM and cooled at 0^{o}C. A droplet has been dispersed on a freshly cleaved mica substrate. After 1 minute the sample has been washed in DI water and blown dry with air (N_2 is not yet available).

Thioflavin-T (ThT) Measurements.

Aliquots (5 μl) of insulin solutions after incubation were added to 995 μl of a 10 mM Na_2H/NaH_2PO_4, 150 mM NaCl, and 50 μM ThT solution and stirred for 30 s. By using a fluorescence spectrophotometer (Cary Eclipse, Varian), fluorescence emission intensity was measured for 30 s at 482 nm (10-nm slit width), exciting at 440 nm (5-nm slit

width). Values were compared with those of the ThT solution and of samples taken from the insulin solution before any incubation.

Atomic Force Microscopy (AFM).

AFM images has been acquired in tapping mode and in true non contact mode with three different tip, from different tip provider (NT-MDT, Nanoworld, ParkScientific instruments). The nominal tip radius was in all the three cases about 10nm, the oscillation frequency was 160kHz, 260kHz and 83kHz respectively. Scanning velocity was kept between 0.5 to 16mm/sec.n.

Results and Discussion

Insulin was incubated at 65°C for 24 h. The reaction was followed using a ThT intensity. The lag phase obtained was 22.3±1.12 hours and the kinetics follow a sigmoidal curve. It was follow using a typical approach of discontinuous assay. The protocol use is base on a a paper that describe the reaction was terminate up to 24 hours at 65°C.

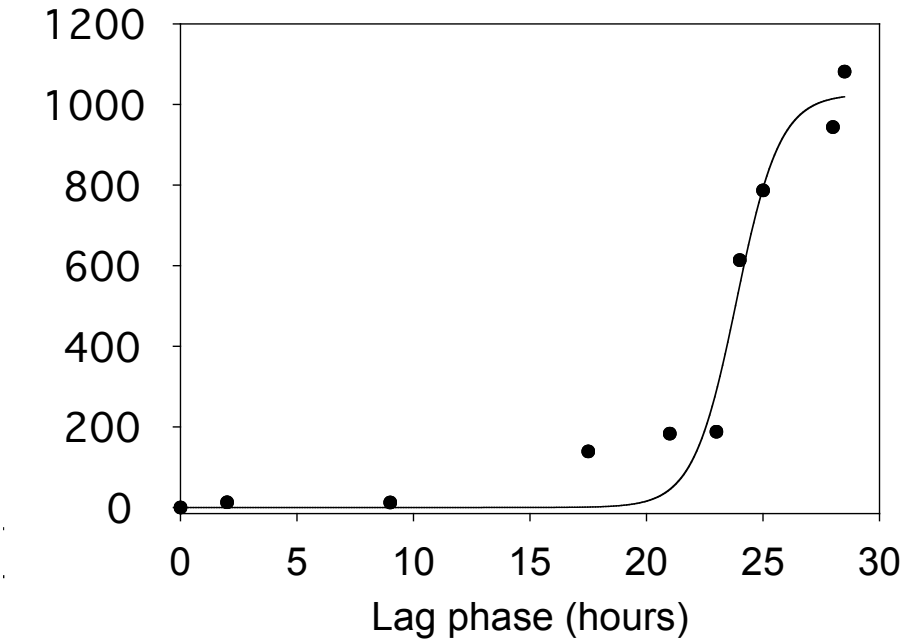

Fig. 1. Kinetics profile of insulin fibrils with ThT. The reaction was performed at 65 °C for 24 hours.

At the end of the reaction, sample was analyzed using atomic force microscopy (AFM). In Fig. 2 it was put enlighten the process of aggregation have success. In the sample some long fibrils (>2μm) were found.

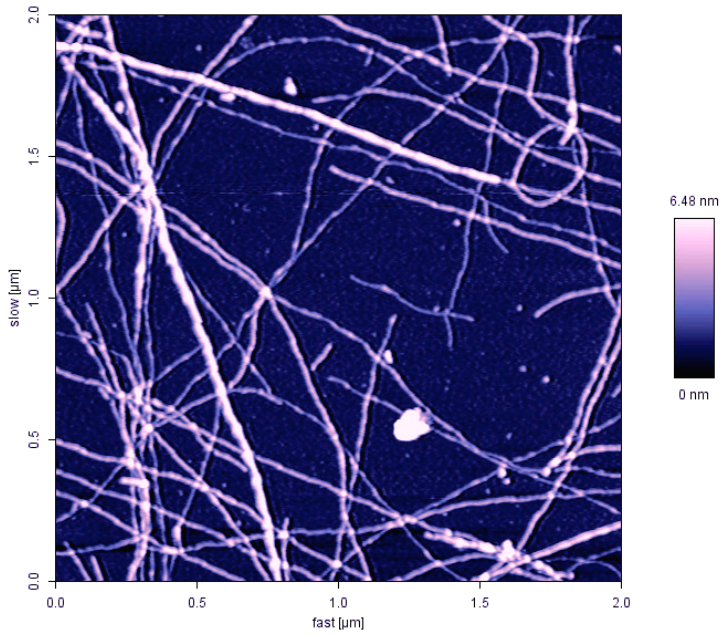

Fig. 2. AFM analysis of the product of aggregation of insulin protein. Fibrils shows a typical image over an area of 2x2μm. In larger images, using standard digitalization parameters (256x256 or 512x512) the pixel size is comparable or larger than the lateral size of the fibrils, and some details are lost. Fibrils appear randomly distributed with several crossings and some loop. Fibril length *often exceeds 2μm (the scanning area).*

Statistic analysis of the insulin fibrils show that typically the fibrils height is 2.5 – 3 nm. Some bundles of fibrils are also present with height never exceeding 10nm. The height distribution was show some particular peaks 10.8 nm, 3.8 nm. Analysis of different region taken with a larger magnification, where all the fibrils are 3nm height. The width of the fibril as measured by AFM range from 10 to 20 nm (Fig. 4). Even if nominally the three tips used are identical, fibrils appeared narrower with the 2nd tip. In order to obtained a more precise evaluation of the lateral size.

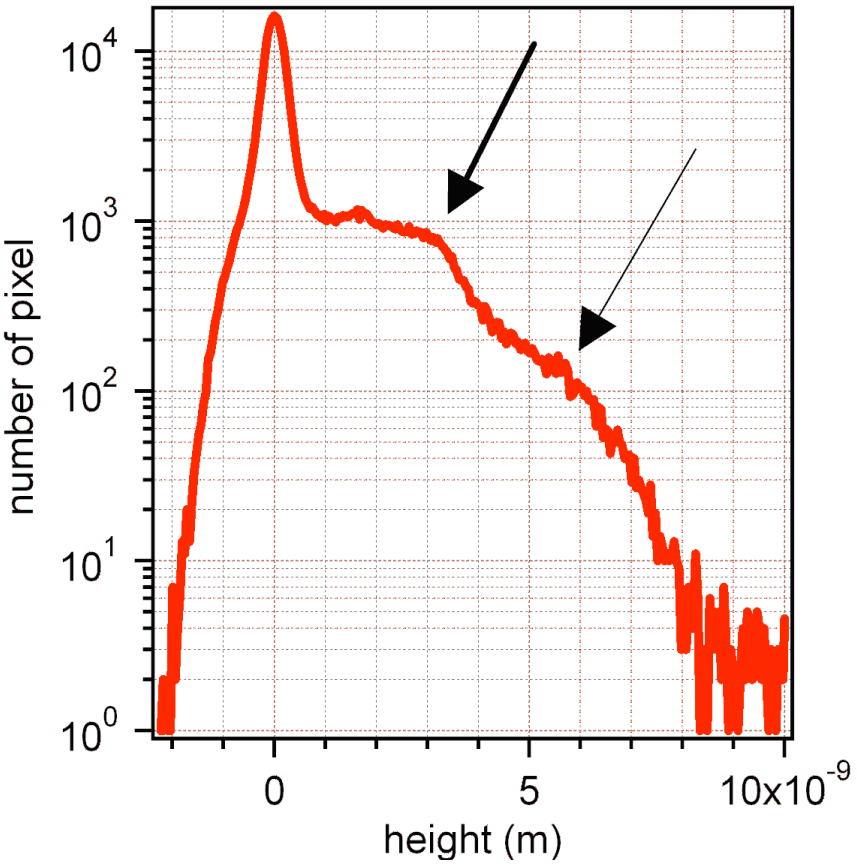

Fig. 3. Height distribution of the image shown in Fig. 1. *Typically the fibrils heigh is 2.5 – 3 nm. Some bundles of fibrils are also present with height never exceeding 10 nm.*

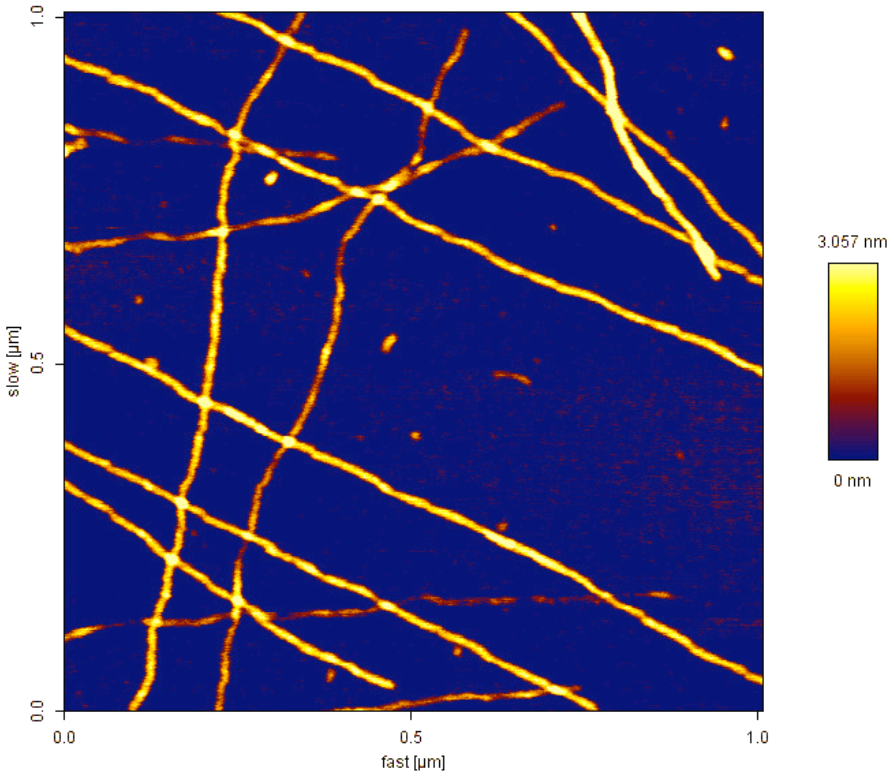

***Fig*. 4**. A different region taken with a larger magnification, where all the fibrils are 3 nm in height. The width of the fibril as measured by AFM range from 10 to 20 nm, depending on the tip used. Typically the observed width is the result of the convolution of the sample size and the tip size.

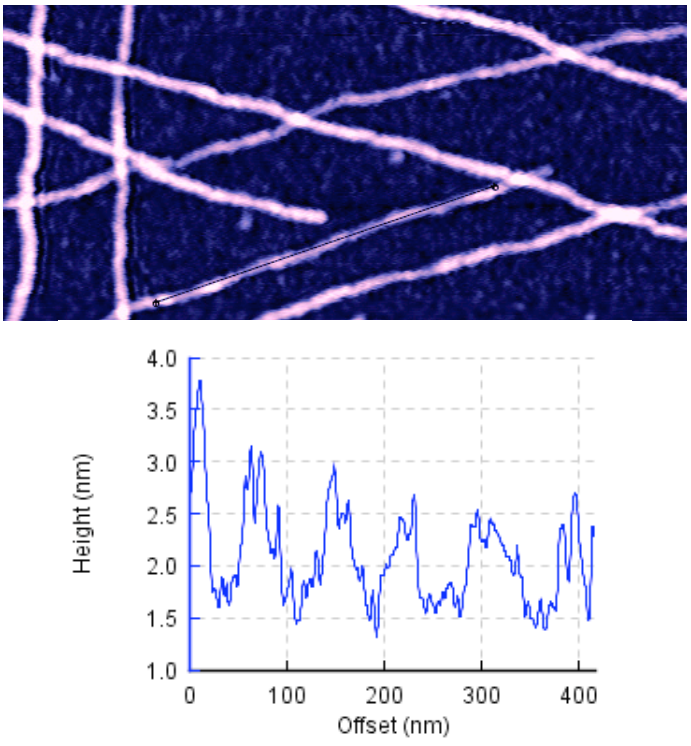

Fig. 5. Details of Fig. 3A. An height profile has been obtained along the fibril marked with a straight line **B** Structures with a periodicity of about 70 nm are highlighted.

Insulin fibrils report a particular periodicity of the height along straight line about 70 nm like it was show in fig 5B. This fits rather well with the twisted structure already reported in literature and observed by TEM spectroscopy [223].

Insulin fibrils show some twisted fibrils; these data is in agremment what was reported by other authors.

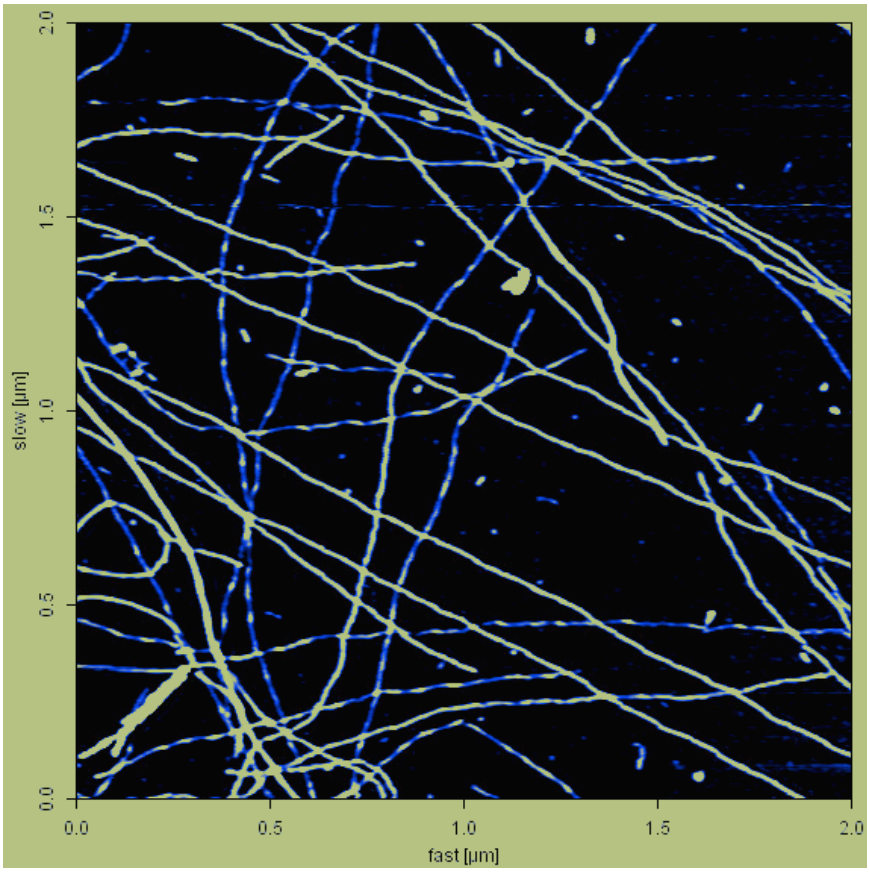

Fig. 6. A large area picture in which the colour scale has been set in order to highlight the twisted structures on the 3 nm height fibrils.

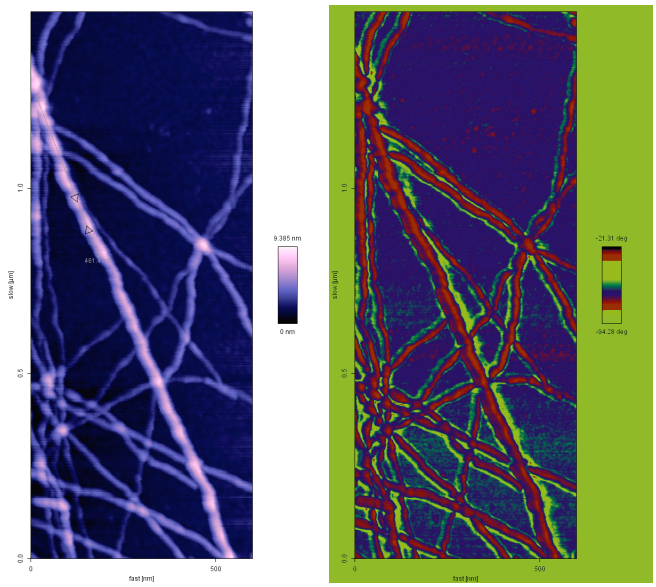

Fig. 7. Lock in phase of insulin aggregates. On the left panel a standard height image is displayed while on the right panel an image where the phase delay between excitation and tip oscillation is plotted.

The lock phase of the fibrils reported in Fig. 8 show the different resistance of insulin and mica surface. In fact the phase delay is significantly different when the tip interacts with the mica and when the tip interacts with the fibrils. This can be attributed to a different hydrophilicity of the two materials, or to different mechanical and/or dissipative properties. Maybe we should try to use this effect to distinguish different kind of fibrils. The differences at the borders (yellow) are due instead to the feedback delay.

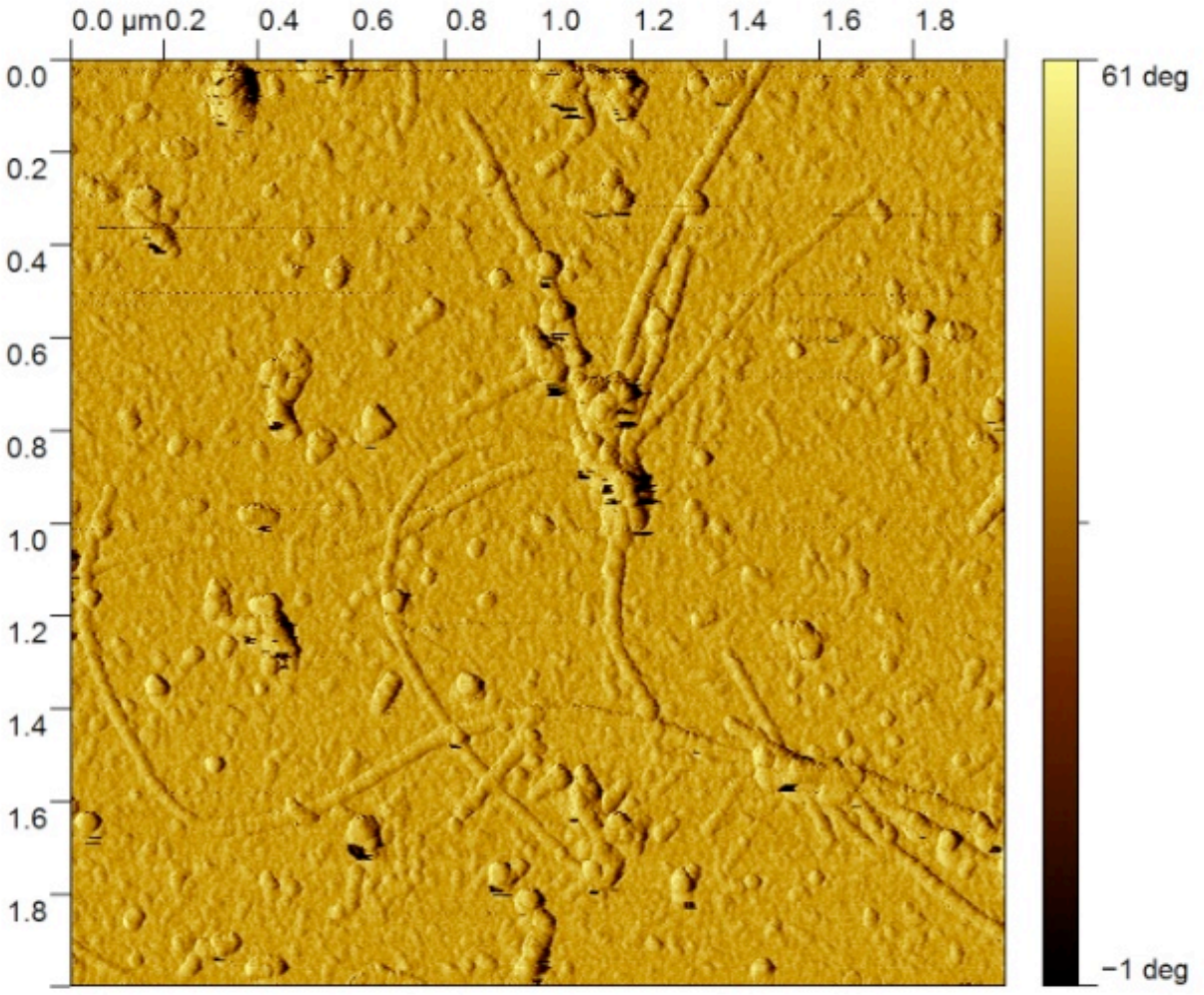

Fig. 8. Lock phase of Insulin fibrils.

APPENDIX III References

1. Brange, J., et al., *Toward understanding insulin fibrillation.* J Pharm Sci, 1997. **86**(5): p. 517-25.
2. Brange, J., et al., *A model of insulin fibrils derived from the x-ray crystal structure of a monomeric insulin (despentapeptide insulin).* Proteins, 1997. **27**(4): p. 507-16.
3. Dische, F.E., et al., *Insulin as an amyloid-fibril protein at sites of repeated insulin injections in a diabetic patient.* Diabetologia, 1988. **31**(3): p. 158-61.
4. Brange, J. and L. Langkjaer, *Insulin formulation and delivery.* Pharm Biotechnol, 1997. **10**: p. 343-409.
5. Jimenez, J.L., et al., *The protofilament structure of insulin amyloid fibrils.* Proc Natl Acad Sci U S A, 2002. **99**(14): p. 9196-201.
6. Devlin, G.L., et al., *The component polypeptide chains of bovine insulin nucleate or inhibit aggregation of the parent protein in a conformation-dependent manner.* J Mol Biol, 2006. **360**(2): p. 497-509.
7. Krebs, M.R., et al., *The mechanism of amyloid spherulite formation by bovine insulin.* Biophys J, 2005. **88**(3): p. 2013-21.

APPENDIX IV: α-Synuclein Amyloid Fibril Formation

Materials and Methods

Expression of α-synuclein

E. coli strain BL21 cells were transformed with the WT and mutant α-synuclein constructs (pET11a:Syn, kindly gave by Professor Gustinchic and dr. Alessandra Chesi). One bacterial colony was inoculated into 5 mL LB broth containing 100 µg/mL ampicillin (QBiogene,Serva), and incubated overnight at 37°C with continuous shaking. Overexpression of the protein was achieved by transferring 2.5 mL pre-culture to 500 mL LB medium supplemented with 70 µg/mL ampicillin. Cells were grown at 37°C, with continuous shaking to an OD_{600} nm of about 0.4-0.6 followed by induction with 1 mM isopropyl-β-thiogalactopyranoside (IPTG) for 3 h. After induction, the bacterial cells were harvested by centrifugation at 5000 g for 10 min and stored at -80°C.

It was also made α-synuclein using bioreactor (BiostaB-plus 2L Sartorius). Single cell was inoculated in 200 mL of LB o/n at 37°C. Following morning it was inoculate in 2 L fermentator with 1.8 L of LB media with 50 mL of preculture. After reach 0.8 OD bacterial was induce with 1mM IPTG for 8 hours.

The cell pellet was re-dissolved in 50 mM Tris (Applichem), 50 mM KCl (Applichem), 5 mM MgAc (Applichem), 0.1% Sodium Azide (Applichem), pH 8.5 (250 mg pellet/mL of buffer). The cell suspension was sonicated for 10 minutes, and the lysate was centrifuged at 8000 g for 30 min. The supernatant was separated from the pellet and the

former was first boiled for 20 min, then centrifuged at 8000 g for 30 min, and finally filtered through a 0.22 µm filter (Millipore).

Purification α-synuclein

The protein was firstly purified through anion exchange chromatography (HiPrep Q FF column, Amersham) in 20 mM Tris, pH 8, 20 mM Tris, 1 M NaCl, pH 8 followed by injection onto a size exclusion chromatography column (Superdex 200 26/30 Amersham) in 50 mM Tris/HCl, pH 7.5. Purified preparations were dialyzed against water for approximately 24 h, then lyophilized and stored at -80°C until use.

Fibrillization conditions

To characterize the aggregation properties of WT and mutant α-synuclein proteins were dissolved in 20 mM Tris (Aldrich)/150 mM sodium chloride (Aldrich), pH 7.4, at a concentrationof 100 fM (500 µL total volume in a 1.5 mL test-tube). The concentration of α-synuclein was determined using its _molar extinction coefficient at 280 nm (*i.e.* ε_{280}=5120) ona Cary 100 Bio spectrophotometer. The purified proteins were then subjected to fibrillization conditions in absence or presence of an equimolar quantity of dopamine hydrochloride (Fluka) at 37 °C with continuous shaking for the indicated time points.

ThT assay.

Fibril formation was monitored by the ThT assay, which was performed by combining10 µL of aggregated α-synuclein with 80 µL of 50 mM Glycine-NaOH (Fluka), pH 8.5, and 10 µL of 100 µM ThT (Sigma) in water. Fluorescence measurements were recorded in an LSB 50 (Perkin Elmer).

Results and Discussion

α-synuclein was expressed using pET11a-syn in flask and also in bioreactors Biostat B plus (Sartorius).

α-synuclein gave a high expression in both approach and the protein was successfully purify using a protocol from Lansbury Lab. Kinetics experiments demonstrate is it possible to obtain fibrils using 96 plate with one glass beads inside. The kinetics obtained demonstrate a low reproducibility. However it after 100 hour of agitation at 37°C the analysis of the sample show presence of the fibrils. Detailed analysis of the height distribution put enlighten two height peaks 10.8 μm and 3.8 μm.

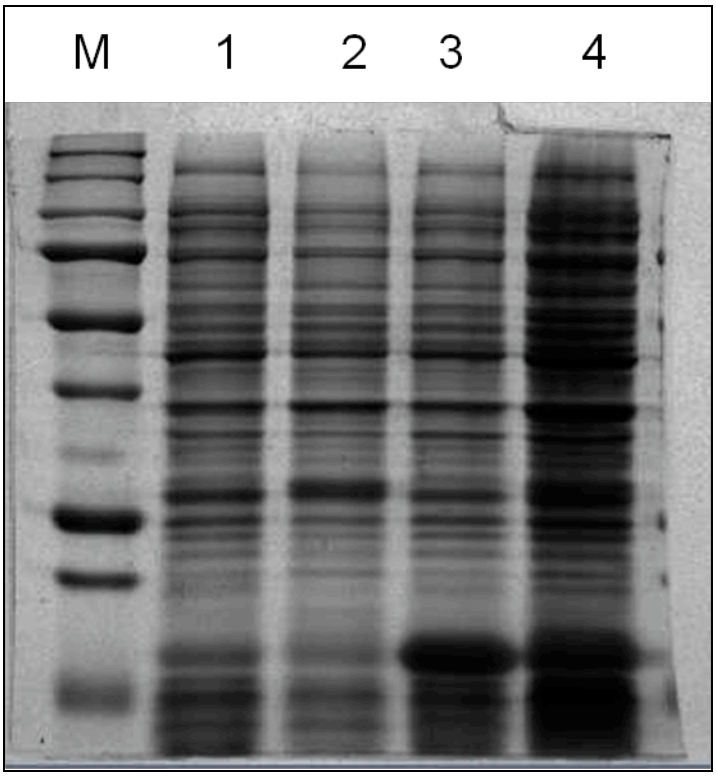

Fig .1. Expression of Synuclein obtained in bioreactor (Biosta B plus) M, Marker ,1: one oD of Inoculum in the bioreactor; 2 one OD of before induction;3 After 4 hours of induction with 1mM IPTG; 4: after o/n induction.

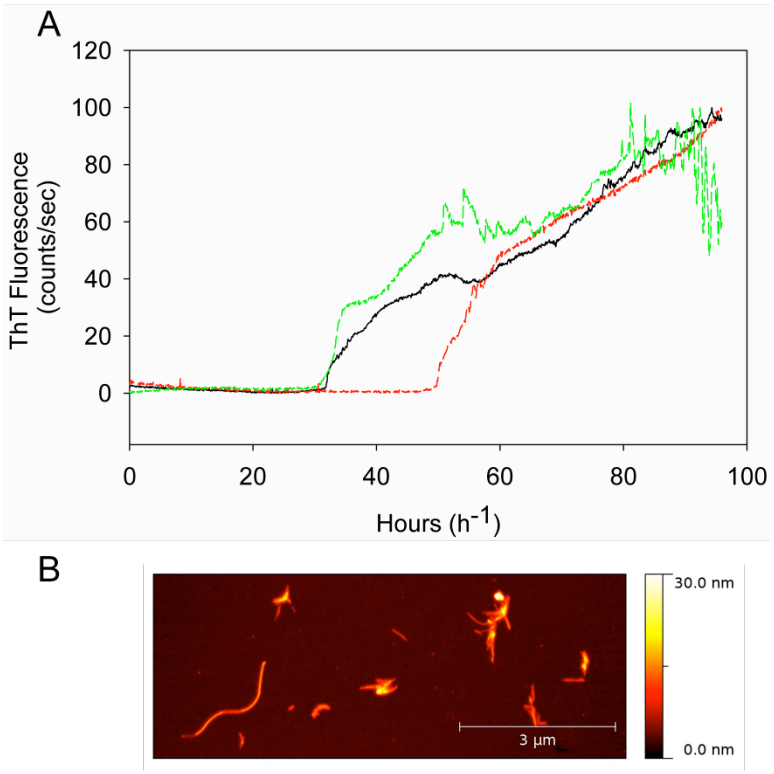

Fig. 2. A: Kinetics profile of α-synuclein in plate readers. **B**: Example of topography of fibrils obtained from α-synuclein protein.

REFERENCES

1. Prusiner, S.B., *Prion biology and diseases.* Harvey Lect, 1991. **87**: p. 85-114.
2. Prusiner, S.B., et al., *Further purification and characterization of scrapie prions.* Biochemistry, 1982. **21**(26): p. 6942-50.
3. Prusiner, S.B., et al., *Prion protein biology.* Cell, 1998. **93**(3): p. 337-48.
4. Griffith, J.S., *Self-replication and scrapie.* Nature, 1967. **215**(5105): p. 1043-4.
5. Pan, K.M., et al., *Conversion of alpha-helices into beta-sheets features in the formation of the scrapie prion proteins.* Proc Natl Acad Sci U S A, 1993. **90**(23): p. 10962-6.
6. Caughey, B.W., et al., *Secondary structure analysis of the scrapie-associated protein PrP 27-30 in water by infrared spectroscopy.* Biochemistry, 1991. **30**(31): p. 7672-80.
7. Caughey, B., et al., *N-terminal truncation of the scrapie-associated form of PrP by lysosomal protease(s): implications regarding the site of conversion of PrP to the protease-resistant state.* J Virol, 1991. **65**(12): p. 6597-603.
8. Safar, J., *The folding intermediate concept of prion protein formation and conformational links to infectivity.* Curr Top Microbiol Immunol, 1996. **207**: p. 69-76.
9. Safar, J., et al., *Conformational transitions, dissociation, and unfolding of scrapie amyloid (prion) protein.* J Biol Chem, 1993. **268**(27): p. 20276-84.
10. Zlotnik, I. and J.T. Stamp, *Scrapie disease of sheep.* World Neurol, 1961. **2**: p. 895-907.
11. Jeffrey, M., I.A. Goodbrand, and C.M. Goodsir, *Pathology of the transmissible spongiform encephalopathies with special emphasis on ultrastructure.* Micron, 1995. **26**(3): p. 277-98.
12. Woolhouse, M.E., et al., *Population dynamics of scrapie in a sheep flock.* Philos Trans R Soc Lond B Biol Sci, 1999. **354**(1384): p. 751-6.
13. M'Gowan, *Investigation into the disease of sheep called "scrapie"*, ed. W.B.a. sons. 1914, Edinburg Scostland UK: Edinburg Scostland UK.
14. Cuille J., C.P.-L., *La tremblante du mouton est bien*

inoculable. CR Acad. Sci. , 1938. **206**: p. 1687-1688.

15. Gordon W.S., B.A., Wilson D.R., *Studies in the louping-ill, tick-born fevera nd scrapie.*, in *Proc. 3rd*

Int. Congress of Microbiologists. 1939: New York,. p. 130-130.

16. Gordon W.S., B.A., Wilson D.R. *Review of work on scrapie at Compton, January 27-30, 1964* in *Report of scrapie seminar, (Washington, D.C England, 1953-1964.* . 1946. Washington: US Dept. Agric.

17. Pattison, I.H. and G.C. Millson, *Scrapie produced experimentally in goats with special reference to the clinical syndrome.* J Comp Pathol, 1961. **71**: p. 101-9.

18. Wilson, C., *Intersecting discourses: MMR vaccine and BSE.* Sci Cult (Lond), 2004. **13**(1): p. 75-88.

19. Liberski, P.P., et al., *Ultrastructural studies of experimental scrapie and Creutzfeldt-Jakob disease in hamsters. II. Astrocytic and macrophage reaction towards axonal destruction.* Acta Neurobiol Exp (Wars), 2002. **62**(3): p. 131-9.

20. Morris, J.A., D.C. Gajdusek, and C.J. Gibbs, Jr., *Spread of scrapie from inoculated to uninoculated mice.* Proc Soc Exp Biol Med, 1965. **120**(1): p. 108-10.

21. Chandler, R.L., *Encephalopathy in mice produced by inoculation with scrapie brain material.* Lancet, 1961. **1**(7191): p. 1378-9.

22. Hunter, G.D. and G.C. Millson, *Attempts to release the scrapie agent from tissue debris.* J Comp Pathol, 1967. **77**(3): p. 301-7.

23. Hunter, G.D., R.H. Kimberlin, and R.A. Gibbons, *Scrapie: a modified membrane hypothesis.* J Theor Biol, 1968. **20**(3): p. 355-7.

24. Alper, T., *The scrapie enigma: insights from radiation experiments.* Radiat Res, 1993. **135**(3): p. 283-92.

25. Adams, D.H., *The nature of the scrapie agent. A review of recent progress.* Pathol Biol (Paris), 1970. **18**(9): p. 559-77.

26. Diener, T.O., *Is the scrapie agent a viroid?* Nat New Biol, 1972. **235**(59): p. 218-9.

27. Bastian, F.O., R.A. Jennings, and W.A. Gardner, *Antiserum to scrapie-associated fibril protein cross-reacts with Spiroplasma mirum fibril proteins.* J Clin Microbiol, 1987. **25**(12): p. 2430-1.

28. Manuelidis, L., et al., *Viral particles are required for infection in neurodegenerative Creutzfeldt-Jakob disease.* Proc Natl Acad Sci U S A, 1995. **92**(11): p. 5124-8.

29. Akowitz, A., E.E. Manuelidis, and L. Manuelidis, *Protected endogenous retroviral sequences copurify with infectivity in experimental Creutzfeldt-Jakob disease.* Arch Virol, 1993. **130**(3-4): p. 301-16.

30. Marsh, R.F. and W.J. Hadlow, *Transmissible mink encephalopathy.* Rev Sci Tech, 1992. **11**(2): p. 539-50.

31. Salman, M.D., *Chronic wasting disease in deer and elk: scientific facts and findings.* J Vet Med Sci, 2003. **65**(7): p. 761-8.

32. Sy, M.S., P. Gambetti, and B.S. Wong, *Human prion diseases.* Med Clin North Am, 2002. **86**(3): p. 551-71, vi-vii.

33. Eggenberger, E., *Prion disease.* Neurol Clin, 2007. **25**(3): p. 833-42, viii.

34. Anders, K.H., *Human prion diseases.* West J Med, 1993. **158**(3): p. 295.

35. Aguzzi, A., *[The prion hypothesis and the human prion diseases].* Berl Munch Tierarztl Wochenschr, 2002. **115**(3-4): p. 91-8.

36. Gajdusek, D.C. and V. Zigas, *[Studies on the pathogenesis of kuru; a clinical, pathological and epidemiological study of a chronic, progressive, degenerative disease of the central nervous system achieving epidemic proportions among the natives of the Eastern Highlands of New Guinea.].* Klin Wochenschr, 1958. **36**(10): p. 445-59.

37. Zigas, V. and D.C. Gajdusek, *Kuru: clinical study of a new syndrome resembling paralysis agitans in natives of the Eastern Highlands of Australian New Guinea.* Med J Aust, 1957. **44**(21): p. 745-54.

38. Lansbury, P.T., Jr., et al., *Structural model for the beta-amyloid fibril based on interstrand alignment of an antiparallel-sheet comprising a C-terminal peptide.* Nat Struct Biol, 1995. **2**(11): p. 990-8.

39. Liberski, P.P. and J. Bratosiewicz-Zapart, *Is the prion structure solved?* Arch Immunol Ther Exp (Warsz), 1997. **45**(2-3): p. 121-40.

40. Hadlow, W.J., *Kuru likened to scrapie: the story remembered.* Philos Trans R Soc Lond B Biol Sci, 2008. **363**(1510): p. 3644.

41. Hadlow, W.J. and C.M. Eklund, *Scrapie--a virus-induced chronic encephalopathy of sheep.* Res Publ Assoc Res Nerv Ment Dis, 1968. **44**: p. 281-306.

42. Liberski, P.P. and P. Brown, *Kuru-fifty years later.* Neurol Neurochir Pol, 2007. **41**(6): p. 548-56.

43. Gibbs, C.J., Jr. and D.C. Gajdusek, *Transmission and characterization of the agents of spongiform virus encephalopathies: kuru, Creutzfeldt-Jakob disease, scrapie and mink encephalopathy.* Res Publ Assoc Res Nerv Ment Dis, 1971. **49**: p. 383-410.

44. Masters, C.L., D.C. Gajdusek, and C.J. Gibbs, Jr., *Creutzfeldt-Jakob disease virus isolations from the Gerstmann-Straussler syndrome with an analysis of the various forms of amyloid plaque deposition in the virus-induced spongiform encephalopathies.* Brain, 1981. **104**(3): p. 559-88.

45. Collinge, J., et al., *Transmission of fatal familial insomnia to laboratory animals.* Lancet, 1995. **346**(8974): p. 569-70.

46. Tateishi, J., *[Human prion diseases and experimental transmission].* Uirusu, 1995. **45**(1): p. 1-4.

47. Jeffrey, M. and G.A. Wells, *Spongiform encephalopathy in a nyala (Tragelaphus angasi).* Vet Pathol, 1988. **25**(5): p. 398-9.

48. Will, R.G., et al., *A new variant of Creutzfeldt-Jakob disease in the UK.* Lancet, 1996. **347**(9006): p. 921-5.

49. Collinge, J. and M. Rossor, *A new variant of prion disease.* Lancet, 1996. **347**(9006): p. 916-7.

50. Collinge, J., et al., *Molecular analysis of prion strain variation and the aetiology of 'new variant' CJD.* Nature, 1996. **383**(6602): p. 685-90.

51. Bruce, M.E., et al., *Transmissions to mice indicate that 'new variant' CJD is caused by the BSE agent.* Nature, 1997. **389**(6650): p. 498-501.

52. Hill, A.F., et al., *The same prion strain causes vCJD and BSE.* Nature, 1997. **389**(6650): p. 448-50, 526.

53. Hill, A.F., et al., *Type of prion protein in UK farmers with Creutzfeldt-Jakob disease.* Lancet, 1997. **350**(9072): p. 188.

54. Scott, M.R., et al., *Compelling transgenetic evidence for transmission of bovine spongiform encephalopathy prions to humans.* Proc Natl Acad Sci U S A, 1999. **96**(26): p. 15137-42.

55. Johnson, R.T. and C.J. Gibbs, Jr., *Creutzfeldt-Jakob disease and related transmissible spongiform encephalopathies.* N Engl J Med, 1998. **339**(27): p. 1994-2004.

56. Donnelly, C.A., et al., *The epidemiology of BSE in cattle herds in Great Britain. I. Epidemiological processes, demography of cattle and approaches to control by culling.* Philos Trans R Soc Lond B Biol Sci, 1997. **352**(1355): p. 781-801.

57. Dormont, D., *Prions, BSE and food.* Int J Food Microbiol, 2002. **78**(1-2): p. 181-9.

58. Watts, J.C., A. Balachandran, and D. Westaway, *The expanding universe of prion diseases.* PLoS Pathog, 2006. **2**(3): p. e26.

59. Dormont, D., *Prion diseases: pathogenesis and public health concerns.* FEBS Lett, 2002. **529**(1): p. 17-21.

60. Walker, D.G., L.F. Lue, and T.G. Beach, *Increased expression of the urokinase plasminogen-activator receptor in amyloid beta peptide-treated human brain microglia and in AD brains.* Brain Res, 2002. **926**(1-2): p. 69-79.

61. Xing, Y. and K. Higuchi, *Amyloid fibril proteins.* Mech Ageing Dev, 2002. **123**(12): p. 1625-36.

62. Korenaga, T., et al., *Transmission of amyloidosis in offspring of mice with AApoAII amyloidosis.* Am J Pathol, 2006. **168**(3): p. 898-906.

63. Stockel, J., et al., *Pathway of detergent-mediated and peptide ligand-mediated refolding of heterodimeric class II major histocompatibility complex (MHC) molecules.* Eur J Biochem, 1997. **248**(3): p. 684-91.

64. Wells, G.A. and J.W. Wilesmith, *The neuropathology and epidemiology of bovine spongiform encephalopathy.* Brain Pathol, 1995. **5**(1): p. 91-103.

65. Cobb, N.J. and W.K. Surewicz, *Prion diseases and their biochemical mechanisms.* Biochemistry, 2009. **48**(12): p. 2574-85.

66. Heikenwalder, M., et al., *Germinal center B cells are dispensable in prion transport and neuroinvasion.* J Neuroimmunol, 2007. **192**(1-2): p. 113-23.

67. Mabbott, N.A. and G.G. MacPherson, *Prions and their lethal journey to the brain.* Nat Rev Microbiol, 2006. **4**(3): p. 201-11.

68. DeArmond, S.J., *Discovering the mechanisms of neurodegeneration in prion diseases.* Neurochem Res, 2004. **29**(11): p. 1979-98.

69. Brandner, S., et al., *Normal host prion protein (PrPC) is required for scrapie spread within the central nervous system.* Proc Natl Acad Sci U S A, 1996. **93**(23): p. 13148-51.

70. Jeffrey, M. and L. Gonzalez, *Pathology and pathogenesis of bovine spongiform encephalopathy and scrapie.* Curr Top Microbiol Immunol, 2004. **284**: p. 65-97.

71. Chesebro, B., et al., *Anchorless prion protein results in infectious amyloid disease without clinical scrapie.* Science, 2005. **308**(5727): p. 1435-9.

72. Aguzzi, A., *Cell biology. Prion toxicity: all sail and no anchor.* Science, 2005. **308**(5727): p. 1420-1.

73. Roucou, X., et al., *Cytosolic prion protein is not toxic and protects against Bax-mediated cell death in human primary neurons.* J Biol Chem, 2003. **278**(42): p. 40877-81.

74. Ma, J. and S. Lindquist, *Wild-type PrP and a mutant associated with prion disease are subject to retrograde transport and proteasome degradation.* Proc Natl Acad Sci U S A, 2001. **98**(26): p. 14955-60.

75. Crozet, C., et al., *The truncated 23-230 form of the prion protein localizes to the nuclei of inducible cell lines independently of its nuclear localization signals and is not cytotoxic.* Mol Cell Neurosci, 2006. **32**(4): p. 315-23.

76. Caramelli, M., et al., *Bovine spongiform encephalopathy in Italian herds.* Vet Rec, 2003. **153**(23): p. 711-2.

77. Casalone, C., et al., *BSE immunohistochemical patterns in the brainstem: a comparison between UK and Italian cases.* Acta Neuropathol, 2006. **111**(5): p. 444-9.

78. Capobianco, R., et al., *Conversion of the BASE prion strain into the BSE strain: the origin of BSE?* PLoS Pathog, 2007. **3**(3): p. e31.

79. Benestad, S.L., et al., *Atypical/Nor98 scrapie: properties of the agent, genetics, and epidemiology.* Vet Res, 2008. **39**(4): p. 19.

80. Benestad, S.L., et al., *Cases of scrapie with unusual features in Norway and designation of a new type, Nor98.* Vet Rec, 2003. **153**(7): p. 202-8.

81. Moum, T., et al., *Polymorphisms at codons 141 and 154 in the ovine prion protein gene are associated with scrapie Nor98 cases.* J Gen Virol, 2005. **86**(Pt 1): p. 231-5.

82. Dickinson, A.G., et al., *Some factors controlling the incidence of scrapie in Cheviot sheep injected with a Cheviot-passaged scrapie agent.* J Comp Pathol, 1968. **78**(3): p. 313-21.

83. Bessen, R.A. and R.F. Marsh, *Distinct PrP properties suggest the molecular basis of strain variation in transmissible mink encephalopathy.* J Virol, 1994. **68**(12): p. 7859-68.

84. Telling, G.C., et al., *Prion propagation in mice expressing human and chimeric PrP transgenes implicates the interaction of cellular PrP with another protein.* Cell, 1995. **83**(1): p. 79-90.

85. Sigurdson, C.J., et al., *Prion strain discrimination using luminescent conjugated polymers.* Nat Methods, 2007. **4**(12): p. 1023-30.

86. Mahal, S.P., et al., *Prion strain discrimination in cell culture: the cell panel assay.* Proc Natl Acad Sci U S A, 2007. **104**(52): p. 20908-13.

87. Legname, G., et al., *Synthetic mammalian prions.* Science, 2004. **305**(5684): p. 673-6.

88. Bruce, M.E. and A.G. Dickinson, *Biological evidence that scrapie agent has an independent genome.* J Gen Virol, 1987. **68 (Pt 1)**: p. 79-89.

89. Vanik, D.L., K.A. Surewicz, and W.K. Surewicz, *Molecular basis of barriers for interspecies transmissibility of mammalian prions.* Mol Cell, 2004. **14**(1): p. 139-45.

90. Jones, E.M. and W.K. Surewicz, *Fibril conformation as the basis of species- and strain-dependent seeding specificity of mammalian prion amyloids.* Cell, 2005. **121**(1): p. 63-72.

91. Legname, G., et al., *Continuum of prion protein structures enciphers a multitude of prion isolate-specified phenotypes.* Proc Natl Acad Sci U S A, 2006. **103**(50): p. 19105-10.

92. King, C.Y. and R. Diaz-Avalos, *Protein-only transmission of three yeast prion strains.* Nature, 2004. **428**(6980): p. 319-23.

93. Toyama, B.H., et al., *The structural basis of yeast prion strain variants.* Nature, 2007. **449**(7159): p. 233-7.

94. Oesch, B., et al., *Identification of cellular proteins binding to the scrapie prion protein.* Biochemistry, 1990. **29**(24): p. 5848-55.

95. Caughey, B. and G.S. Baron, *Prions and their partners in crime.* Nature, 2006. **443**(7113): p. 803-10.

96. Chen, S., et al., *Prion protein as trans-interacting partner for neurons is involved in neurite outgrowth and neuronal survival.* Mol Cell Neurosci, 2003. **22**(2): p. 227-33.

97. Mange, A., et al., *Alpha- and beta- cleavages of the amino-terminus of the cellular prion protein.* Biol Cell, 2004. **96**(2): p. 125-32.

98. Griffoni, C., et al., *The cellular prion protein: biochemistry, topology, and physiologic functions.* Cell Biochem Biophys, 2003. **38**(3): p. 287-304.

99. Chiesa, R. and D.A. Harris, *Prion diseases: what is the neurotoxic molecule?* Neurobiol Dis, 2001. **8**(5): p. 743-63.

100. Wuthrich, K. and R. Riek, *Three-dimensional structures of prion proteins.* Adv Protein Chem, 2001. **57**: p. 55-82.

101. Millhauser, G.L., *Copper binding in the prion protein.* Acc Chem Res, 2004. **37**(2): p. 79-85.

102. Choi, C.J., et al., *Interaction of metals with prion protein: possible role of divalent cations in the pathogenesis of prion diseases.* Neurotoxicology, 2006. **27**(5): p. 777-87.

103. Bueler, H., et al., *Mice devoid of PrP are resistant to scrapie.* Cell, 1993. **73**(7): p. 1339-47.

104. Mallucci, G.R., et al., *Post-natal knockout of prion protein alters hippocampal CA1 properties, but does not result in neurodegeneration.* EMBO J, 2002. **21**(3): p. 202-10.

105. Nishida, N., et al., *A mouse prion protein transgene rescues mice deficient for the prion protein gene from purkinje cell degeneration and demyelination.* Lab Invest, 1999. **79**(6): p. 689-97.

106. Collinge, J., et al., *Prion protein is necessary for normal synaptic function.* Nature, 1994. **370**(6487): p. 295-7.

107. Tobler, I., et al., *Altered circadian activity rhythms and sleep in mice devoid of prion protein.* Nature, 1996. **380**(6575): p. 639-42.

108. Manson, J.C., et al., *129/Ola mice carrying a null mutation in PrP that abolishes mRNA production are developmentally normal.* Mol Neurobiol, 1994. **8**(2-3): p. 121-7.

109. Shyng, S.L., M.T. Huber, and D.A. Harris, *A prion protein cycles between the cell surface and an endocytic compartment in cultured neuroblastoma cells.* J Biol Chem, 1993. **268**(21): p. 15922-8.

110. Pauly, P.C. and D.A. Harris, *Copper stimulates endocytosis of the prion protein.* J Biol Chem, 1998. **273**(50): p. 33107-10.

111. Brown, D.R. and A. Besinger, *Prion protein expression and superoxide dismutase activity.* Biochem J, 1998. **334 (Pt 2)**: p. 423-9.

112. Sakudo, A., et al., *Impairment of superoxide dismutase activation by N-terminally truncated prion protein (PrP) in PrP-deficient neuronal cell line.* Biochem Biophys Res Commun, 2003. **308**(3): p. 660-7.

113. Suazo, M., et al., *CCS and SOD1 mRNA are reduced after copper supplementation in peripheral mononuclear cells of individuals with high serum ceruloplasmin concentration.* J Nutr Biochem, 2008. **19**(4): p. 269-74.

114. Mouillet-Richard, S., et al., *Modulation of serotonergic receptor signaling and cross-talk by prion protein.* J Biol Chem, 2005. **280**(6): p. 4592-601.

115. Spielhaupter, C. and H.M. Schatzl, *PrPC directly interacts with proteins involved in signaling pathways.* J Biol Chem, 2001. **276**(48): p. 44604-12.

116. Martins, V.R., et al., *Insights into the physiological function of cellular prion protein.* Braz J Med Biol Res, 2001. **34**(5): p. 585-95.

117. Chiarini, L.B., et al., *Cellular prion protein transduces neuroprotective signals.* EMBO J, 2002. **21**(13): p. 3317-26.

118. Chiarini, L.B., et al., *Cytoplasmic c-Jun N-terminal immunoreactivity: a hallmark of retinal apoptosis.* Cell Mol Neurobiol, 2002. **22**(5-6): p. 711-26.

119. Gauczynski, S., et al., *The 37-kDa/67-kDa laminin receptor acts as the cell-surface receptor for the cellular prion protein.* EMBO J, 2001. **20**(21): p. 5863-75.

120. Warner, R.G., et al., *Identification of the heparan sulfate binding sites in the cellular prion protein.* J Biol Chem, 2002. **277**(21): p. 18421-30.

121. Kurschner, C. and J.I. Morgan, *The cellular prion protein (PrP) selectively binds to Bcl-2 in the yeast two-hybrid system.* Brain Res Mol Brain Res, 1995. **30**(1): p. 165-8.

122. Toni, M., et al., *Cellular prion protein and caveolin-1 interaction in a neuronal cell line precedes fyn/erk 1/2 signal transduction.* J Biomed Biotechnol, 2006. **2006**(5): p. 69469.

123. Schmitt-Ulms, G., et al., *Binding of neural cell adhesion molecules (N-CAMs) to the cellular prion protein.* J Mol Biol, 2001. **314**(5): p. 1209-25.

124. Della-Bianca, V., et al., *Neurotrophin p75 receptor is involved in neuronal damage by prion peptide-(106-126).* J Biol Chem, 2001. **276**(42): p. 38929-33.

125. Kocisko, D.A. and B. Caughey, *Searching for anti-prion compounds: cell-based high-throughput in vitro assays and animal testing strategies.* Methods Enzymol, 2006. **412**: p. 223-34.

126. Dobson, C.M. and M. Karplus, *The fundamentals of protein folding: bringing together theory and experiment.* Curr Opin Struct Biol, 1999. **9**(1): p. 92-101.

127. Dobson, C.M., *Protein misfolding, evolution and disease.* Trends Biochem Sci, 1999. **24**(9): p. 329-32.

128. Dobson, C.M., *Protein folding and misfolding.* Nature, 2003. **426**(6968): p. 884-90.

129. Chiti, F. and C.M. Dobson, *Protein misfolding, functional amyloid, and human disease.* Annu Rev Biochem, 2006. **75**: p. 333-66.

130. Ross, C.A. and M.A. Poirier, *Protein aggregation and neurodegenerative disease.* Nat Med, 2004. **10 Suppl**: p. S10-7.

131. Aguzzi, A. and C. Haass, *Games played by rogue proteins in prion disorders and Alzheimer's disease.* Science, 2003. **302**(5646): p. 814-8.

132. Murphy, R.M., *Peptide aggregation in neurodegenerative disease.* Annu Rev Biomed Eng, 2002. **4**: p. 155-74.

133. Bates, G., *Huntingtin aggregation and toxicity in Huntington's disease.* Lancet, 2003. **361**(9369): p. 1642-4.

134. Lashuel, H.A., et al., *Mixtures of wild-type and a pathogenic (E22G) form of Abeta40 in vitro accumulate protofibrils, including amyloid pores.* J Mol Biol, 2003. **332**(4): p. 795-808.

135. Mallucci, G., et al., *Depleting neuronal PrP in prion infection prevents disease and reverses spongiosis.* Science, 2003. **302**(5646): p. 871-4.

136. Horiuchi, M. and B. Caughey, *Specific binding of normal prion protein to the scrapie form via a localized domain initiates its conversion to the protease-resistant state.* EMBO J, 1999. **18**(12): p. 3193-203.

137. Bucciantini, M., et al., *Inherent toxicity of aggregates implies a common mechanism for protein misfolding diseases.* Nature, 2002. **416**(6880): p. 507-11.

138. Kayed, R., et al., *Common structure of soluble amyloid oligomers implies common mechanism of pathogenesis.* Science, 2003. **300**(5618): p. 486-9.

139. Kayed, R., et al., *Annular protofibrils are a structurally and functionally distinct type of amyloid oligomer.* J Biol Chem, 2009. **284**(7): p. 4230-7.

140. Roth M, T.B., Blessed G., *Correlation between scores for dementia and counts of 'senile plaques' in*

cerebral grey matter of elderly subjects. Nature., 1966 **1Jan 1**(209(5018)): p. 109-10.

141. Treusch, S., D.M. Cyr, and S. Lindquist, *Amyloid deposits: protection against toxic protein species?* Cell Cycle, 2009. **8**(11): p. 1668-74.

142. Baglioni, S., et al., *Prefibrillar amyloid aggregates could be generic toxins in higher organisms.* J Neurosci, 2006. **26**(31): p. 8160-7.

143. Cohen, A.S. and E. Calkins, *Electron microscopic observations on a fibrous component in amyloid of diverse origins.* Nature, 1959. **183**(4669): p. 1202-3.

144. Westermark, P., et al., *Amyloid fibril protein nomenclature -- 2002.* Amyloid, 2002. **9**(3): p. 197-200.

145. Stefani, M. and C.M. Dobson, *Protein aggregation and aggregate toxicity: new insights into protein folding, misfolding diseases and biological evolution.* J Mol Med, 2003. **81**(11): p. 678-99.

146. Sunde, M., et al., *Common core structure of amyloid fibrils by synchrotron X-ray diffraction.* J Mol Biol, 1997. **273**(3): p. 729-39.

147. Sipe, J.D. and A.S. Cohen, *Review: history of the amyloid fibril.* J Struct Biol, 2000. **130**(2-3): p. 88-98.

148. Serpell, L.C., P.E. Fraser, and M. Sunde, *X-ray fiber diffraction of amyloid fibrils.* Methods Enzymol, 1999. **309**: p. 526-36.

149. Chimon, S. and Y. Ishii, *Capturing intermediate structures of Alzheimer's beta-amyloid, Abeta(1-40), by solid-state NMR spectroscopy.* J Am Chem Soc, 2005. **127**(39): p. 13472-3.

150. Zandomeneghi, G., et al., *FTIR reveals structural differences between native beta-sheet proteins and amyloid fibrils.* Protein Sci, 2004. **13**(12): p. 3314-21.

151. Puchtler, H. and F. Sweat, *Congo red as a stain for fluorescence microscopy of amyloid.* J Histochem Cytochem, 1965. **13**(8): p. 693-4.

152. LeVine, H., 3rd, *Quantification of beta-sheet amyloid fibril structures with thioflavin T.* Methods Enzymol, 1999. **309**: p. 274-84.

153. O'Nuallain, B., et al., *Thermodynamics of A beta(1-40) amyloid fibril elongation.* Biochemistry, 2005. **44**(38): p. 12709-18.

154. Lomakin, A., et al., *On the nucleation and growth of amyloid beta-protein fibrils: detection of nuclei and quantitation of rate constants.* Proc Natl Acad Sci U S A, 1996. **93**(3): p. 1125-9.

155. Kelly, J.W., *The alternative conformations of amyloidogenic proteins and their multi-step assembly pathways.* Curr Opin Struct Biol, 1998. **8**(1): p. 101-6.

156. Gosal, W.S., et al., *Competing pathways determine fibril morphology in the self-assembly of beta2-microglobulin into amyloid.* J Mol Biol, 2005. **351**(4): p. 850-64.

157. Jahn, T.R., et al., *Amyloid formation under physiological conditions proceeds via a native-like folding intermediate.* Nat Struct Mol Biol, 2006. **13**(3): p. 195-201.

158. Forloni, G., *beta-Amyloid neurotoxicity.* Funct Neurol, 1993. **8**(3): p. 211-25.

159. Gasset, M., et al., *Predicted alpha-helical regions of the prion protein when synthesized as peptides form amyloid.* Proc Natl Acad Sci U S A, 1992. **89**(22): p. 10940-4.

160. Tagliavini, F., et al., *Synthetic peptides homologous to prion protein residues 106-147 form amyloid-like fibrils in vitro.* Proc Natl Acad Sci U S A, 1993. **90**(20): p. 9678-82.

161. Supattapone, S., et al., *Prion protein of 106 residues creates an artifical transmission barrier for prion replication in transgenic mice.* Cell, 1999. **96**(6): p. 869-78.

162. Baskakov, I.V., et al., *Self-assembly of recombinant prion protein of 106 residues.* Biochemistry, 2000. **39**(10): p. 2792-804.

163. Mehlhorn, I., et al., *High-level expression and characterization of a purified 142-residue polypeptide of the prion protein.* Biochemistry, 1996. **35**(17): p. 5528-37.

164. Zhang, H., et al., *Physical studies of conformational plasticity in a recombinant prion protein.* Biochemistry, 1997. **36**(12): p. 3543-53.

165. Negro, A., et al., *The complete mature bovine prion protein highly expressed in Escherichia coli: biochemical and structural studies.* FEBS Lett, 1997. **412**(2): p. 359-64.

166. Baskakov, I.V., *Autocatalytic conversion of recombinant prion proteins displays a species barrier.* J Biol Chem, 2004. **279**(9): p. 7671-7.

167. Kundu, B., et al., *Nucleation-dependent conformational conversion of the Y145Stop variant of human prion protein: structural clues for prion propagation.* Proc Natl Acad Sci U S A, 2003. **100**(21): p. 12069-74.

168. Hope, J., et al., *Cytotoxicity of prion protein peptide (PrP106-126) differs in mechanism from the cytotoxic activity of the Alzheimer's disease amyloid peptide, A beta 25-35.* Neurodegeneration, 1996. **5**(1): p. 1-11.

169. Hornemann, S. and R. Glockshuber, *Autonomous and reversible folding of a soluble amino-terminally truncated segment of the mouse prion protein.* J Mol Biol, 1996. **261**(5): p. 614-9.

170. Jackson, G.S., et al., *Reversible conversion of monomeric human prion protein between native and fibrilogenic conformations.* Science, 1999. **283**(5409): p. 1935-7.

171. Baskakov, I.V., et al., *Folding of prion protein to its native alpha-helical conformation is under kinetic control.* J Biol Chem, 2001. **276**(23): p. 19687-90.

172. Baskakov, I.V., et al., *Pathway complexity of prion protein assembly into amyloid.* J Biol Chem, 2002. **277**(24): p. 21140-8.

173. Morillas, M., D.L. Vanik, and W.K. Surewicz, *On the mechanism of alpha-helix to beta-sheet transition in the recombinant prion protein.* Biochemistry, 2001. **40**(23): p. 6982-7.

174. Bocharova, O.V., et al., *In vitro conversion of full-length mammalian prion protein produces amyloid form with physical properties of PrP(Sc).* J Mol Biol, 2005. **346**(2): p. 645-59.

175. Swietnicki, W., et al., *pH-dependent stability and conformation of the recombinant human prion protein PrP(90-231).* J Biol Chem, 1997. **272**(44): p. 27517-20.

176. Torrent, J., et al., *Alternative prion structural changes revealed by high pressure.* Biochemistry, 2003. **42**(5): p. 1318-25.

177. Baskakov, I.V., et al., *The peculiar nature of unfolding of the human prion protein.* Protein Sci, 2004. **13**(3): p. 586-95.

178. Leffers, K.W., et al., *The structural transition of the prion protein into its pathogenic conformation is induced by unmasking hydrophobic sites.* J Mol Biol, 2004. **344**(3): p. 839-53.

179. Leffers, K.W., et al., *Assembly of natural and recombinant prion protein into fibrils.* Biol Chem, 2005. **386**(6): p. 569-80.

180. Kocisko, D.A., et al., *Cell-free formation of protease-resistant prion protein.* Nature, 1994. **370**(6489): p. 471-4.

181. Bossers, A., et al., *In vitro conversion of normal prion protein into pathologic isoforms.* Clin Lab Med, 2003. **23**(1): p. 227-47.

182. Aguzzi, A. and M. Polymenidou, *Mammalian prion biology: one century of evolving concepts.* Cell, 2004. **116**(2): p. 313-27.

183. Prusiner, S.B. and S.J. DeArmond, *Prion diseases of the central nervous system.* Monogr Pathol, 1990(32): p. 86-122.

184. Come, J.H., P.E. Fraser, and P.T. Lansbury, Jr., *A kinetic model for amyloid formation in the prion diseases: importance of seeding.* Proc Natl Acad Sci U S A, 1993. **90**(13): p. 5959-63.

185. Lansbury, P.T., *Mechanism of scrapie replication.* Science, 1994. **265**(5178): p. 1510.

186. Bessen, R.A., et al., *Non-genetic propagation of strain-specific properties of scrapie prion protein.* Nature, 1995. **375**(6533): p. 698-700.

187. Soto, C., *Diagnosing prion diseases: needs, challenges and hopes.* Nat Rev Microbiol, 2004. **2**(10): p. 809-19.

188. Kaneko, K., et al., *A synthetic peptide initiates Gerstmann-Straussler-Scheinker (GSS) disease in transgenic mice.* J Mol Biol, 2000. **295**(4): p. 997-1007.

189. Legname, G., et al., *Strain-specified characteristics of mouse synthetic prions.* Proc Natl Acad Sci U S A, 2005. **102**(6): p. 2168-73.

190. Tremblay, P., et al., *Mutant PrPSc conformers induced by a synthetic peptide and several prion strains.* J Virol, 2004. **78**(4): p. 2088-99.

191. Soto, C., G.P. Saborio, and L. Anderes, *Cyclic amplification of protein misfolding: application to prion-related disorders and beyond.* Trends Neurosci, 2002. **25**(8): p. 390-4.

192. Soto, C., *Constraining the loop, releasing prion infectivity.* Proc Natl Acad Sci U S A, 2009. **106**(1): p. 10-1.

193. Deleault, N.R., et al., *Protease-resistant prion protein amplification reconstituted with partially purified substrates and synthetic polyanions.* J Biol Chem, 2005. **280**(29): p. 26873-9.

194. Colby, D.W., et al., *Prion detection by an amyloid seeding assay.* Proc Natl Acad Sci U S A, 2007. **104**(52): p. 20914-9.

195. Wille, H., et al., *Structural studies of the scrapie prion protein by electron crystallography.* Proc Natl Acad Sci U S A, 2002. **99**(6): p. 3563-8.

196. Govaerts, C., et al., *Evidence for assembly of prions with left-handed beta-helices into trimers.* Proc Natl Acad Sci U S A, 2004. **101**(22): p. 8342-7.

197. DeMarco, M.L. and V. Daggett, *From conversion to aggregation: protofibril formation of the prion protein.* Proc Natl Acad Sci U S A, 2004. **101**(8): p. 2293-8.

198. Wickner, R.B., *[URE3] as an altered URE2 protein: evidence for a prion analog in Saccharomyces cerevisiae.* Science, 1994. **264**(5158): p. 566-9.

199. Wickner, R.B., et al., *Yeast prions: evolution of the prion concept.* Prion, 2007. **1**(2): p. 94-100.

200. Uptain, S.M. and S. Lindquist, *Prions as protein-based genetic elements.* Annu Rev Microbiol, 2002. **56**: p. 703-41.

201. Glover, J.R., et al., *Self-seeded fibers formed by Sup35, the protein determinant of [PSI+], a heritable prion-like factor of S. cerevisiae.* Cell, 1997. **89**(5): p. 811-9.

202. Tanaka, M., et al., *Conformational variations in an infectious protein determine prion strain differences.* Nature, 2004. **428**(6980): p. 323-8.

203. Saupe, S.J., et al., *The product of the het-C heterokaryon incompatibility gene of Neurospora crassa has characteristics of a glycine-rich cell wall protein.* Genetics, 1996. **143**(4): p. 1589-600.

204. Wasmer, C., et al., *Infectious and noninfectious amyloids of the HET-s(218-289) prion have different NMR spectra.* Angew Chem Int Ed Engl, 2008. **47**(31): p. 5839-41.

205. Wasmer, C., et al., *Amyloid fibrils of the HET-s(218-289) prion form a beta solenoid with a triangular hydrophobic core.* Science, 2008. **319**(5869): p. 1523-6.

206. Ritter, C., et al., *Correlation of structural elements and infectivity of the HET-s prion.* Nature, 2005. **435**(7043): p. 844-8.

207. Siemer, A.B., et al., *Observation of highly flexible residues in amyloid fibrils of the HET-s prion.* J Am Chem Soc, 2006. **128**(40): p. 13224-8.

208. Siemer, A.B., et al., *13C, 15N resonance assignment of parts of the HET-s prion protein in its amyloid form.* J Biomol NMR, 2006. **34**(2): p. 75-87.

209. Bishop, M.F.F.F., *KINETICS OF NUCLEATION-CONTROLLED*

POLYMERIZATION. BIOPHYSICAL JOURNAL 1984. **46**.

210. Sun, Y., et al., *Conformational stability of PrP amyloid fibrils controls their smallest possible fragment size.* J Mol Biol, 2008. **376**(4): p. 1155-67.

211. Caughey, B., et al., *Aggregates of scrapie-associated prion protein induce the cell-free conversion of protease-sensitive prion protein to the protease-resistant state.* Chem Biol, 1995. **2**(12): p. 807-17.

212. Baskakov, I.V. and L. Breydo, *Converting the prion protein: what makes the protein infectious.* Biochim Biophys Acta, 2007. **1772**(6): p. 692-703.

213. Castilla, J., C. Hetz, and C. Soto, *Molecular mechanisms of neurotoxicity of pathological prion protein.* Curr Mol Med, 2004. **4**(4): p. 397-403.

214. Tanaka, M., et al., *Mechanism of cross-species prion transmission: an infectious conformation compatible with two highly divergent yeast prion proteins.* Cell, 2005. **121**(1): p. 49-62.

215. Tanaka, M., *[Final proof of "prion hypothesis" in the yeast prion [PSI+] system].* Tanpakushitsu Kakusan Koso, 2005. **50**(3): p. 207-14.

216. Tanaka, M. and J.S. Weissman, *An efficient protein transformation protocol for introducing prions into yeast.* Methods Enzymol, 2006. **412**: p. 185-200.

217. Tanaka, Y., et al., *Progressive phenotype and nuclear accumulation of an amino-terminal cleavage fragment in a transgenic mouse model with inducible expression of full-length mutant huntingtin.* Neurobiol Dis, 2006. **21**(2): p. 381-91.

218. Rezaei, H., et al., *Amyloidogenic unfolding intermediates differentiate sheep prion protein variants.* J Mol Biol, 2002. **322**(4): p. 799-814.

219. Lee, S. and D. Eisenberg, *Seeded conversion of recombinant prion protein to a disulfide-bonded oligomer by a reduction-oxidation process.* Nat Struct Biol, 2003. **10**(9): p. 725-30.

220. Swietnicki, W., et al., *Aggregation and fibrillization of the recombinant human prion protein huPrP90-231.* Biochemistry, 2000. **39**(2): p. 424-31.

221. Breydo, L., O.V. Bocharova, and I.V. Baskakov, *Semiautomated cell-free conversion of prion protein: applications for high-throughput screening of potential antiprion drugs.* Anal Biochem, 2005. **339**(1): p. 165-73.

222. Apetri, A.C., D.L. Vanik, and W.K. Surewicz, *Polymorphism at residue 129 modulates the conformational conversion of the D178N variant of human prion protein 90-231.* Biochemistry, 2005. **44**(48): p. 15880-8.

223. Cohlberg, J.A., et al., *Heparin and other glycosaminoglycans stimulate the formation of amyloid fibrils from alpha-synuclein in vitro.* Biochemistry, 2002. **41**(5): p. 1502-11.

224. Baskakov, I.V. and O.V. Bocharova, *In vitro conversion of mammalian prion protein into amyloid fibrils displays unusual features.* Biochemistry, 2005. **44**(7): p. 2339-48.

225. Novitskaya, V., et al., *Amyloid fibrils of mammalian prion protein are highly toxic to cultured cells and primary neurons.* J Biol Chem, 2006. **281**(19): p. 13828-36.

226. Anderson, M., et al., *Polymorphism and ultrastructural organization of prion protein amyloid fibrils: an insight from high resolution atomic force microscopy.* J Mol Biol, 2006. **358**(2): p. 580-96.

227. Bocharova, O.V., et al., *Synthetic prions generated in vitro are similar to a newly identified subpopulation of PrPSc from sporadic Creutzfeldt-Jakob Disease.* Protein Sci, 2005. **14**(5): p. 1222-32.

228. Lundmark, K., et al., *Transmissibility of systemic amyloidosis by a prion-like mechanism.* Proc Natl Acad Sci U S A, 2002. **99**(10): p. 6979-84.

229. Soto, C., *Alzheimer's and prion disease as disorders of protein conformation: implications for the design of novel therapeutic approaches.* J Mol Med, 1999. **77**(5): p. 412-8.

230. Nilsson, M.R., *Techniques to study amyloid fibril formation in vitro.* Methods, 2004. **34**(1): p. 151-60.

231. Kaneko, K., et al., *Prion protein (PrP) synthetic peptides induce cellular PrP to acquire properties of the scrapie isoform.* Proc Natl Acad Sci U S A, 1995. **92**(24): p. 11160-4.

232. Sicorello, A., et al., *Agitation and high ionic strength induce amyloidogenesis of a folded PDZ domain in native conditions.* Biophys J, 2009. **96**(6): p. 2289-98.

233. Makarava, N., et al., *Conformational Switching within Individual Amyloid Fibrils.* J Biol Chem, 2009. **284**(21): p. 14386-95.

234. Breydo, L., N. Makarava, and I.V. Baskakov, *Methods for conversion of prion protein into amyloid fibrils.* Methods Mol Biol, 2008. **459**: p. 105-15.

235. Ostapchenko, V.G., et al., *The polybasic N-terminal region of the prion protein controls the physical properties of both the cellular and fibrillar forms of PrP.* J Mol Biol, 2008. **383**(5): p. 1210-24.

236. Sim, V.L. and B. Caughey, *Ultrastructures and strain comparison of under-glycosylated scrapie prion fibrils.* Neurobiol Aging, 2008.

237. Morris, A.M., et al., *Fitting neurological protein aggregation kinetic data via a 2-step, minimal/"Ockham's razor" model: the Finke-Watzky mechanism of nucleation followed by autocatalytic surface growth.* Biochemistry, 2008. **47**(8): p. 2413-27.

238. Brange, J., et al., *Toward understanding insulin fibrillation.* J Pharm Sci, 1997. **86**(5): p. 517-25.

239. Brange, J., et al., *A model of insulin fibrils derived from the x-ray crystal structure of a monomeric insulin (despentapeptide insulin).* Proteins, 1997. **27**(4): p. 507-16.

240. Dische, F.E., et al., *Insulin as an amyloid-fibril protein at sites of repeated insulin injections in a diabetic patient.* Diabetologia, 1988. **31**(3): p. 158-61.

241. Brange, J. and L. Langkjaer, *Insulin formulation and delivery.* Pharm Biotechnol, 1997. **10**: p. 343-409.

242. Jimenez, J.L., et al., *The protofilament structure of insulin amyloid fibrils.* Proc Natl Acad Sci U S A, 2002. **99**(14): p. 9196-201.

243. Devlin, G.L., et al., *The component polypeptide chains of bovine insulin nucleate or inhibit aggregation of the parent protein in a conformation-dependent manner.* J Mol Biol, 2006. **360**(2): p. 497-509.

244. Krebs, M.R., et al., *The mechanism of amyloid spherulite formation by bovine insulin.* Biophys J, 2005. **88**(3): p. 2013-21.